Diss. ETH N° 20129

MODELING THE GROWTH AND IMPACT OF THE WOOD-DECAY FUNGUS *PHYSISPORINUS VITREUS*

A dissertation submitted to
ETH ZURICH

for the degree of
Doctor of Sciences

presented by
MATTHIAS JÖRG FUHR

MSc ETH Civil Eng
born December 25, 1982

citizen of
Sufers GR, Switzerland

accepted on the recommendation of
Prof. Dr. Hans Jürgen Herrmann, examiner
Prof. Dr. Lynne Boddy, co-examiner
Prof. Dr. Francis Schwarze, co-examiner

2012

Preface

This thesis is the outcome of my research at the Institute for Building Materials (IFB) of the Swiss Federal Institute of Technology Zurich (ETH Zurich) into the development of a mathematical model to optimize the process of enhancing the permeability of Norway spruce wood by *Physisporinus vitreus* (Swiss National Foundation of Science No. 205321-121701).

I would particularly like to thank my supervisor, Professor Dr Hans J. Herrmann, for his interest in this work and for giving me the opportunity to explore an additional field of civil engineering after my master course in construction and mechanics at ETH Zurich. I was supported by Dr M. Schubert and Professor F.W.M.R. Schwarze from the Swiss Federal Laboratories for Material Science and Technology (EMPA) at St. Gallen, who initiated the project and continually motivated me to gain and broaden my knowledge in the field of wood-decay fungi. I would like to thank my PhD colleague, C. Stührk, because without his engagement the experimental part of this project would not have been possible. Our teamwork was the key to the success of this interdisciplinary project, which involved a multitude of fields from computational physics to microbiology.

The cooperation with other projects was a source of inspiration for my thesis. I would like to express my gratitude to E. Fehr from the IFB and M. Meyer from the Institute of Cell Biology, ETH Zurich, for the exciting work on modelling the healing of wounds, Dr B. Münch from EMPA Dübendorf for help with using digital image processing, Dr C. Lehringer from EMPA Dübendorf for helpful discussions about *P. vitreus*, Dr D. Derome from EMPA Dübendorf for the climate chamber used in the tomographic experiments at PSI Villigen, E. Strub from EMPA Dübendorf for help with the microtome, G. Peschke from IFB for assisting with visualizing the fungus using scanning electron microscopy and Dr F.K. Wittel from the IFB for cooperation in the field of finite elements and mechanics. I am

indebted to all my colleagues at the IFB for their interesting discussions and varying advice about daily life as a PhD student.

Dr Kerry Brown (Melbourne, Australia) is thanked for proofreading my papers and most parts of my thesis.

Last, but by no means least, my special thanks go to my family for their support at all times.

Matthias Jörg Fuhr
Zurich, October 2011

Abstract

The wood-decay fungus, *Physisporinus vitreus*, degrades the bordered pit membranes of Norway spruce wood in its first stage of colonization. By degrading these closed valve-like connections between the pores, *P. vitreus* increases the permeability of this wood species, which is generally considered to be refractory to preservatives or modification agents, but does not significantly reduce the strength of the timber. This biotechnological process is termed 'bioincising' and it can be used to improve the uptake of substances that will enhance the wood's quality in terms of durability, fire resistance or hardness. The growth and effect of the fungus strongly depends on environmental factors, such as temperature, water activity and pH, as well as the incubation conditions. Previous studies have investigated the anatomy, permeability and mechanical properties of bioincised wood in order to reduce negative side effects and determine the optimal growth conditions of the fungus. Such *in vitro* experiments are time- and cost-intensive, and often it is not possible to link the microscopic degradation pattern of the fungus with the macroscopic properties of wood, such as permeability, because of the material's opacity.

In such a situation where it is impossible to look inside the material, mathematical models in combination with laboratory experiments enable to study of the growth behaviour of the fungus by identifying on a microscopic scale the key processes that determine the interaction between wood and fungus, and simplifying a complex biological system to a (simpler) mathematical model. The aim of the present work was to develop a fungal growth model (FGM) of *P. vitreus* based on its microscopic parameters in order to optimize the bioincising process.

The three main areas of focus of this study are the anatomy of bioincised Norway spruce wood and the simulation of the growth and impact of the fungus. Each subject is presented in a chapter, after a general introduction to the kingdom of

fungi. The first focus is on quantifying the elements of the cell wall in Norway spruce, such as intrinsic defects, pits and cell wall alterations by the fungus, by using high-resolution synchrotron X-ray computed tomography (XCT) and digital image processing. This is believed to be the first time that the cell wall elements have been segmented automatically, enabling their three-dimensional distribution in wood to be studied. Knowledge of the three-dimensional distribution of the pits in untreated Norway spruce, as well as the distribution of the impact of the fungus, is of significance for the simulation of *P. vitreus*. The second focus is the simulation of the growing fungus using the FGM. The basic idea is to model the penetration of the fungus into the wood by a pit-to-pit growth pattern, whereby the position of the mycelium and its interaction with the wood is restricted to the pits. This assumption is a simplification and does not take into account fungal activities such as bore holes, cavities or notches, but enables the enormously complex wood structure to be reduced to a network of pits, thereby showing that the fungus captures the wood tissue in a stepwise growth pattern, which is mainly dominated by the rate of degradation of the pits and the specific growth rate of the hyphae. The third focus is a permeability model of the impact of *P. vitreus*. Knowledge of the distribution of the pits, obtained in the first focus, enables calculation of the precise hydraulic resistance of each cell wall based on the resistance of a single pit. This method links the microscopic degradation of the pits (measured using the FGM or high-resolution synchrotron data) with the macroscopic permeability of a wood sample. Results of the FGM suggest that the total number of destroyed pits may principally explain permeability changes.

The interaction between fungus and wood is extremely complex and determined by environmental factors such as temperature, water activity and pH. Despite the difficulties in modelling a wood-decay fungus such as *P. vitreus*, the present work demonstrates the suitability of the FGM in optimizing the bioincising process. Furthermore, studying the growth strategy of other wood-decay fungi is possible with the (FGM).

Zusammenfassung

Holz ist ein organisches, zellulares Material, welches als vielseitiger Baustoff im Bauwesen geschätzt wird. In der Schweiz wird dabei hauptsächlich Fichtenholz eingesetzt. Dieses besticht durch seine ausgezeichneten mechanischen Eigenschaften, wie z.B. eine hohe Reisfestigkeit und ein niedriges Quellen und Schwinden, während dessen Dauerhaftigkeit durch Schädlinge wie Pilze oder andere Mikroorganismen limitiert wird. Fichtenholz ist eine schwer tränkbar Holzart und eine Verbesserung der Dauerhaftigkeit mittels technischen Verfahren ist deshalb sehr kosten- und energieintensiv. Die gängige Verfahren zur Verbesserung des Fichtenholzes mittels Holzschutzmittel oder holzmodifizierenden Substanzen, wie z.B. UV-Schutzmittel, Brandschutzmittel und Harze, sind die Druckimprägnierung oder das Einschneiden mittels Messern. Die Ergebnisse und Effizienz der bestehenden Verfahren sind unbefriedigend und ein neues Verfahren, genannt Bioincising, wurde entwickelt. Dabei wir die Tränkbarkeit von Fichtenholz mit Hilfe des holzzersetzenden Pilzes *Physisporinus vitreus* verbessert. Dieser baut in einem Frühstadium der Holzbesiedelung unter anderem die Hoftüpfel im Fichtenkernholz ab ohne dessen Festigkeit signifikant zu beeinträchtigen. Die Hoftüfpel sind ventilartige Verbindungen zwischen den Holzzellen und spielen für den Baum bei der Regulierung des Wassertransports von der Wurzel zur Krone eine wichtige Rolle. Im Fichtenkernholz, welches der tote Teil des Baumes ist, sind die Hoftüpfel verschlossen. Es konnte gezeigt werden, dass pilzbehandelte Fichtenholzproben ein stark verbessertes Tränkungsverhalten aufweisen. Dabei ist das Wachstumsverhalten des Pilzes stark von Umweltfaktoren wie der Temperatur, der Feuchtigkeit und dem Substrat abhängig und es wurden Parameterstudien über das Wachstumsverhalten des Pilzes erstellt. Solche Laborversuche sind sehr aufwendig und eine Beobachtung des Pilzwachstums *in vivo* auf einer mikroskopischen Skala im Holz ist mit heutigen experimentellen Methoden noch nicht möglich. Deshalb wird vorgeschlagen, die Auswirkung von mikroskopischen Parametern, z.B. wie Hyphenwachstumsgeschwindigkeit oder Tüpfelabbaugeschwindigkeit auf

makroskopische Messgrössen wie Eindringtiefe oder Permeabilität, mittels eines mathematischen Modelles zu untersuchen. Ziel dieser Arbeit ist die Entwicklung eines mathematischen Modelles des Wachstums von *P. vitreus* in Fichtenholz zur Optimierung des Bioincisig Verfahrens.

Die vorliegende Arbeit behandelt drei Schwerpunkte. Der erste Schwerpunkt ist eine Methode zur Quantifizierung von Fichtenholz-Zellwandelementen, wie z.B. intrinsische Defekte in der Zellwand, Tüpfel und Pilzschäden, mittels hochauflösender Synchrotron Tomographie und digitaler Bildbearbeitung. Mit Hilfe dieser Methode konnte erstmalig die dreidimensionale Verteilung der Tüpfel und die durch den Pilz verursachten Zellwandschäden im Fichtenholz automatisch detektiert und analysiert werden. Die Kenntnisse über die dreidimensionale Verteilung der Tüpfel in einem Jahrring sind für die Simulation des Pilzwachstums und des Pilzangriffs von enormer Bedeutung. Der zweite Schwerpunkt behandelt die Simulation des Pilzes im Fichtenholz mittels eines mathematischen Modelles, genannt Fungal Growth Model (FGM). Das FGM basiert auf der Idee, dass das Wachstum des Pilzes lediglich durch ein Tüpfel zu Tüpfel wachsen abgebildet werden kann. Diese starke Vereinfachung ermöglicht es die enorm komplexe Holzstruktur auf ein Netzwerk von Tüpfel zu reduziert. Mit diesem gitterfreien Modell konnte gezeigt werden, dass der Pilz das Substrat schrittweise besiedelt und die Ausbreitungsgeschwindigkeit der Pilzfront im Holz vom Verhältnis zwischen der Tüpfelabbaugeschwindigkeit und Ausbreitungsgeschwindigkeit der einzelnen Hyphen dominiert wird. Die Auswirkungen des Tüpfelabbaus durch den Pilz auf die Permeabilität des Holzes werden im dritten Schwerpunkt behandelt. Hier wird ein hydraulisches Modell präsentiert, welches einen repräsentativen hydraulischen Widerstand aus den einzelnen Tüpfel einer Zellwand berechnet. Damit kann aus dem mikroskopischen Abbau der Tüpfel, welcher z.B. im FGM oder in tomographischen Experimenten beobachtet werden kann, direkt auf die makroskopische Permeabilität einer Fichtenholzprobe geschlossen werden. Ein Vergleich mit experimentellen Daten ergab, dass die Erhöhung der Permeabilität hauptsächlich durch den Abbau der Tüpfel erklärt werden kann.

Die Interaktion zwischen Pilz und Holz ist enorm komplex und häng von vielen Umweltfaktoren ab. Trotz dieser Schwierigkeiten konnten mathematische und experimentelle Methoden entwickelt und angewendet werden, welche zur Optimierung des Bioincising Verfahren gut geeignet sind. Des Weiteren können die vorge-

schlagenen Modelle zur Erforschung von Wachstumsstrategien anderer Pilzarten benutzt werden.

Contents

List of Symbols

$\dot{\alpha}_c$	Pit degradation rate (enzymatic)
$\dot{\alpha}_I$	Initial pit degradation
$\dot{\alpha}_p$	Pit degradation rate (pressure)
β	Branching threshold, variable
ϵ	Growth costs factor
η	Dynamic viscosity
κ	Opening threshold
λ	Mean hyphal growth rate
μ	Hyphal growth rate
ν	Initial amount of nutrients
ω	Scale parameter
ρ	Density
τ	Time
θ	Angle
ξ	Angle, cut-off length
Δ	Degradation rate
Γ	Transport
Λ	Transport
Ω	Cost of Growth
Π	Penetration capacity

a	Variable
a_{ij}	Adjacency matrix
A	Area
b	Variable
B	Pressure
c	Variable, Orientation of node
d	Variable, diameter
D	Diameter
E	Young's modulus
f	Nutrients at a node
F	Nutrients at a pit
G	Shear modulus
G_r	Radial growth rate
k	Variable
K	Permeability, Stiffness matrix
l	Length
L	Total hyphal length
m	Iteration step
M	Biomass
p	Polarization, pressure
q	Degree of a node
Q	Volume flow
r	Coordinate
R	Radius
R_h	Hydraulic resistance
s	Tip
t	Time
v	Velocity
w	Thickness, width
W	Penetration work

List of indices and operators

0	Reference configuration
i,j,k	Variable indices
c	Characteristic, critical
$\mathcal{H}(x)$	HEAVISIDE step function: $\mathcal{H}(x) = \begin{cases} 0, & \text{for} \quad x < 0 \\ 1, & \text{for} \quad x \geq 0 \end{cases}$
R	Radial
T	Tangential
L	Longitudinal
n	Node
e	Edge
p	Pit
t	Tracheid
<>	Arithmetic mean
N	Number of
δ_{ij}	Kroencker delta

List of abbreviations

1D, 2D, 3D	One-, two and three-dimensional
CCD	Charge-coupled device
CLSM	Confocal laser scanning microscopy
CWE	Cell wall element
EMC	Equilibrium moisture content
EMPA	Eidgenössische Materialprüfungsanstalt (Swiss Federal Laboratories for Materials and Technology)
ETH	Eidgenössische Technische Hochschule (Swiss Federal Institute of Technology)
FGM	Fungal growth model
FSP	Fibre saturation point
HGU	Hyphal growth unit
IFB	Institute for Building materials
LM	Light microscopy
LNA	Low-nutrient agar
MC	Moisture content
MEA	Malt extract agar
pH	pH (potential hydrogenium)
PSI	Paul Scherrer Institute, Villigen (Switzerland)
RH	Relative humidity
ROI	Region of interest
RT, LT, RL	Radial tangential, longitudinal tangential, radial tangential
SE	Structuring element
SEM	Scanning electron microscopy
SLS	Swiss Light Source
TOMCAT	TOmographic Microscopy and Coherent rAdiology experiments
VOXEL	Volumetric pixel element
WFM	Wide-field microscopy
XCT	X-ray computed tomography

1 Introduction

1.1 Motivation

Wood is an organic and renewable natural resource widely used as a building material. Its excellent mechanical properties, ready availability, simple processing requirements of the raw material and ecological aspects have ensured the use of wood by humans since the earliest days, as documented in a prehistoric pile village near Sutz-Lattringen, Switzerland [73, 74], for example. On the other hand, its use as a building material is limited by organisms, such as wood-inhabiting fungi [147, 47, 167, 159], wood-destroying insects (e.g. wood borers and termites [35, 188]), bacteria [47] and marine animals [34], and by weathering by high temperature, emissions and ultraviolet radiation [201]. In order to protect wood against these biotic and abiotic factors, its quality is usually enhanced by the application of wood preservatives [151] or wood-modification substances [80].

Typically, wood preservatives are organic or synthetic substances that increase the wood's durability and resistance against pests, whereas wood-modification agents are treatments that improve the wood's material properties, such as hardness [61], UV-protection [124], strength [89] or hygroscopicity [205, 88]. Most techniques of impregnating wood are based on either non-pressure procedures, such as brushing, spraying or dipping, or pressure procedures, such as full-cell and boucherie processing. The treatability of the wood is mainly governed by its microstructure and the molecular size of the agent's components. However, many tree species have refractory wood; that is, the tissue has low treatability and effective impregnation is often impossible. In such situations, the surface of the raw material is mechanically incised with spokes, needles, lasers or drills [138, 152] in order to enhance the effectiveness of the impregnation techniques described. However, perforating the wood's surface by incising is, especially in combination with pressure impregnation, a time-, energy- and cost-intensive pro-

cedure. Besides the traditional incising techniques, biotechnological approaches using bacteria, enzymes and fungi are common (for a review see Lehringer et al. [101]), but the results of both traditional and biotechnological incising techniques are often unsatisfactory [114, 101].

1.2 Problem and objective

Norway spruce (*Picea abies* (L.) H.Karst.) is the most common tree species in central Europe and an important renewable natural resource of Switzerland. Its excellent mechanical properties and wide availability qualify it as a construction material. However, it has a refractory wood (i.e. low treatability) and the low durability reduces its usage, and technical upgrading of its resistance to microorganisms using wood preservatives is limited because of the low permeability of the heartwood, the dead part of the tree that is characterized by closed bordered pits. It is this closing, called aspiration [141], of the valve-like connection between the pores in the cell walls that makes efficient treatment of this wood species without energy- and cost-intensive technical processing impossible.

Recent studies suggest that the white-rot basidiomycete, *Physisporinus vitreus*, can increase permeability by degrading the bordered pit membranes in Norway spruce heartwood [168, 169]. This process, which occurs in the first stage of the fungal colonization of wood, is termed 'bioincising' and it can be used as an alternative to common techniques of improving the uptake of wood protection and wood-modification substances [170, 101, 98], without significantly reducing the strength of the wood. However, detailed *in vitro* experimental studies of fungal growth and its impact are essential for upscaling bioincising [99, 163, 100, 102], but such experiments are complex and expensive, or even impossible, because of the opacity of wood. In such a situation, mathematical models in combination with laboratory experiments can enable the study of the growth behaviour of the fungus.

The aim of the present work was to develop a mathematical model of the growth and impact of *P. vitreus* in Norway spruce wood in order to optimize the biotechnological process of bioincising. A filamentous wood-decay fungus exploits the host tissue by thin root-like structures (i.e. hyphae) that form a tree-like network

(i.e. mycelium). In order to explain the macroscopic properties of the wood-fungus system, such as the penetration depth of the fungus or the permeability of the wood, the model used to optimize bioincising has to be based on the microscopic interaction between the hyphae and the wood (i.e. 'bottom-up approach'). Explaining the effect of the growth velocities of the hyphae, their uptake of nutrients and the rate of degradation of the pits will support the design of laboratory experiments. For example, uniformity of wood colonization by the fungus strongly depends on the incubation conditions, because the main fungal penetration pathways are in a radial direction along the wood rays and in longitudinal direction via the tracheids. Once established, a mathematical model can evaluate the optimal distribution of fungal mycelia on the surface of the wood specimen in order to homogeneously increase the wood's permeability by a defined degree.

Bioincised Norway spruce wood can be used as the basis for wood products. Enhanced uptake of wood preservatives or wood-modification substances will improve the durability and sustainability of this native wood. The demand for such advanced wood products has increased in Switzerland since the institution of the revised Swiss construction codes and fire standards in 2003 [130, 131], which now enable the construction in Switzerland of modern multistorey wood buildings up to six floors [111]. Moreover, knowledge of the behaviour of *P. vitreus* may provide additional aspects of this exceptional organism for a better understanding of the mystery of superior violins [172, 1] or the colonization strategy of wood-decay fungi in general.

1.3 Outline

My thesis is structured in three parts dealing with the fundamental aspects of *P. vitreus* and Norway spruce wood (Ch. 2), the methods used to analyze the growth and impact of *P. vitreus* (Ch. 3) and the results of its activities in two- and three-dimensional environments (Ch. 4). Chapters 3 and 4 are based on publications written by me as principal investigator and published/or submitted to peer-reviewed scientific journals. These journals explicitly allow me to include the articles, in full or part, in a dissertation.

The first part (Ch. 2) presents the basic concept of Norway spruce wood and the

white-rot basidiomycete, *P. vitreus*. Knowledge of the anatomy, chemistry and ecology of Norway spruce, as well as the physiology of *P. vitreus*, is crucial for developing methods of analyzing fungal growth in wood.

The second part of the thesis (Ch. 3) deals with the methods of analyzing the growth and impact of *P. vitreus*. First, a framework for analyzing and quantifying the cell wall elements in Norway spruce is developed from three-dimensional tomographic data provided by high-resolution synchrotron tomographic microscopy and analyzed by digital image processing (based on Fuhr et al. [57]). Second, I analyze and discuss the three-dimensional distribution of the bordered pits in a growth ring (based on Fuhr et al. [54]). These results are the basis for modelling the growing fungus in Chapters 4 and 5. Chapter 4 presents the fungal growth model (FGM). This mathematical framework is used to analyze the growth and impact of *P. vitreus* in homogeneous (Sec. 4.2 is based on Fuhr et al. [58]) and inhomogeneous wood-like substrates (Sec. 4.3 and Sec. 4.4 are based on Fuhr et al. [55] and Fuhr et al. [56]). Chapter 5 presents a hydraulic model for analyzing the permeability changes in fungally-modified wood (based on Fuhr et al. [53]).

The thesis closes with a summary of the main findings and discusses the proposed methods and results in the context of future developments in the field of wood-decay fungi.

2 Basic aspects of Norway spruce wood and *Physisporinus vitreus*

Studying wood-decay fungi is exciting because it involves a multitude of scientific fields at all levels of biological organization (Fig. 2.1). The large scale ($> 10^{-1}$ m) comprises studies in which detailed knowledge of the physiology of the fungal mycelium and the fine structure of the wood play a secondary role. Engineering applications mainly deal with the economic impact of wood-decay fungi on structures, whereas ecological studies investigate the relation of wood-decay fungi to other organisms and their environments. On a finer scale (10^{-2}–10^{-4} m), the focus is on the microscopic structure and behaviour of the biological tissues (i.e. wood or fungal cell wall). Scientific experiments at this scale typically take place in laboratories (i.e. laboratory scale). Ultrascopical aspects ($\sim 10^{6}$ m) of wood-decay fungi and their applications are the field of material technologies and molecular biology, such as the use of fungal enzymes for the production of wood-fibre composites [161]. In addition, in recent years a growing number of studies have dealt with complex interactions in biological systems. Summarized by the term 'systems biology', these projects are often interdisciplinary and use computational resources extensively. Systems biology is related to other relatively young scientific disciplines such as bioinformatics and computational biology. On the atomic scale ($\sim 10^{-8}$ m), methods of the physical sciences are applied to biological systems in order to study the structure and function of molecules. However, all of the mentioned scientific disciplines have in common that they tend to span more and more levels of biological organization. Multiscale approaches are increasingly popular and classical boundaries between disciplines vanish.

The present work also developed a multiscale approach to studying *P. vitreus*, because the wood-decay fungus and its substrates have a complex cellular and hierarchical structure from the nanoscopic to the macroscopic scale (Fig. 2.1). Understanding the chemical composition and anatomical structure of its environ-

ment (Sec. 2.1), as well as the physiology and morphology of the fungal mycelium (Sec. 2.2), was crucial in the development of a mathematical framework of the growth and impact of *P. vitreus*. An introduction to models of fungal growth (i.e. discrete and continuum approaches) is given in Sec. 2.3.

2.1 Norway spruce wood

2.1.1 Anatomical structure

Wood is a porous material with a complex cellular and hierarchical structure as shown in Figs. 2.1 and 2.2. On the macroscopic scale, wood consists of growth rings.

Stem and growth ring

The three orientations of wood are denoted as longitudinal (along the trunk), radial (from the pith to the bark) and tangential (tangent to the growth ring) as shown in Fig. 2.2. In regions of the world with distinct seasons the growth rings correspond to the stem's annual increase in diameter. On the mesoscopic scale, the growth rings comprise cells that vary significantly in their geometry and dimensions according to their function. At the beginning of the vegetative period, the tree produces wood with a high porosity (early-wood) to transport nutrients in the lumens, whereas latewood is denser in order to stabilize the tree. In Switzerland, trees may produce early-wood from March to August, latewood from September to November and the dormant season, in which the trees are photosynthetically inactive, is typically from December to March. The width of the stem's growth rings strongly depends on the microclimate of the tree's location. The width decreases from the pith to the bark and smaller growth rings have more latewood [158]. Lindström [112] reported values for the width (percentage of latewood) between 0.5 (30%) and 8 (5%) mm. Fig. 2.3 shows a scanning electron microscopy (SEM) image of a radial tangential (RT) section of a Norway spruce growth ring. The size of the sample is approximately 0.7 mm (tangential) $\times$ 2.4 mm (radial). The respective fractions of latewood, transition wood and early-wood are approximately 7%, 15% and 78%. The corresponding

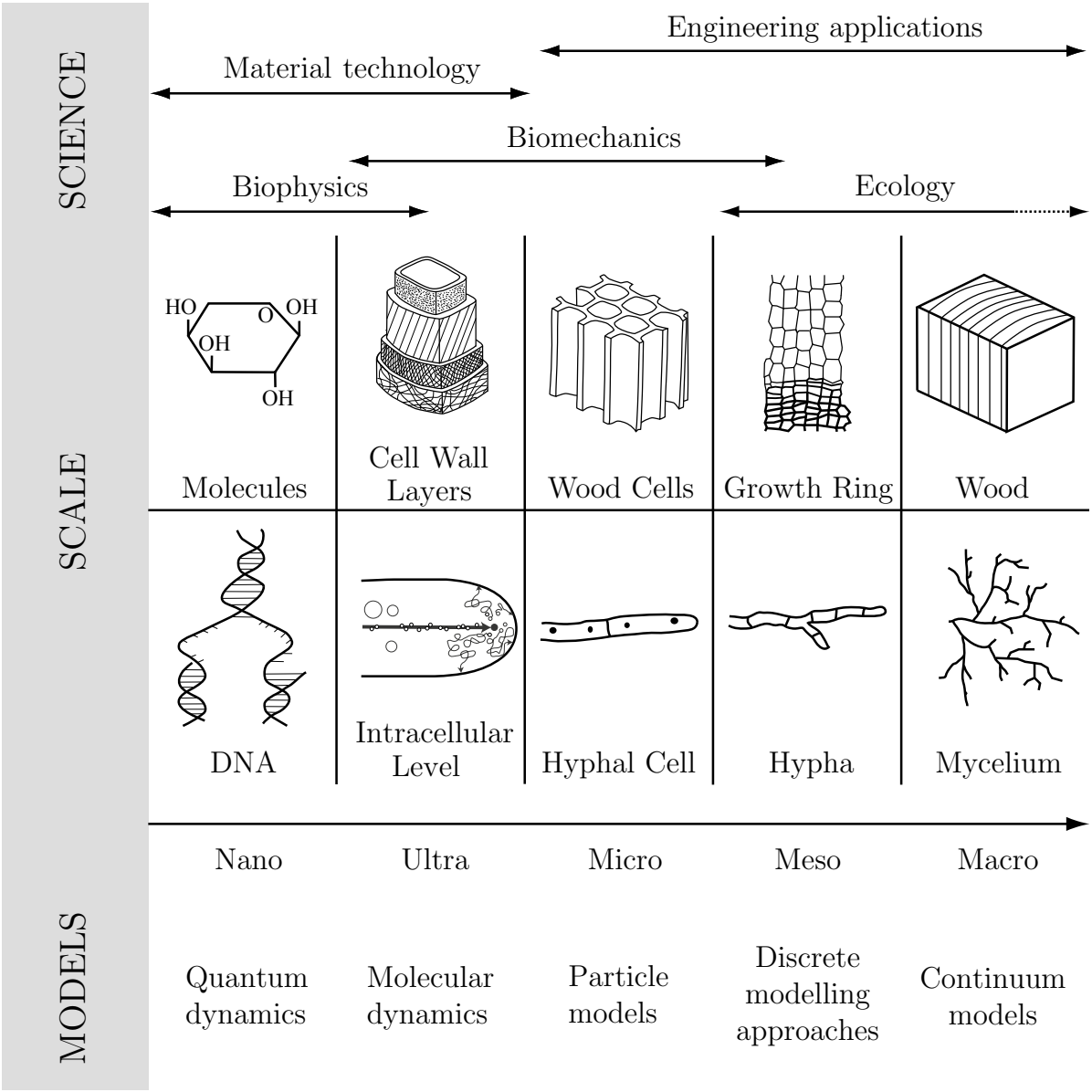

Figure 2.1: Hierarchical structure of wood and fungi, and the application in science and technology. Wood-decay fungi and their substrates have a complex cellular and hierarchical structure from the nanoscopic to the macroscopic scale, which involves a multitude of scientific fields at all levels of biological organization. Modelling wood-decay fungi is a challenge because the processes governing the growing mycelium are performed on different scales; for example, uptake of nutrients is on the microscopic scale whereas transport of nutrients takes place on the macroscopic scale.

density $\rho^*(x)$ along the growth ring (radial direction) is measured by counting all 'wood pixels' (i.e. pixels above a specific threshold) in the tangential direction of the image. Thus, the relative density, which is the density of a growth ring $\rho^*(x)$

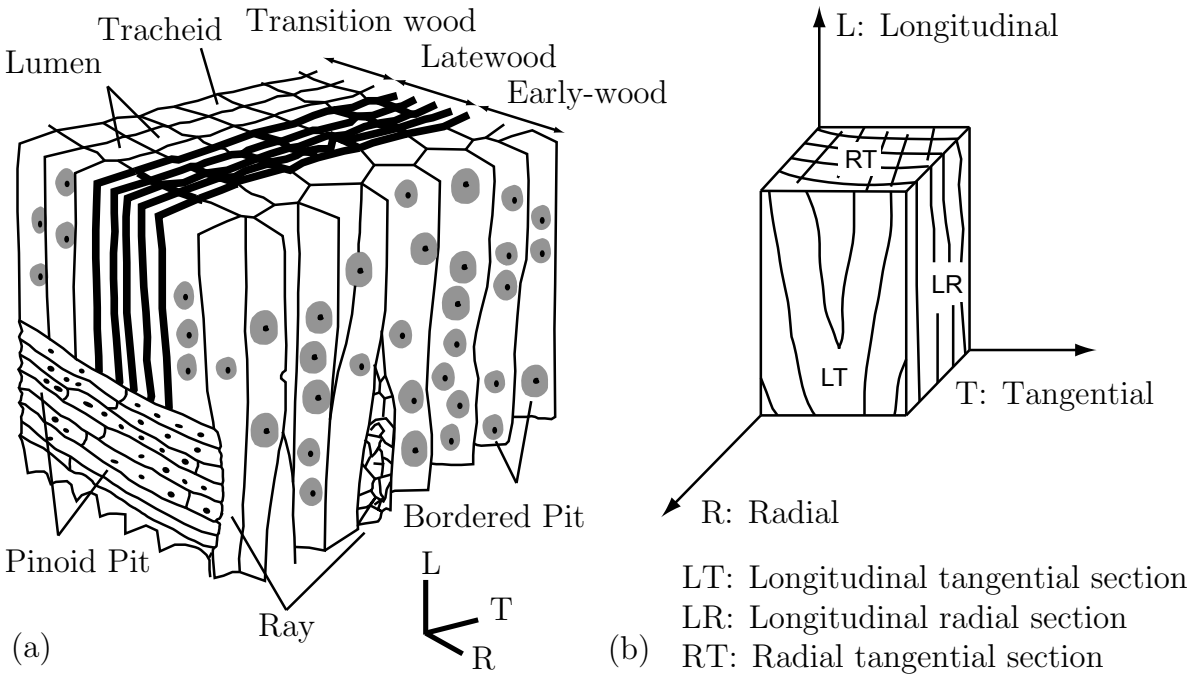

Figure 2.2: Cellular structure of Norway spruce wood. (a) Mainly tracheids and rays comprise the cellular structure of Norway spruce. Bordered and piceoid pits connect the cell lumens (i.e. the void within the cell). The cells vary significantly in their geometry and dimensions and form a growth ring consisting of a continuous transition from early-wood (high porosity) and transition wood to latewood (low porosity). As shown, at the boundary between adjacent growth rings there is a sharp transition from early- to latewood. (b) The three orientations of wood are denoted as longitudinal (L), radial (R) and tangential (T).

normalized by the density of the cell wall $\rho_c = 1500$ kg/m^3 [129], may be given by calculating $\rho^*(x)$ according to Wittel [202] as

$$\rho^* = \rho_{min}(1 + 2a_1 \cdot x^{b_1} \cdot e^{c_1 x}) \tag{2.1}$$

using $a_1 = 2.5$, $b_1 = 0.25$, $c_1 = -10$ and $\rho_{min} = 350$ kg/m^3 (Fig. 2.3), which is in good agreement with the mean value of approximately 420 kg/m^3 reported by Niemz [129]. In addition, the porosity of the wood is approximately 0.13 - 0.61 (Tab. 2.1).

Wood type	**Area total** A_{tot} [mm^2]	**Lumen area** A_L [mm^2]	**Porosity** A_L/A_{tot} [-]
Early-wood	2.23	1.35	0.61
Transition wood	0.45	0.17	0.38
Latewood	0.17	0.02	0.11

Table 2.1: Porosity of Norway spruce wood measured from the scanning electron microscopy image of Fig. 2.3.

Tracheids and rays

In softwood there are six types of cells with distinct functions as shown in Tab. 2.2.

Cell type	**Orientation**	**Form**	**Function**
Early-wood tracheids	Longitudinal	Elongated	Condution
Latewood tracheids	Longitudinal	Elongated	Stability
Ray tracheids	Radial	Elongated	Conduction
Ray parenchymal cells	Radial	Prismatic	Storing
Longitudinal parenchymal cells	Longitudinal	Prismatic	Storing
Epithelial cells (resin canals)	Longitudinal/radial	Circular	Secreting

Table 2.2: Softwood cell types and their orientation, form and function (after Wagenführ & Scholz [198]).

The early- and latewood tracheids are the main cells (90 - 95%) and the remainder are ray parenchymal cells in the radial and longitudinal directions, ray tracheids and resins canals [50, 139]. For simplicity, in this thesis early- and latewood tracheids are termed 'tracheids' and ray parenchymal cells in the radial direction (including tracheid rays) are 'rays'. Tracheids and rays are the main growth path of *P. vitreus* in the longitudinal and radial direction respectively.

Tracheids are tube-like objects with a complex polygonal shape and two tapered ends. Brändström [22] distinguishes two tips, two tip zones (or transition zones)

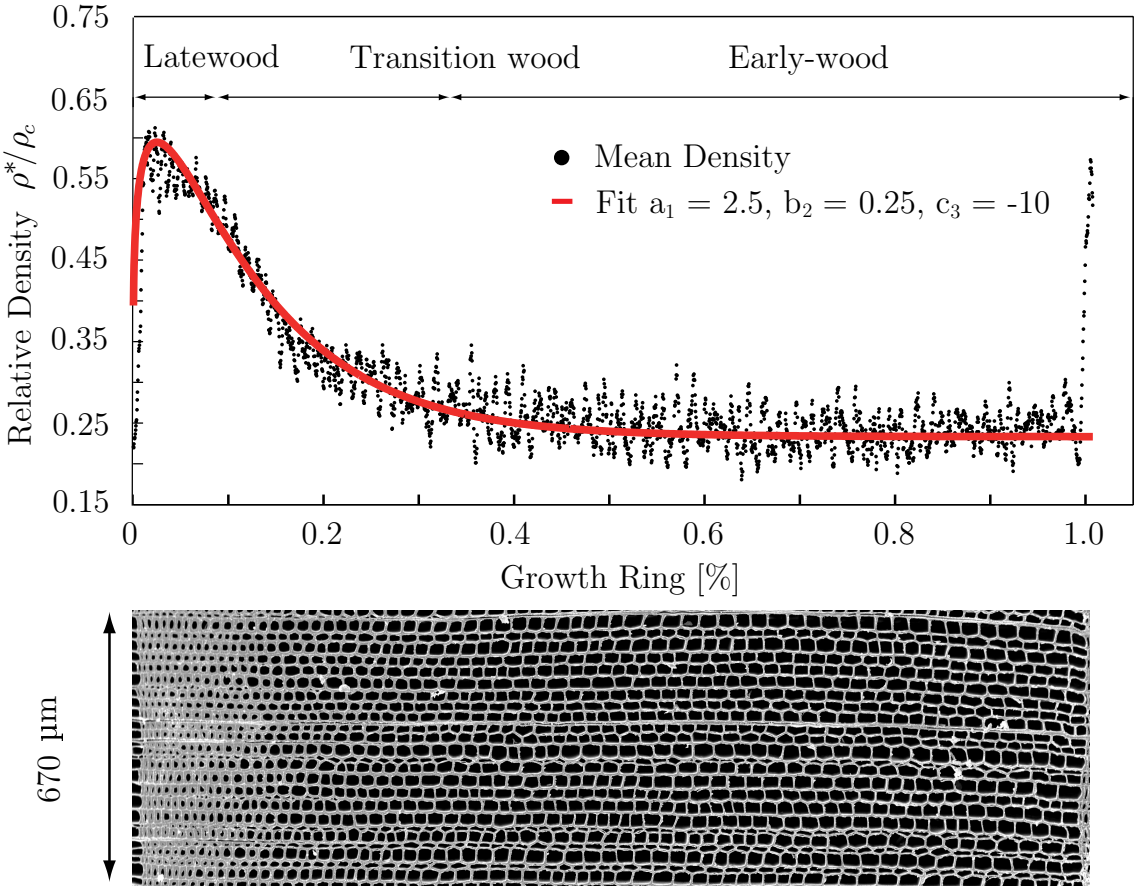

Figure 2.3: Radial tangential (RT) section of a Norway spruce growth ring and the corresponding density along the growth ring (radial direction).

and a middle zone, whereby one tip is approximately 50% longer than the other. The middle zone comprises approximately 70% of the tracheid's length. The average length of Norway spruce tracheids is approximately 2 - 5 mm [22] and their lengths increase from the pith to the bark [155, 116]. Fig. 2.4 shows Norway spruce early-wood, transition wood and latewood tracheids using high-resolution synchrotron X-ray computed tomographic (XCT) microscopy. Further details about the 3D XCT technique are presented in Sec. 2.3.1.

The cross-sections of early-wood and transition wood tracheids are roughly hexagonal, whereas latewood tracheids have a square-shaped middle zone (Figs 2.3 and 2.4). The fibre geometry [202], which is defined as the ratio between the radial (l_R) and tangential size (l_T) of a tracheid's middle zone, may be given by

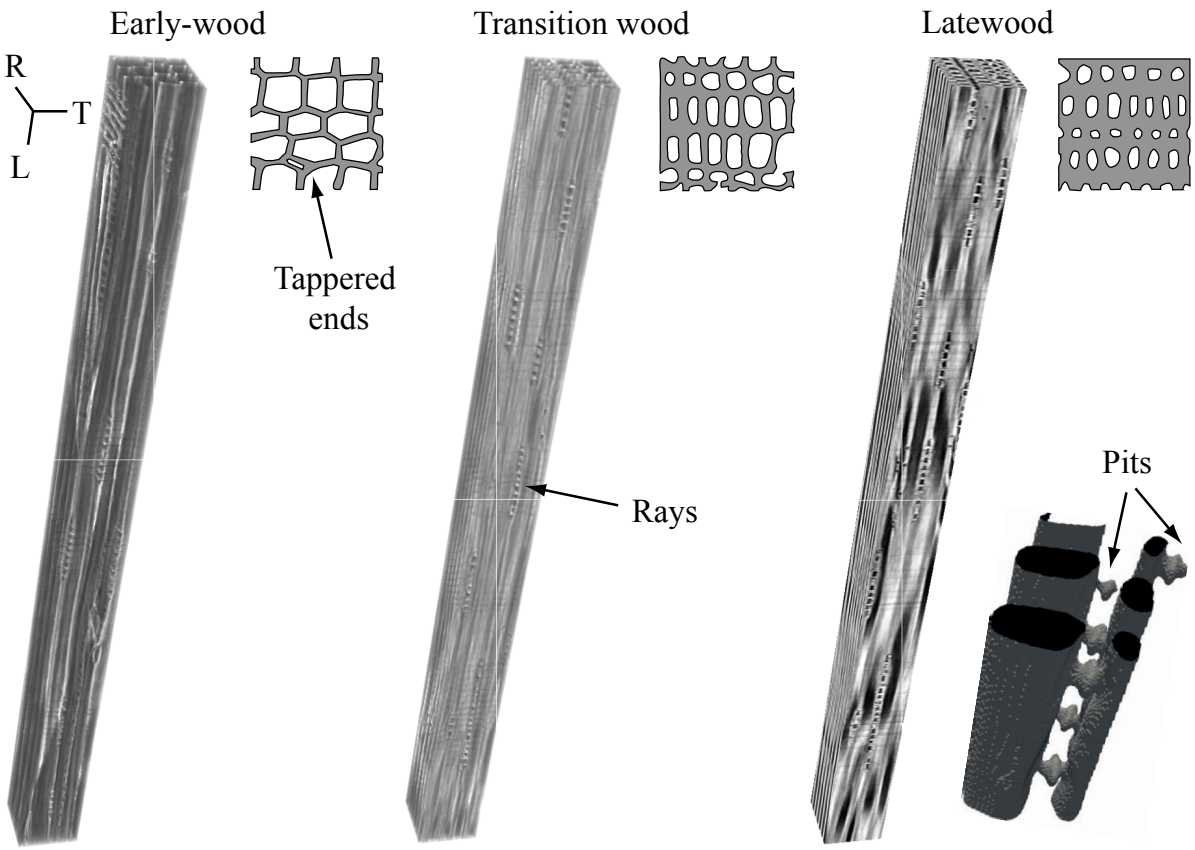

Figure 2.4: Synchrotron XCT images of Norway spruce tracheids. The 3D tomograms have a total size of 1.85 × 0.14 × 0.14 mm (R × T × L) and a resolution of approximately 1.85 µm^3 per volumetric pixel element (i.e. VOXEL). The inset has a resolution of approximately 0.37 µm^3/VOXEL and shows the pits in latewood.

$$\frac{l_R}{l_T} = a_2 \cdot (x + b_2)^{c_2} + d_2 \tag{2.2}$$

where $a_2 = 1.215$, $b_2 = 0.0025$, $c_2 = 0.2153$ and $d_2 = 0.135$ (Fig. 2.5), using the experimental data from the growth ring shown in Fig. 2.3. The thickness of the cell wall can be calculated from Eq. 2.1 as

$$\tau^*(x) = t_{min}(1 + 2 \cdot a_2 \cdot x^{b_3} \cdot e^{c_1 x}) \tag{2.3}$$

using $b_3 = 0.35$ and $t_{min} = 2.25$ µm.

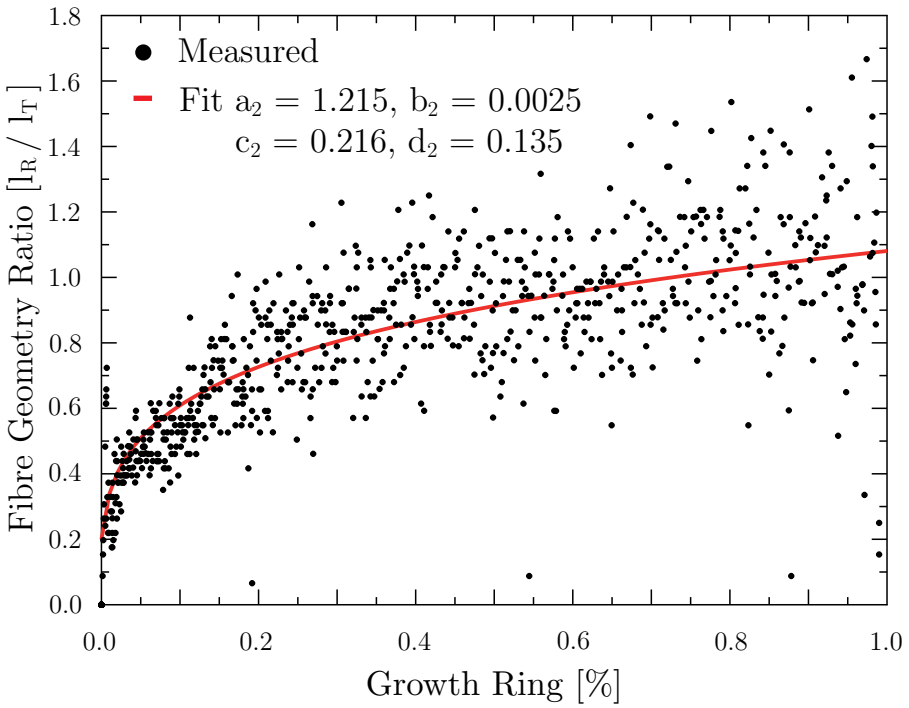

Figure 2.5: (a) Fibre geometry ratio (Eq. 2.2) for a Norway spruce growth ring measured from the scanning electron microscopy image in Fig. 2.3. The cell wall thickness is between 0.2 and 0.5 µm.

Lewis [106] described the 3D conifer tracheid as a stretched 14-sided polyhedron (i.e. 8 hexagonal faces and 6 square faces).

Rays are positioned radially in order to store and transport nutrients across the growth rings. Often, the rays consist of a single or double row of ray parenchymal cells enclosed top and bottom by ray tracheids. In addition, there are rays with and without horizontal resin canals. The rays are known as the main fungal pathway in the radial direction [147, 167], as is the case for *P. vitreus* in the early stage of Norway spruce wood colonization [99].

Pits

At the microscopic level, the lumens of wood cells are interconnected through pits (Fig. 2.6). There are three types of pits in Norway spruce: bordered, half-bordered (or piceoid) and simple (or pinoid) pits. The bordered pits connect adjacent tracheids and have a cap (i.e. torus), which is flat and disc-shaped in early-wood [10], consisting mainly of pectin and hemicelluloses. The torus is fixed by small

fibres, forming a permeable membrane (i.e. margo) made of cellulose [10], in order to control fluid flow in the tree. The spacing between the cellulose fibres of the margo is approximately 130 - 200 nm[109]. In Norway spruce sapwood the pits are open, whereas in the heartwood the torus attaches to the cell wall and hydrogen bonds irreversibly close the pit [190], a process called aspiration. Additionally, lignification of the margo and the torus occurs in the heartwood [108, 49]. The respective diameters of the porus, torus and pit chamber are approximately 4, 8 and 16 µm in early-wood [158], but the pits in latewood are much smaller. Most of the bordered pits are located on the radial walls of the early-wood tracheids [22]), whereas partial pitting exists on the tangential walls [175], that is, the boundary between the early- and latewood of two growth rings [95]. Bordered pits are more frequent in early-wood than in latewood [95, 94], with most of the pits found in the areas of overlap of early-wood tracheids. Sirviö & Kärenlampi [176] measured approximately 20 - 40 pits/mm in early-wood tracheids. However, the 3D distribution of bordered pits is not well known.

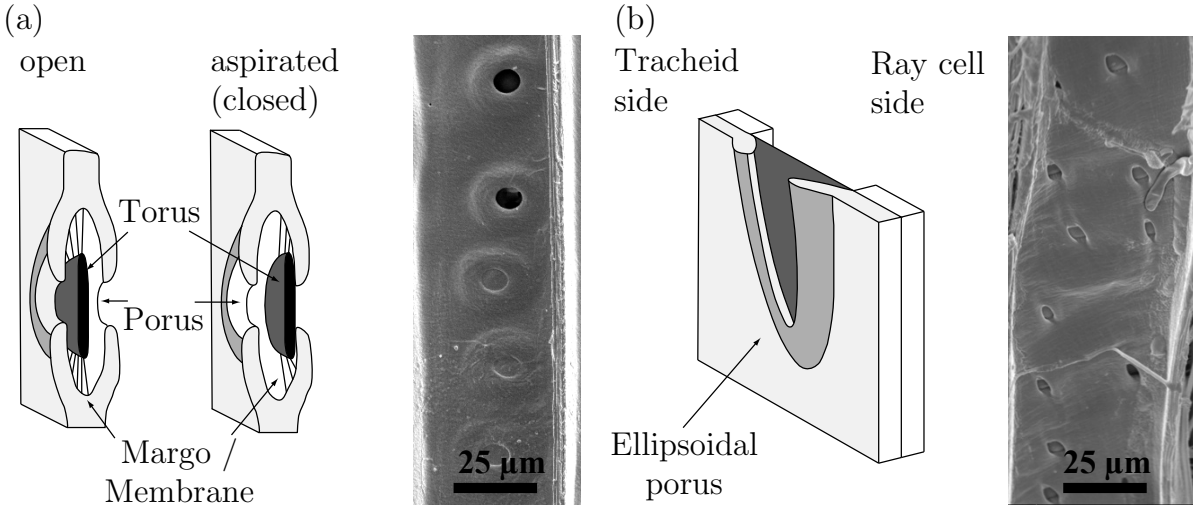

Figure 2.6: Bordered and half-bordered pits in Norway spruce. (a) The bordered pits in sapwood consist of a pit chamber (porus) and a cap (torus), which is fixed by small fibres forming a permeable membrane (margo). In the heartwood, the torus closes the pit by attaching its margo to the cell wall, a process called aspiration. Additionally, the torus is sealed with lignin (lignification). (b) Half-bordered pits (piceoid pits) connect rays and tracheids in their crossfields.

Half-bordered (piceoid) pits connect tracheids and rays and are much smaller

(∼ 5 µm). They are also lignified in Norway spruce heartwood. There are approximately four piceoid pits in a crossfield [158].

Simple pits are holes with a membrane formed by the middle lamella and they connect adjacent parenchymal cells such as rays [158]. Microscopic channels (i.e. plasmodesmata) enable the exchange of substances [49]. Simple pits were of minor importance in the studies presented here.

Cell wall

At the submicroscopic level the cell wall is composed of layers that consist of cellulose macromolecules encrusted by an envelope of hemicellulose and embedded in a matrix of lignin. The cellulose macromolecules mainly form long chains called microfibrils, which are further packed into macrofibrils (i.e. microfibril aggregates [44]). The micro- and macrofibrils (i.e. fibrils) are linked by hemicelluloses to the lignin matrix. Thereby, a complex laminate of fibrils, celluloses, hemicelluloses and lignin is formed as shown in Fig. 2.7.

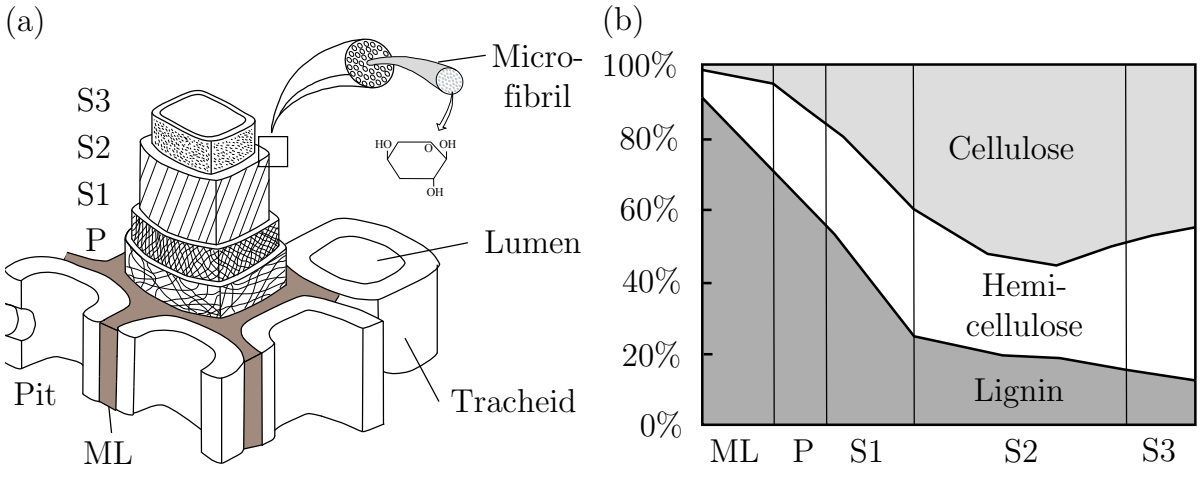

Figure 2.7: Ultrastructural aspects of the cell wall. (a) The cell wall has three layers: middle lamella (ML), primary wall (P) and secondary wall (S1, S2 and S3). (b) The quantity of cellulose, hemicelluloses and lignin varies within the cell wall (modified after Fengel & Wegener [50]).

The cell wall consists of three layers according to Kerr & Baily [90]: the middle

lamella (∼ 2 - 5 µm), the primary wall (∼ 0.1 µm) and the secondary wall (∼ 1 - 5 µm). The secondary wall is further subdivided into S1 (∼ 0.2 µm), S2 (∼ 1 - 5 µm) and S3 (∼ 0.1 µm) layers (thickness after [129]). The middle lamella is rich in pectin and cements adjacent cells together. The large amount of lignin (∼ 90%) gives the middle lamella a high compressive strength [129]. The primary cell wall is a thin layer and composed of irregularly oriented fibrils with a large amount of lignin. The middle lamella and the primary cell wall form the so-called 'compound middle lamella'. The secondary cell wall also has three layers [50]). The S1 layer is adjacent to the primary cell wall and consists of fibrils perpendicularly oriented to the wood cell axis [129], while the S2 layer consists of densely packed fibrils that spiral around the axis of the wood cell. The composition of the S3 layer is similar to that of the primary cell wall and is only found in parenchymal cells. The orientation of the fibrils to the cell axis is 60 - 80° (S1), 10 - 30° (S2) and 60 - 90° (S3) [198]).

2.1.2 Chemical composition

Principal chemical composition

Hyphal growth and the impact of a fungus are inextricably linked to the chemical composition of wood tissue and the extracellular digestion of organic matter. Knowledge of the specific decay pattern of a wood-decay fungus (i.e. the pattern of colonization and the mechanical properties of wood) and the chemical composition of wood tissue enables conclusions to be deduced from the enzymatic activity of the organism.

Wood consists mainly of organic molecules that are based on the chemical elements carbon (C, 50%), oxygen (O, 43%), hydrogen (H, 6%), nitrogen (N, < 1%) and other elements such as metals (< 1%). An overview of the principal chemical elements of wood is given in Tab. 2.3.

	Function	Constituent
Principal components	Structural components of the cell wall	Celluloses (40 - 55%) and Hemicelluloses (15 - 35%)
	Mainly responsible for the strengthening of wood	Lignin (hardwood 18 - 25%, softwood 28 - 41%)
	Intercellular cement for the cell wall layers	Pectin
Extractives	Extractives often affect the chemical, biological and physical properties of wood (e.g. the resistance to microorganisms)	Fats, fatty acids, resins and waxes. Starch and sugars. Phenols, terpenes and steroids. Inorganic and organic salts and acids. Minerals.

Table 2.3: Chemical composition of wood.

Cellulose

Hygroscopy is the ability of a material to bind water from its environment [183]. Cellulose is a polysaccharide consisting of an unbranched chain of many β-glucose molecules and it is the hydroxyl groups (-OH) of this molecule that are important for the chemical absorption of water. Blocking these hydroxyl groups (e.g. with wood-modification substances containing acetic acid) hampers the uptake of water and therefore reduces the hygroscopical behaviour of wood.

Cellulose gives wood its bending strength [129] and is the most abundant chemical compound found in plants. Norway spruce wood contains several modifications of crystalline cellulose, such that crystalline, semi-crystalline and amorphous regions alternate [129]. Crystalline cellulose is tightly packed and the absorption of chemical compounds is limited, whereas the amorphous regions bind water, fungal enzymes and other substances to a greater degree [129]. Microcrystalline cellulose has a Young's modulus of 25 GPa [46] and therefore a bending strength that is twice as high as Norway spruce wood (Tab. 2.4). Thus, the bending strength and other mechanical properties of wood are only partly explained by its components and are mainly governed by the architecture of the cell wall (Sec. 2.1.2).

Property	Symbol	Value	Unit
Growth ring width	w_g	2	mm
Early-wood tracheid length / height / width / length of tapered end	$l_L/l_R/l_T/l_O$	2/0.6/0.4/0.15	mm
Cell wall thickness	w_t	0.005-0.05	mm
Density cell wall	ρ_c	1500	kg/m^3
Density wood	ρ_w	450	kg/m^3
Young'smodulus (L)	E_L	11	GPa
Shear modulus (L)	G_L	780	MPa

Table 2.4: Selected properties of Norway spruce wood [158].

Hemicellulose

Hemicelluloses are non-cellulotic polysaccharides that are shorter and have more functional groups than celluloses [129]. These reactive groups enable hemicelluloses to take up more water than celluloses and therefore they are mainly responsible for the swelling and shrinking of wood [198].

The functions of hemicelluloses in wood are to support the cell wall (i.e. celluloses and lignin), control the cell membrane's permeability and an adhesive effect between several components in the cell wall [129]. The latter characteristic is important for the thermal modification of timber [198], which enhances the durability of Norway spruce wood against wood-decay fungi [177].

Lignin

Lignin is a 3D polymer and responsible for the compressive strength of the cell wall [129]. Its highly cross-linked structure consists of phenylpropanoids and it is hydrophobic compared with celluloses and hemicelluloses [198].

Gymnosperms (27%), i.e. 'softwood', contain more lignin than wood from angiosperm trees (21%), i.e. 'hardwood', as reported by Wagenführ & Scholz [198]. Lignins are sensitive to photochemical reactions. UV light can delignify unpro-

tected wood surfaces, which, in combination with weathering, causes the grey-silver colour of exposed timber. Wood-modification substances are able to prevent such a delignification and conserve the initial colour of wood.

Water

Wood is hygroscopic, which means it can give off or take up water from the environment either by absorption (i.e. incorporation of a substance into another substance) or adsorption (i.e. adhesion of a molecule to a surface). There are two forms of water in wood: free water in the cells lumina, which are the largest pores within wood (Sec. 2.1.2), and bound water within the cell wall. Bound water diffuses into the wood in a liquid or gaseous form, whereas the uptake of free water by capillary forces is only possible where there is direct contact of the wood tissue with liquid water. The moisture content (MC) of wood is usually defined as the mass of the wet wood as a percentage of its oven-dry mass [173]. For wood tissue without direct contact with liquid water, the MC is governed by the relative humidity (RH), which is the partial pressure of water vapour as a percentage of the saturated vapour pressure of the air-water mixture under specific environmental conditions (i.e. absolute humidity, temperature and pressure). The equilibrium moisture content (EMC) is the MC at which the wood neither gains nor loses water.

The EMC for Norway spruce wood under standard conditions (i.e. 20°C and 65% RH) is approximately 12% [129]; that is, water vapour is bound within the cell wall by absorption. Stamm [183] distinguishes five types of adsorption by wood, but the most important are chemical adsorption (EMC $\sim$ 0 - 6%), physical adsorption (EMC $\sim$ 6 - 15%) and capillary condensation (EMC $>$ 15%) as shown in Fig. 2.8. In addition, wood has a remarkable 'sorption hysteresis', which means that its MC is different for adsorption (wetting) and desorption (drying).

The chemical bonding of water on hydrophilic groups, such as hydroxyl, carboxyl or carbonyl, is termed 'chemical adsorption', whereas physical adsorption is the binding of water by van der Waals' forces. In addition, condensation of vapour in the small capillaries of the cell wall occurs because of the lower saturated vapour pressure in such voids [183]. The MC at 100% RH is called the fibre saturation

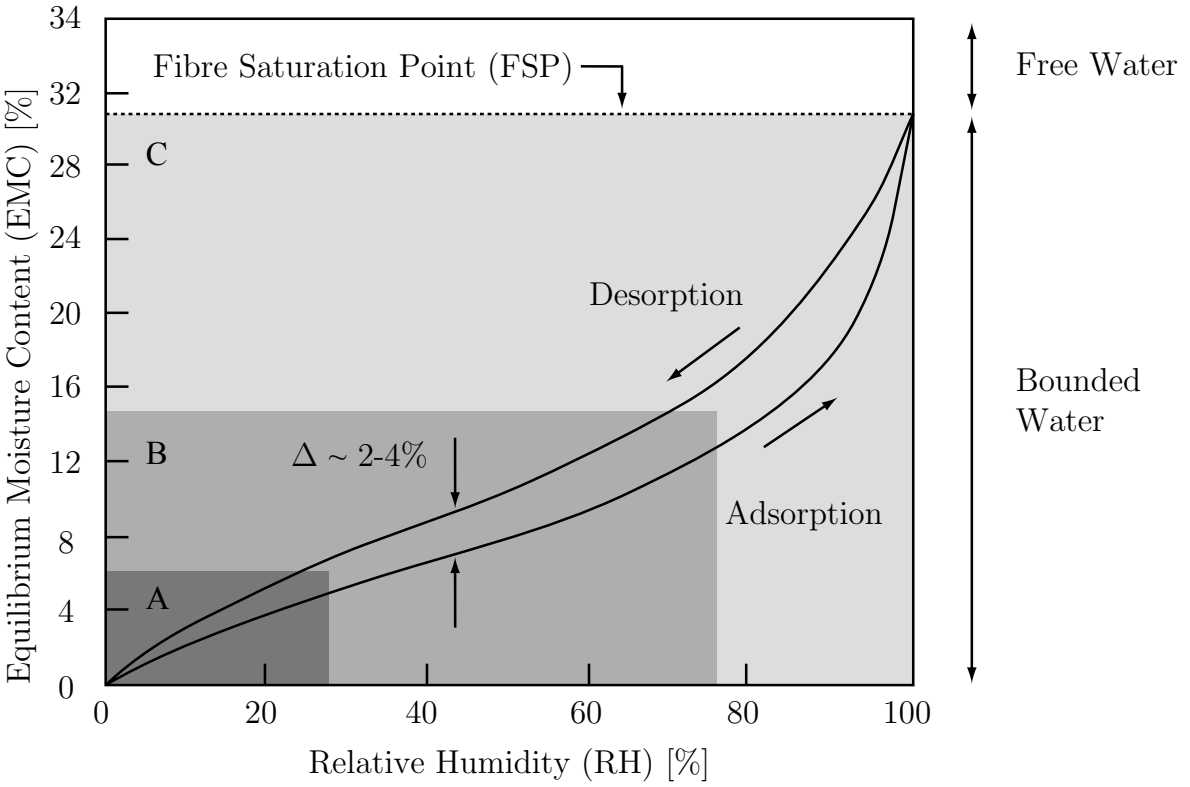

Figure 2.8: Equilibrium moisture content of White spruce (*Picea glauca* (Moench) Voss) wood as a function of the relative humidity at 25°C. Most important types of adsorption are chemical adsorption (A), physical adsorption (B) and capillary condensation (C). Modified after Stamm [183] and Wagenführ & Scholz [198].

point (FSP), which for Norway spruce is approximately 38% MC [158]. Below the FSP, the relation between the EMC of wood and the RH of the environment may be described by the Hailwood-Horrobin [75] or Brunauer-Emmett-Teller equation [183].

The sorption of water in the cell wall causes swelling and shrinking, whereas the uptake of free water above the FSP has a negligible effect on the dimensions of a wood specimen. Typical values for swelling in the principal directions of spruce (Sec. 2.1.2) are approximately 0.2 - 0.4% in the longitudinal, 4% in the radial and 6 - 8% in the tangential direction [93, 129, 158].

Extractives

Chemical compounds other than celluloses, hemicelluloses, lignin or water are extractives (e.g. lipids, waxes, alkaloids, proteins, sugars, resins, starches, oils and minerals [82]). Most extractives are soluble in neutral solutions [140]. They do not contribute to the mechanical properties of the wood, but affect its colour, odour and decay resistance. For example, pectins are a prominent group of amorphous polysaccharides and serve many wood-decay fungi as a carbon source [68].

2.1.3 Economic aspects

Approximately one-third of Switzerland is covered by forests, which fulfil a multitude of economic and ecological functions, such as wood production, protection against natural hazards (i.e. avalanches in the mountains or landslides), habitat for animals and recreational activities. Swiss forests consist of approximately 405M m^3 of wood, of which the most common species is the spruce with 179M m^3 (41%), followed by the beech with 73M m^3 (17%), as reported by the Swiss National Forest Inventory (LFI3). Other relevant species are fir, pine, larch, ash and sycamore. In total, 69% are softwoods and 31% are hardwoods.

The spruce is the economically most relevant species, especially as a building material, because of its excellent mechanical properties (i.e. high strength and low hygroscopicity), wide availability and relatively easy processing of the raw material. Switzerland has an annual production of approximately 2.5M m^3 of timber (softwood), 0.4M m^3 particle board and 0.4M m^3 fibre board [71]. Beech wood is a hardwood and has better mechanical properties than spruce, but is not commonly used as a construction material because of its high hygroscopicity and high variability of its mechanical properties. However, a number of Swiss research projects deal with the use of beech as a construction material in order to reduce Switzerland's dependence on spruce; for example, hardwood girders [185] or wood adhesive bonds [77, 120].

Most buildings in Switzerland are made of steel and concrete, and wood construction is uncommon, especially for multistorey buildings. However, there is a trend to using wood as a construction material since the complete revision of the

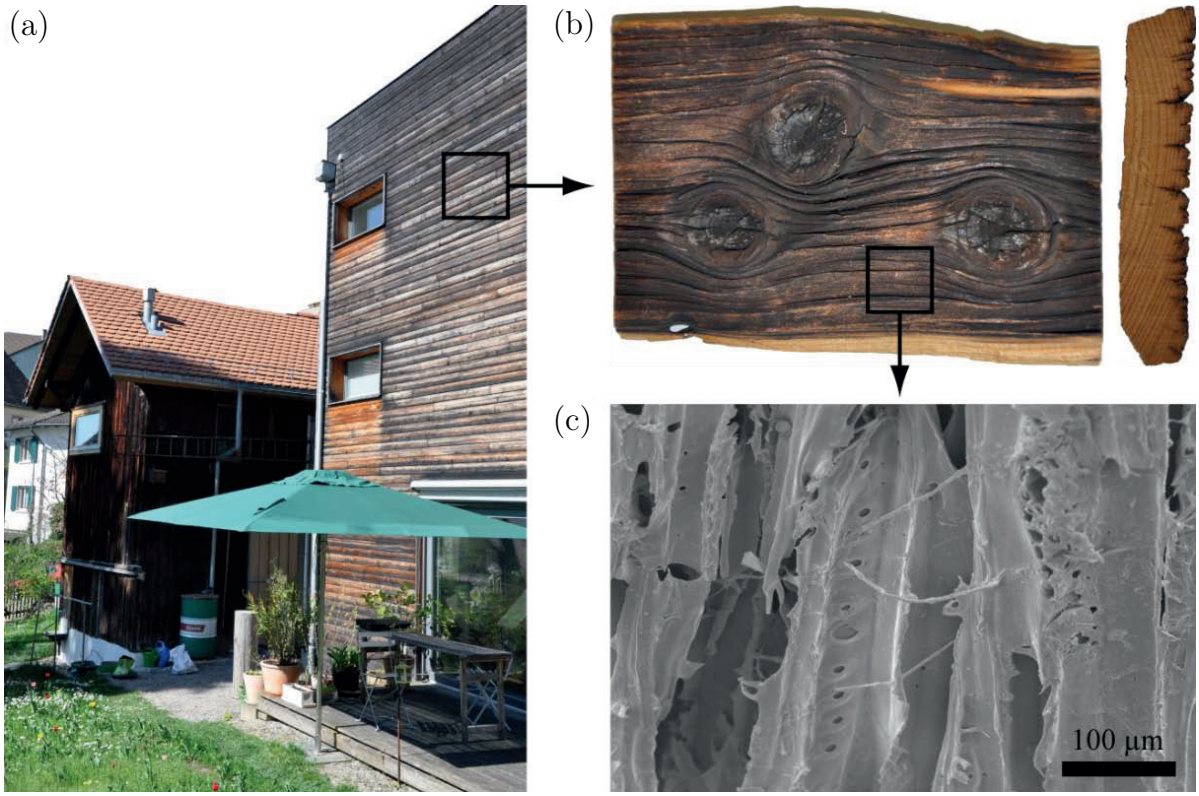

Figure 2.9: (a) Ancient wood constructions typically have a saddle roof, whereas modern wood buildings do not have such protection and are more exposed to (b) weathering and (c) wood-decay fungi (e.g. *Physisporinus vitreus*). Bioincising may improve the impregnation of refractory wood and support the construction of modern wood buildings in Switzerland. Picture of Norway spruce wood sample taken with kind permission of P. Niemz.

Swiss construction codes in 2003. Two factors may influence the use of timber in Switzerland. First, the new codes and subsequent documentation enable the construction of multistorey buildings [111]. However, such modern wood buildings are often constructed with a flat roof (Fig. 2.9), which exposes them to weathering and wood-decay fungi. Bioincising may improve the impregnation of refractory wood, such as Norway spruce, and thus support the construction of modern wood buildings in Switzerland. Second, the Swiss population may increase approximately 14% by 2050 [92] and hence the demand on living space will also increase. More living space may be provided by additional storeys on existing buildings. Such constructions should be very light, in order to reduce the load for the existing structure of the building. Therefore, light wood constructions are ideally suited for such concerns [8, 125].

2.2 *Physisporinus vitreus*

Wood-decay fungi degrade their substrate (wood), which is a complex anisotropic material featuring several hierarchical levels of organization (see Fig. 2.1) from the macroscopic (e.g. growth rings) over the mesoscopic (e.g. set of wood cells) down to the microscopic and nanoscopic scales (e.g. wood cells and fibrils), by extracellular, degradative enzymes. The fungi play an important role in natural ecosystems by recycling the carbon and minerals fixed in plants, but thereby they cause significant damage to the wood's structure and limit the use of wood as a building material. Wood-decay fungi are classified into three types according to their decay pattern (Tab. 2.5): brown rot, white rot (i.e. selective delignification and simultaneous rot), and soft rot (types 1 and 2).

2.2.1 Morphology

Physisporinus vitreus (Pers.: Fr.) P.Karst is a filamentous fungus and belongs to the Division Basidiomycota [36]. Filamentous fungi exploit their environment by tubular, elongated cells (i.e. hyphae) that form a complex tree-like network (i.e. mycelium) as shown in Fig. 2.10. The mycelium's morphology strongly depends on environmental factors such as pH, water activity and temperature [163], and the type, quantity and form of nutrients. Studying wood-decay fungi involves disciplines at all levels of biological organization (Fig. 2.1).

Mycelium

The mycelium is the vegetative part of a filamentous fungus and consists of a dense network of hyphae. Growth starts typically from a single spore and over time a hyphal network can cover huge areas up to the kilometre scale. The mycelium of an *Armillaria bulbosa* species in Oregon, USA, has an estimated size of 15 hectares and is considered to be the largest organism on earth [178].

Filamentous fungi are often considered as modular organisms (Tab. 2.6), because a mycelium has a repetitive structure. Branching and anastomosis (i.e. fusion of hyphae) of the mycelium typically results in a complex network [87, 17, 14].

	Brown rot	**White rot**		**Soft rot**
		Simultaneous rot	*Selective delignification*	
Host	Especially in coniferous trees	Broad-leaved trees, but seldom in conifers	Broad-leaved trees and conifers	Extensive decay in living broad-leaved trees
Fungi	Basidiomycetes, especially from the family of the Polyporaceae	Basidiomycetes and Ascomycetes	Basidiomycetes and Ascomycetes	Ascomycetes
Degradation	Cellulose and hemicellulose degradation	Cellulose, lignin and hemicelluloses	First lignin and hemicelluloses, later cellulose	Cellulose and hemicelluloses; Lignin slightly
Consistency	Fragile, powdery, brown; cracks and clefts	Brittle	Fibrous (stringy)	Brittle
Strength	Drastic reduction of bending and impact strength	Brittle	Less drastic than in brown rot	Between brown and white rot

Table 2.5: Wood-decay fungi are classified into three types according to their decay pattern (Schwarze et al. [167]). *Physisporinus vitreus* may be considered as causing white rot [157, 168, 169, 99]. An overview of wood-decay fungi is presented by Rayner & Boddy [147], Schmidt [159] and Schwarze & Engels [167]. In the present work we studied the growth of the white-rot fungus, *P. vitreus*, in the heartwood of Norway spruce.

A hyphal network is not a static object, rather a dynamic and highly adaptive system [146] that responds very sensitively to its environment as shown in Fig. 2.10(a).

Hypha

A hypha of *P. vitreus* consists of one or more connected cells that are separated from each other by internal cross-walls called septa. This septation is a characteristic of the 'higher fungi' Division (i.e. Ascomycota, Basidiomycota). Wood-decay fungi build several types of hypha [159], with variable diameters of 0.1 - 0.4 µm

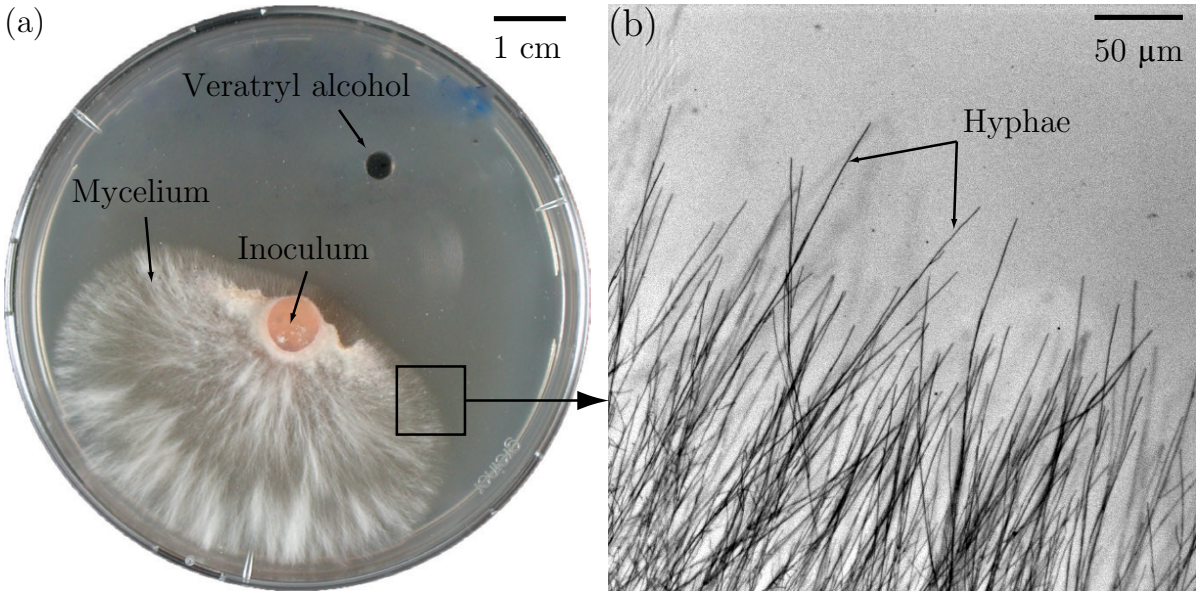

Figure 2.10: (a) The filamentous basidiomycete, *Physisporinus vitreus*, explores its environment by tubular cells (i.e. hyphae), forming a complex tree-like structure (i.e. mycelium). (a) The mycelium's morphology strongly depends on environmental factors, such as the type of nutrients, as shown by the response of *P. vitreus* to the presence of an inoculum of 96% Veratryl alcohol. (b) Hyphae have a diameter of approximately 1 - 2 µm. Images with kind permission of C. Stührk.

(microhyphae of *Phyellinus pini*), 1 - 5 µm (vegetative hypha of *P. vitreus*) and 60 µm ('vessel' hyphae of *Serpula lacrymans*).

The growth of a hypha is localized to its tip, a process called polarization [189]. The hyphal morphogenesis of higher fungi seems to be inextricably linked with the existence of a sub-apical phase-dark structure [62] called the Spitzenkörper [24], which is only found in ascomycetes and basidiomycetes [63]. The Spitzenkörper plays a crucial role in the growth and orientation of hyphal tips. Harris et al. [76] describe the Spitzenkörper as a 'complex, multicomponent structure dominated by vesicles'. Vesicles are bubble-like objects that can store and transport substance (e.g. elements for the formation of the cell wall). Mathematical models [7, 6, 60, 191] show that the characteristic hyphoidal form of the tip can be explained by the concentration of vesicles in the apical region [153, 150, 174].

	Unitary organism *(e.g. M. J. Fuhr)*	**Modular organism** *(e.g. Physisporinus vitreus)*
Growth	Growth is accompanied by change in form	Growth is an iteration of modular units
Development	Growth is determinate and ends when development is complete	Growth is open and continues as long as the conditions are favourable
Response	Responds to environment as an integrated whole	Localized response to environment

Table 2.6: Growth, development and response of unitary and modular organisms (modified after Carlile & Gow [26]).

Fungal cell wall

Fungal cell walls consist of several layers and contain chitin, whereas the cell walls of plants contain cellulose [199]. The presence of chitin enables fungal cells and plant cell tissue to be distinguished (e.g. using fluorescence labelling techniques as shown in Fig. 2.11).

2.2.2 Physiology

The growth and degradation pattern of *P. vitreus* depends on various physical, chemical and biological factors such as nutrients, water, air, temperature, pH, light, gravity force and interaction with other organisms [159]. Water activity (a_w), temperature and pH are the key factors in the growth behaviour and development of the fungal mycelium [147]. These factors are discussed below.

Water activity, temperature and pH

Water activity is defined as the ratio of the vapour pressure of a liquid and the vapour pressure of pure water at the same temperature (i.e. pure distilled water has a_w of 1). Schubert et al. [163] found that the growth of *P. vitreus* mainly depends on a_w (0.950 - 0.998) and temperature (10 - 30°C), whereas pH (4 - 6)

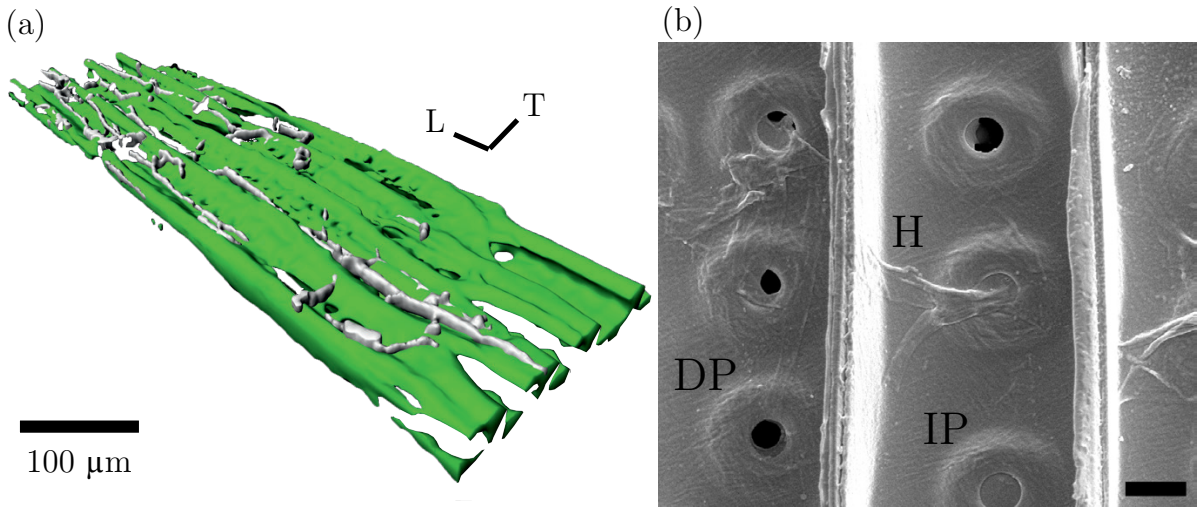

Figure 2.11: (a) Confocal laser scanning microscopy image showing a radial longitudinal section of Norway spruce heartwood colonized by the hyphae (white) of *Physisporinus vitreus* (image modified after Stührk et al. [187]). (b) Scanning electron microscopy images of a longitudinal-tangential section of Norway spruce heartwood infested by hyphae (H) of *P. vitreus*. The image shows intact and aspirated bordered pits (IP) and degraded bordered pits (DP). Scale bar 10 µm.

affected the growth rate to a lesser extent. The acid environment of pH 4 - 6 is known as an optimum range for Basidiomycetes [159]. The optimal growth conditions of *P. vitreus* were at T = 20°C, pH = 5 and $a_w = 0.998$. No growth was observed at $a_w < 0.955$.

Oxygen supply

Schmidt et al. [157] observed that *P. vitreus* colonizes water-saturated specimens with a low oxygen content. This colonization pattern is remarkable because a lack of oxygen normally hampers fungal growth within wood [13, 137].

Nutrient supply

The ratio between carbon and nitrogen (i.e. the C/N ratio) influences the growth pattern of wood-decay fungi ([97] and references therein). Eastern white pine has a nitrogen content between 0.1% and 0.2% of dry weight [147] and Norway spruce wood has a C/N ratio of approximately 250 (Sec. 2.1.2). The original discovery

of *P. vitreus* was in the water-saturated timber of a cooling tower [157], which obviously has high humidity and a low oxygen supply. Such conditions, in combination with a low concentration of nitrogen (e.g. C/N > 200) in the medium, may support the selective degradation of lignin as hypothesized by Dill & Kraepelin [43], whereas a narrow C/N ratio facilitates the degradation of polysaccharides [97]. Thus, the incubation of wood specimens on agar with a wide C/N ratio is prefered in order to support a selective pit membrane degradation [99, 166].

Enzymatic activity

P. vitreus shows a heterogeneous decay pattern (Sec. 2.2.3) and determining the enzymatic processes behind this exceptional behaviour is still in progress, as reported in a review by Schwarze & Schubert [171]. They found that *P. vitreus* excretes small amounts of polygalacturonase and the lignolytic enzymes, mangan peroxidase and lignin peroxidase, were not detected. In addition, *P. vitreus* produces and secretes large amounts of laccase with only one isoform [85] and a mass of approximately 53 kDa, which is in the range of a bacterial laccase. Furthermore, Ihssen et al. [85] found that this laccase has reduced reactivity in comparison with commercially available forms. This observation is in agreement with the small loss of wood mass during the first stage of the colonization process, as reported by Schwarze et al. [169], and the selective delignification of the secondary wood cell wall without affecting the middle lamellae, even at advanced stages of degradation [171].

2.2.3 Growth and decay pattern

Petri dish

The growth kinetics of fungal colonies is often observed in Petri dishes, which in the standard size have a radius of 90 mm and are made of an optical transparent material such a glass or polymethyl methacrylate. Common types of media are malt extract agar (MEA) and low-nutrient agar (LNA). LNA has a composition which is more representative of the nutritional status in wood [182], i.e. C/N ratio.

The growth kinetics of filamentous fungi (e.g. *P. vitreus*) on a solid media can be divided into four characteristic stages of radial expansion [97]. The first stage is the lag phase, in which the spores start germinating or the hyphae of an inoculum begin to growth. After the lag phase, the hyphae are able to divide and grow without any restriction by neighbouring hyphae or a lack of nutrients. This exponential phase is followed by a linear increase in colony radius. In this stage, the expansion of the fungal colony is restricted to the tips in the peripheral growth zone, whereas the hyphae in the centre of the colony start differentiating, forming anastomoses [148, 79] or cords ([51] and reference therein). The linear phase continues until the margin of the Petri dish is reached and the environmental conditions are favourable.

Norway spruce wood

Norway spruce wood is a chemically and physically complex material consisting of cellulose, hemicellulose, lignin and extractives (Sec. 2.1.2). These macromolecules and the microfibrils (Sec. 2.1.1) are the main nutrient sources of wood-decay fungi, besides water, oxygen and carbohydrates in the rays. Over time, fungi have evolved different strategies to exploit these nutrients in complex substrates such as wood (Tab. 2.5).

Generally, in its primary stage of growth, *P. vitreus*, which is a filamentous basidiomycete, selectively degrades the lignin and pectin of wood. In the secondary stage it degrades cellulose. Schwarze & Landmesser [168] have reported that *P. vitreus* also degrades pit membranes in the heartwood of Norway spruce and that this degradation of pit membranes is pronounced in the primary stage of growth. The pits are elements of the cell walls and play an important role in the resource capture of fungi [69]. Therefore, in the initial stage of its growth *P. vitreus* significantly increases the water uptake by wood without significantly reducing the breaking strength of the wood, but it alters the breaking strength during the secondary stage of its growth. Thus, *P. vitreus* can be used for biotechnological applications, as shown by Schwarze & Schubert [170] and Lehringer et al. [98, 101].

The growth and impact of *P. vitreus* have been the subject of many previous studies, although most have dealt with the decay pattern of the fungus [168, 99]

or have tried to quantify the effect of the fungus on macroscopic wood properties such as density [168], Young's modulus and sound velocity [172, 181], microtensile strength [102], surface hardness [100] and permeability [159, 170]. Lehringer et al. [99] used light microscopy (LM) to quantify the patterns of decay of bordered pits, half-bordered pits and cell walls and classified these elements according to fungal activity as 'intact', 'degraded' or 'strongly degraded'. However, physical quantification of the microscopic decay patterns of the fungus is difficult because of the opacity of wood and the heterogeneity of its structure, so synchrotron XCT (Ch. 3) or mathematical modelling (Ch. 4) can potentially be powerful and efficient methods of investigation. Besides their role as biodeteriorators, wood-decay fungi can be used for biotechnological applications.

2.2.4 Biotechnological applications

Recent investigations have shown that wood-decay fungi have many valuable biotechnological purposes in the pure and applied wood sciences [172, 114, 122]. Alterations in the cell wall structure and/or distribution of the cell wall constituents are reflected in the plasticity of the wood degradation modes of different fungi [172, 40]. The specificity of their enzymes and the mild conditions under which degradation proceeds potentially make them suitable agents for wood-modification processes such as biopulping, bioremediation or bioincising [115, 122, 170]. The biotechnological process of bioincising is a promising approach to improving the uptake of preservatives and wood-modification substances by refractory wood via the degradation of bordered pits by *P. vitreus*. [168, 169]. Furthermore, because of its exceptional pattern of degradation, *P. vitreus* is successfully used to improve the acoustic properties of the tone wood of Norway spruce wood used for musical instruments by its selective delignification of the secondary cell walls without affecting the middle lamellae, even at advanced stages of decay [172, 181, 180, 1, 200]. However, successful upscaling of the biotechnological processes in which *P. vitreus* is used to improve substrate properties requires a set of investigations for the identification and detection of important growth parameters [165, 163, 160] and elucidation of the wood-fungus interactions [99]. Hence, visualizing and quantifying the microscopic decay patterns are of interest for the study of wood-decay fungi in general, as well as for wood-decay fungi and microorganisms with possible applications for biotechnol-

ogy. However, quantification of microscopic cell wall alterations (e.g. their size and distribution in space and time) is difficult because of the opacity of wood and the heterogeneity of its structure. Novel experimental techniques using confocal laser scanning microscopy (CLSM) or high-resolution synchrotron XCT microscopy enables measurement of the hyphal network or the impact of fungi on wood at the micrometre scale [186].

2.2.5 Network measures

Growing filamentous fungi form a complex hyphal network [87] and it is convenient to abstract such a network into nodes and edges as shown in Fig. 2.12. Such discretization enables the definition of network measures, which are useful both for analyzing laboratory experiments (i.e. CLSM images of the mycelium [187, 186]) and mathematical modelling (i.e. FGM [55]). Fricker et al. [51] present a summary of common network measures.

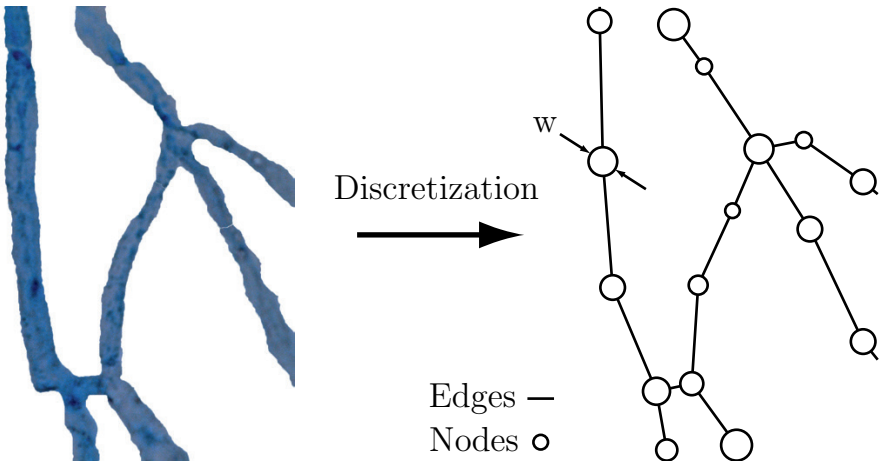

Figure 2.12: Discretization into nodes and edges enables the definition of network measures, which are useful both for analyzing laboratory experiments and for mathematical modelling.

Nodes, edges and tips

Let us consider a hyphal network consisting of N_n nodes connected by N_e edges. The adjacency matrix of the network has the order $(N_n \times N_n)$ and is defined as

$$\begin{aligned} a_{ij} &\in 0, 1, \\ a_{ii} &= 0, \\ a_{ij} &= a_{ji}, \end{aligned} \tag{2.4}$$

where each entry of a_{ij} represents a connection between two nodes, (i) and (j), receiving the values of 1 and 0 for connected and unconnected nodes, respectively. Thus, the degree q_i and the total length l_i of mycelium associated with a node (i) are given by

$$q_i = \sum_{j=1}^{N_n} a_{ij}, \tag{2.5}$$

$$l_i = 0.5 \sum_{j=1}^{N_n} a_{ij} \cdot \|r_i - r_j\|, \tag{2.6}$$

where r is the position vector of a node and $\|\cdot\|$ denotes the Euclidian norm.

Hyphal length and biomass

The total hyphal length L and the biomass M are given by

$$L = \sum_{i=1}^{N_n} l_i, \tag{2.7}$$

$$M = \rho_h \sum_{i=1}^{N_n} w_i \cdot l_i, \tag{2.8}$$

where $\rho_h \sim 1000$ kg/m^3 is the density of the hyphae and w_i their diameter as shown in Fig. 2.12.

Hyphal growth unit

The hyphal growth unit (HGU) is the average length of a hypha associated with each tip of the mycelium. First postulated by Plomley [144], the HGU is defined as

$$HGU = \frac{\sum_{i=1}^{N_n} l_i}{N_t}, \tag{2.9}$$

where N_t is the number of tips in the mycelium , l_i is the total length of mycelium associated with node (i). The HGU depends on the environmental conditions and is constant during unrestricted growth of the mycelium [192].

Growth front and radial growth rate

The radial expansion of a fungal colony is often used as a measure of the metabolic activity of the fungus. The radius R of a fungal colony is defined as the radius, which contains 95% of the mycelium's biomass, starting as a circular inoculum. Thus,

$$R_{95} = min\left\{ r : \frac{\sum_{(i)\forall(d_i^2<r^2)}^{N_n} l_i}{\sum_{i=1}^{N_k} l_i} \geq 0.95 \right\}, \tag{2.10}$$

where N_n is the number of nodes of the mycelium and d_i is the distance of node (i) from the centre of gravity of the inoculum. The radial growth rate G_r is given by $G_r = dR_{95}/dt$.

2.3 Tools for analyzing wood-decay fungi

2.3.1 Laboratory experiments

Wood is an opaque material, so to analyze its 3D structure, samples are usually sliced into thin sections and analyzed by LM, SEM and CLSM [59, 187, 186] or, for non-destructive analysis, X-ray tomography [57, 196, 195]. Stührk et al. [187, 186] present a review of these methods for analyzing the hyphal growth of *P. vitreus*.

Light microscopy (LM) and scanning electron microscopy (SEM)

Classical destructive methods of analyzing wood-decay fungi include LM and SEM. The advantage of LM is the elucidation and interpretation of wood-decay patterns with the help of specific staining techniques [156], whereas SEM provides brilliant high-resolution images down to the nanometre scale (Fig. 2.11). However, classical microscopy techniques only provide two-dimensional (2D) information and vigorous efforts are required to quantify alterations in the cell wall structure [99]. However, the growth of fungi in wood is a complex 3D process because of the diverse alignment of wood cells and the distribution of nutrients. In order to successfully model the growth and impact of wood-decay fungi, more quantitative information on the distribution of fungal activity at the microscopic level in space and time is required [55]. CLSM and XCT microscopy, for example, provide 3D information.

Confocal laser scanning microscopy (CLSM)

CLSM is a technique for acquiring 2D and 3D optical images using a laser beam. The advantage of CLSM is that the focus of the beam is on a selected plane and therefore enables point-by-point scanning of an object in sections. In addition, staining the object with specific fluorescent dyes enables identification and separation of constituents during image acquisition (e.g. wood and fungus as shown in Fig. 2.13). CLSM in combination with fluorescence labelling has been widely used for analyzing wood [91, 175] and wood-decay fungi [203, 204, 42]. Fricker

et al. [52] and Patel et al. [136] present a review of quantitative fluorescence microscopy.

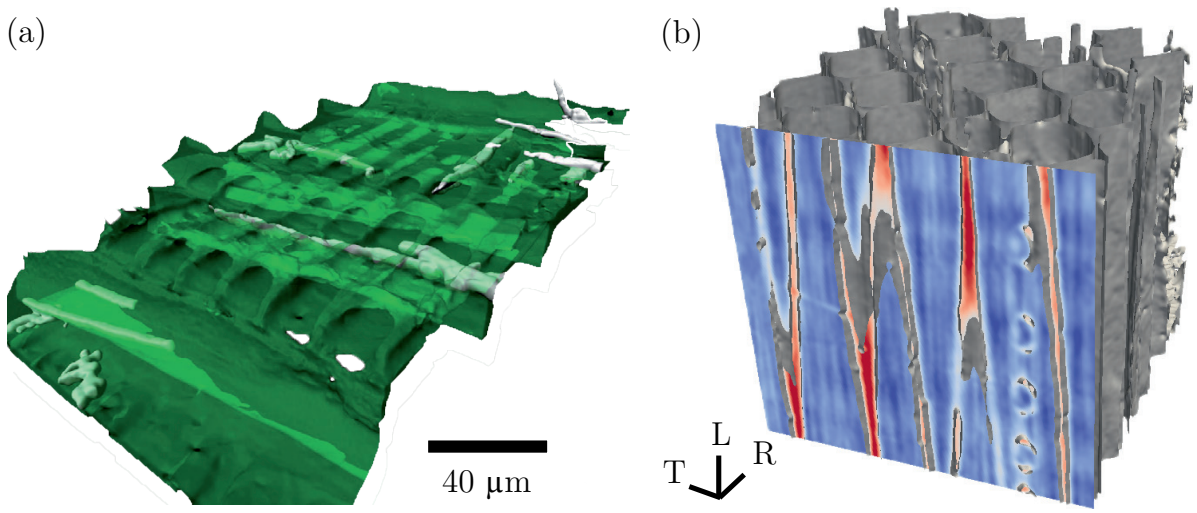

Figure 2.13: (a) CLSM image of a transverse section of Norway spruce heartwood colonized by the hyphae (white) of *Physisporinus vitreus*. Hyphae are stained with the fluorescence dye, Alexa Fluor 633 + WGA (i.e. Alexa Fluor conjugated with wheat germ agglutinin), which binds to chitin. Wood shows autofluorescence at approximately 350 nm and is transparent for CLSM up to a range of 200 µm. Wood and hyphae are visualized and rendered via isosurfaces [57, 187]. (b) Synchrotron XCT microscopy of the impact of *P. vitreus* on Norway spruce heartwood after 20 days (e.g. degraded cell walls and pits).

Synchrotron X-ray computed tomography microscopy

At the microscopic scale, non-destructive techniques based on XCT microscopy have been mostly used in wood research for 3D investigation of mycelial expansion and the impact of wood-decay fungi. In XCT, the beam attenuation is acquired either by absorption or by scattering according to the atomic number of the constituents at each VOXEL. The 2D projections are subsequently reconstructed into a 3D attenuation map. McGovern et al. [119] measured the mass loss of wood specimens using XCT with a VOXEL size of approximately 0.34 mm^3. Illman & Dowd [86] and Van den Bulcke et al. [196] used high-resolution XCT microscopy to analyze the density and structure of incubated wood. Van den

Bulcke et al. [197] identified a single hypha of *Aureobasidium pullulans* with a diameter of approximately 10 µm in wood using high-resolution XCT microscopy. However, automated separation of fungus and wood was not accomplished. It seems that CLSM is the appropriate technique for analyzing the 3D structure of the mycelium in wood, because of its capacity to separate fluorescence-stained fungi from the wood substrate during measurement [187, 186, 42]. However, the penetration depth of laser light into wood is limited and cell wall damage is not clearly visible, because of the weak autofluorescence of wood. Therefore, the use of high-resolution XCT microscopy for analyzing the impact of wood-decay fungi is suggested.

2.3.2 Mathematical models

Mathematical models describe a system (e.g. fungus-wood) by a set of variables using mathematical language. An analytical solution of complex systems is often very expensive or even not possible and only computers enable an efficient investigation (i.e. computer simulation). The objective of a mathematical model is not to mimic reality with an extremely complex system of equations, but rather the reduction of a complex (biological) system into a simpler (mathematical) system in order to identify, isolate and investigate the key properties. Mathematical models are often classified according to the type of equations and variables, the time dependency or the discretization (e.g. linear or non-linear, deterministic or probabilistic, static or dynamic and discrete or continuous). Because several authors provide excellent reviews of the mathematical modelling of fungi [25, 12, 48, 145, 128, 38, 51, 19], the following paragraph focuses on the challenges of modelling a wood-decay fungus such as *P. vitreus*. A selection of mathematical models dealing with the growth of fungi is given in Tab. 2.7.

Computational modelling in combination with laboratory experiments can give a deeper insight into the complex interactions between organisms and their environment. For example, growth has been extensively investigated in the context of cancer growth, dendritic growth, gelation and penetration in porous media [30, 83, 78, 2]. The hyphal growth and expansion of *P. vitreus* can be modelled by stochastic processes in both time and space. Wood-decay fungi and their substrates have complex cellular structures from the nanoscopic to the macroscopic

Scale	**Continuous**	**Cellular automata**	**Vector**	**Abstract Networks**
Micro	[7, 149, 191, 65]	[48]		[3]
Meso	[45, 39, 20]	[113, 21, 18]	[31, 84, 103, 121, 28]	[107, 179, 194]
Macro	[4, 96, 135]			

Table 2.7: Classification of selected models of fungi according to Davison [38].

level (Fig 2.1). Growth of filamentous fungi, especially in such 'multiscale' materials as soils or wood, is a challenge to quantify and different modelling techniques have been used [145, 38]. Modelling of filamentous fungi on the colony scale is difficult because the processes governing the growth of the mycelium occur on different scales; for example, uptake of nutrients occurs on the microscopic scale, whereas the transport of nutrients takes place on the meso- or even macroscopic scale. In addition to the chemical alteration of their substrate, growing fungi change the spatial (i.e. physical) structure of their substrate according to the type of fungi (e.g. wood-decay fungi often degrade specific parts of the wood such as bordered pits) and the wood species and thereby often increase the permeability of the wood. The creation of new pathways is an inherent part of their strategy to capture the resource.

3 3D Visualization and quantification of microscopic cell wall elements of Norway spruce wood by tomographic microscopy

The visualization and the quantification of microscopic decay patterns are important for the study of the impact of wood-decay fungi in general, as well as for wood-decay fungi and microorganisms with possible applications in biotechnology. In the present work, a method was developed for the automated localization and quantification of microscopic cell wall elements (CWE) of Norway spruce wood such as bordered pits, intrinsic defects, hyphae or alterations induced by white-rot fungus *P. vitreus* using high-resolution XCT microscopy. In addition to classical destructive wood anatomical methods such as LM or CLSM (Sec. 2.3.1), this method allows for the first time to compute the properties (e.g. area, orientation and size distribution) of CWE of the tracheids in a sample. This is essential for modelling the influence of microscopic CWE on macroscopic properties such as wood strength and permeability.

To the best of my knowledge, this chapter describes for the first time a computer based automated procedure for the localization and quantification of cell wall elements such as bordered pits, intrinsic defects and alterations induced by *P. vitreus* by means of high-resolution XCT microscopy. The quantitative information arising from this procedure allows to e.g. analyze the distribution of the fungal activity of *P. vitreus* in the late- and early wood of Norway spruce depending on the incubation conditions, which is essential for the successful manufacture of fungal modified wood.

3.1 Automated quantification of microscopic decay pattern

3.1.1 Materials and methods

Wood and fungus

I use defect-free heartwood wood from a Norway spruce tree grown in Switzerland. The three alignments of wood cells are longitudinal (parallel to the fibre), radial (perpendicular to the fibre) and tangential (parallel to the growth rings) as shown in Fig. 2.2. There are mainly two types of cells in softwoods, tracheids and rays. The cell walls of tracheids consist of several layers denoted as secondary wall S_1, S_2, S_3 and primary wall (PW) from the lumen (i.e. voids within the cells) to the middle lamella (ML) forming the border of two adjacent tracheids (Fig. 2.6). In order to transport water and nutrients in longitudinal and radial direction, the cell lumina are connected via bordered and simple pits (Fig. 2.7).

Specimens with dimensions of approximately 400 µm (radial) × 10 mm (tangential) × 6 mm (longitudinal) were produced with a microtome. All specimen faces, except the radial ones, were subsequently coated by brushing (Nuvovern ACR Emaillack, Walter Mäder AG, Killwangen, Switzerland). After 24 h, the procedure was repeated to guarantee a solid sealing. Subsequently, the specimens were conditioned for two weeks at 22°C and 50% RH. Thereafter, the specimens were sterilized with hot steam (121°C, 20 min and 200 kPa vapour pressure) and placed on a 'feeder block' of Scots pines *Pinus sylvestris* previously colonized with *P. vitreus*. Specimens were incubated under sterile conditions for seven weeks at 22°C and 70% RH. After incubation, the specimens were cut into elongated wood prisms of approximately 400 µm (radial) × 400 mm (tangential) × 6 mm (longitudinal) using a microtome.

For the tomographic experiments, the samples were glued onto cylindrical sample holders using double-side adhesive tape, the longitudinal axis of the sample being located at the rotation axis of the tomographic stage.

Synchrotron Tomographic Microscopy

Synchrotron radiation facilities provide photon beams of energy densities that outrange conventional X-ray sources by orders of magnitude. Among other benefits, the high brilliance and brightness of synchrotron based X-rays enable tomographic microscopy at sub-micrometer scale.

In the present study, tomographic experiments were performed at the TOMCAT (Tomographic Microscopy and Coherent Radiology experiments) beam line at the synchrotron radiation facility Swiss Light Source (SLS) at the Paul Scherrer Institute (PSI) in Villigen (Switzerland). The TOMCAT beam line operates in both, absorption and phase-contrast mode. Phase-contrast tomography analyzes the Zernike phase-contrasts of the X-ray beam induced by refraction [127] and is preferable for materials with low absorption contrast such as wood. Trtik et al. [193] and Mannes [117] demonstrated the use of phase-contrast tomography for the analysis of 3D structures in Norway spruce wood down to the microscopic level.

In order to minimize dehydration of the specimen during measurements a climatic chamber to control the air humidity at 95% RH was used (Derome et al. [41]). The temperature remained constant during measurements at 25°C. For each specimen, a set of 1501 projections over 180° was acquired with a photon energy of 9.9 and 20.2 keV for absorption or phase-contrast mode, respectively. The X-rays were converted into visible light by a YAG:Ce 20 µm scintillator and projected to a charge coupled device (CCD) featuring a resolution of 2048 × 2048 pixels and a dynamic range of 14-bit. The nominal edge length of a cubic VOXEL was 0.37 µm by using an optical objective with the magnification (20×) and a field of view of 0.75 × 0.75 mm. The total scanning time was approximately 15 minutes for both, absorption and phase-contrast mode. Stampanoni et al. [184] provides further technical specifications for TOMCAT.

The reconstruction of the original projections into a stack of 2048 transverse sections termed tomograms was based on Filtered-Back-Projection using the Parzen filter supporting noise suppression. The tomograms are 16-bit gray-level TIFF images. The projection values were initially corrected with dark- and flat-field images and the attenuation values thereof were obtained by Lambert-inversion.

Stripe artifacts originating from defective detector pixels were eliminated [126] and centering artifacts remedied.

Analysis of tracheid cell wall elements

Fig. 3.1 illustrates the cell wall analysis process and Fig. 3.2 presents the core algorithm. The original data, a stack of n sequential tomograms of the specimen is displayed in Fig. 3.1(a), the data processing yielding the CWE in Figs. 3.1(b) - (d). Initially, the region of interest (ROI) of each tracheid is manually identified in the 3D tomograms. The 3D tracheid objects are subsequently mapped into 2D by applying a cylindrical projection, each point representing the mean attenuation of the cell wall VOXELs at an angle α, referring to the centre of gravity of the tracheid. The resulting tracheidal 2D-map is a gray-level image of size $n \times s$, where $s \sim 2 \cdot \pi/\alpha$, in which regions of low attenuation values (i.e. CWE) are clearly visible. After segmentation, the distribution of the CWE size and the orientation was determined.

First, a ROI was selected and transformed into a binary mask separating air (black pixels) and wood material (white pixels). Segmentation was based on gray-level thresholding using Otsu's method [132]. Fig. 3.1(b) shows the original tomograms after applying a morphological closing operation by using a spherical structuring element (SE) with the radius of 3 pixels, in order to remove small objects mainly originating from noise [64]. The resulting filtered mask is the basis for the segmentation and mapping of the tracheids.

Tracheids were segmented by constructing the watersheds between adjacent and closed lumina [123]. Since the lumina might not be closed because of CWE (arrow in Fig. 3.3(a), a morphological closing operation using a SE of $3 \times 3 \times 150$ pixels was applied (Fig. 3.1(c)) prior to watershed construction. Subsequently, each spanning cluster is labeled as shown by the colors in Fig. 3.1(c). The obtained label mask of each tomogram makes the segmentation of a tracheid in the filtered mask possible and therefore the construction of a 3D tracheid mask, which is finally used to select and map the cell wall VOXELs to a tracheidal 2D-map by using a cylindrical projection. Fig. 3.1 illustrates this process for one of the tomograms.

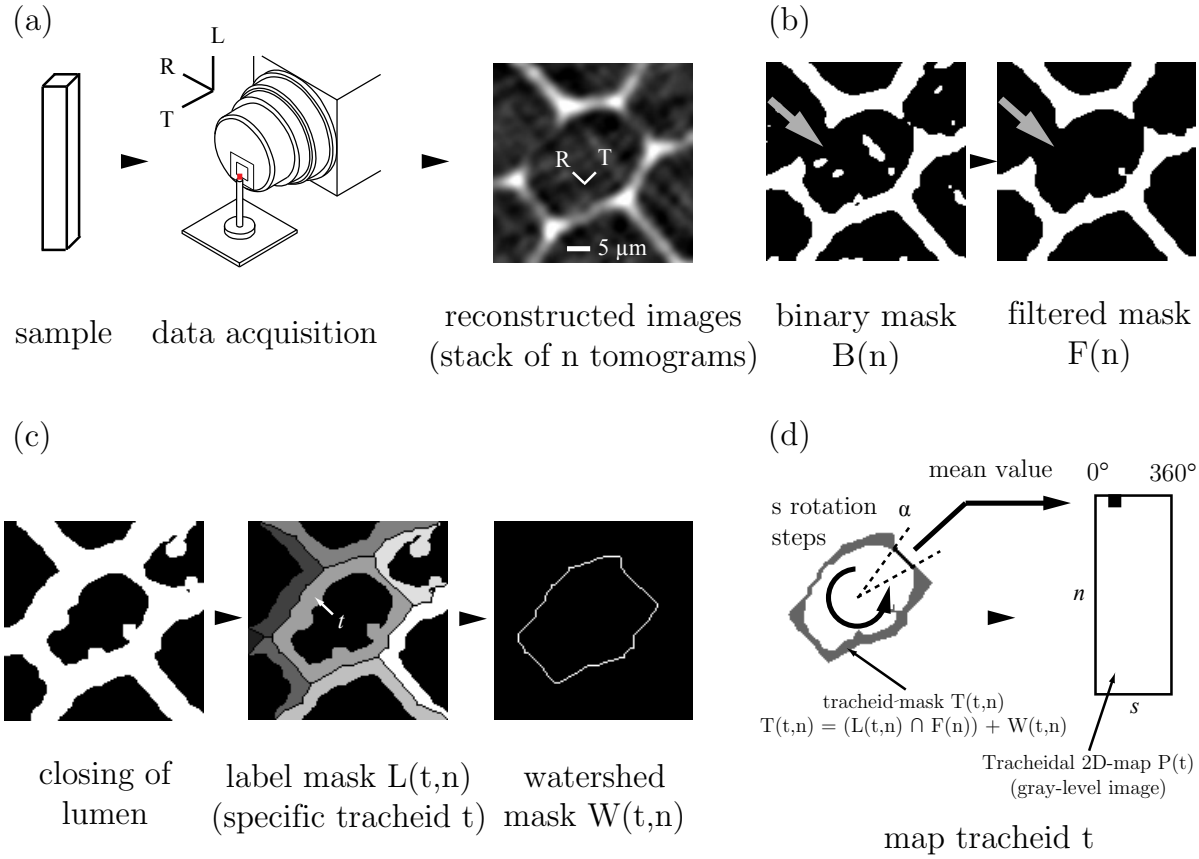

Figure 3.1: Schematic workflow from (a) tomographic experiment to (b - d) quantification of cell wall elements. (a) Acquisition of original data, a stack of n subsequent tomograms, and manual identification of a region of interest. (b) Segmentation of the tomograms to a binary mask and removing of artifacts. (c) Closing of the cell lumina in the filtered mask in order to obtain a label mask and a watershed mask to identify the pixels corresponding to a specific tracheid. (d) Construction of the tracheid mask and mapping procedure. The 3D tracheid object is subsequently mapped into 2D by using a cylindrical projection, where each point represents the mean attenuation of the cell wall VOXELs at an angle α, referring to the centre of gravity of the tracheid. Based on the resulting tracheidal 2D-map, which is a gray-level image of size $n \times s$, it is possible to segment and determine the distribution of the CWE size and orientation.

```
program Size_Distribution
#Read Data
I <- Read Stack of n Tomograms
Ic <- Crop ROI of I

#Construction 2D Map
for i to n do
    B <- Compute binary mask of Ic(n)
    Bc <- Morphological closing of B
    F(n) <- Remove objects < p pixels from Bc
end Return Filtered mask (F)

Fc <- Morphological closing of F
for i to n do
    S <- Compute skeleton of Fc(n)
    Sr <- Remove spur pixels from S
    L(n) <- Compute label mask from Sr and Fc
end Return Label mask L

t <- Choose specific tracheid
for i to n do
    L(t,n) <- Find all pixels of tracheid t in L(n)
    W(t,n) <- Compute watershed of tacheid t
    Compute tracheid mask T(t,n) = ( L(t,n) ∩ F(n) ) + W(t,n)
    P(t,n) <- Normal cylindric projection P(t,n)
end Return Normal cylindrical projection P(t)

#Size distribution
Pb(t) <- Construct binary image of P(t)
Compute size distribution of cell wall elements in Pb(t)
end program Size_Distribution
```

Figure 3.2: Core algorithm for computing the size-distribution of cell wall elements of a tracheid.

3.1.2 Results and discussion

In order to demonstrate the potential of the method I analyzed single tracheids of a ROI with the size of 125 × 125 × 400 pixels using synchrotron XCT in absorption (Fig. 3.3(a)) and phase-contrast mode (Fig. 3.3(b)) visualized by isosurfaces in Figs. 3.3(a) and (b) respectively. CWE such as bordered pits (P), intrinsic defects or cell wall alterations induced by *P. vitreus* (F, L) were marked. The tracheidal 2D-map of this tracheid is shown in Fig. 3.3(a). The CWE are clearly visible and their segmentation was possible (Fig. 3.3(b)). Fig. 3.3(c) shows the histogram of the CWE areas. Their mean attenuation can be interpreted as a measure of

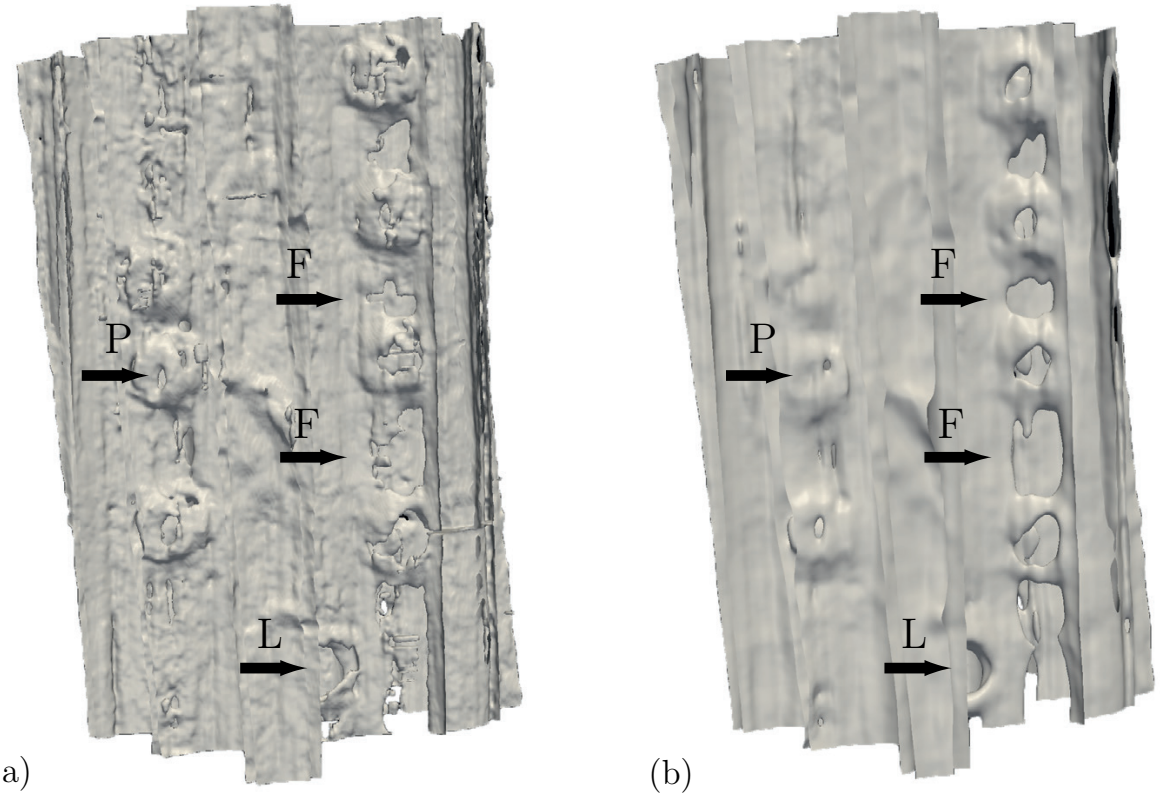

(a) (b)

Figure 3.3: Region of interest with a size of 125 × 125 × 400 pixels of a specimen incubated with *Physisporinus vitreus* for 8 weeks. The sample was measured by using the synchrotron tomographic microscopy in (a) absorption and (b) phase-contrast mode and visualized by isosurfaces. The clusters of pixels with a very low attenuation indicate cell wall elements such as pits (P), intrinsic defects or cell wall alterations may induced by *P. vitreus* (F,L).

cell wall damage as shown in the inset. The results revealed the tracheid's lateral surface of approximately 9800 µm^2 had a total number of 18 CWEs with an area of approximately 285 µm^2, which relates to approximately 3% of the tracheid's lateral surface. The largest and the smallest CWE had areas of 72 µm^2 and 0.05 µm^2, respectively. Most of the CWEs were smaller than 40 µm^2. In Addition, most CWEs occurred in the tangential cell walls (Fig. 3.4(a) and (b)) and different shapes of CWEs were recorded in tangential and radial cell walls. Larger CWE showed a lower mean attenuation than smaller CWE.

The detection and computing of the CWE revealed clusters of pixels with a very low attenuation as illustrated in the tracheidal 2D-map (Fig. 3.3(b) and Fig. 3.4(a)). However, the shape of the cell wall and of the 'holes' strongly depends on the constant value for the isosurfaces (Figs. 3.3(a) and (b)) and the binary

mask of the tracheidal 2D-map (Fig. 3.4(a)). Thus, for future measurements it is necessary to compare the tracheids before and after fungal exposure in order to identify alterations of the cell wall accurately. Therefore, the scanning procedure may be time consuming, but recent developments make laboratory-based phase-contrast XCT microscopy available [118].

Since tracheids exhibit a complex 3D shape the presented cylindrical projection distorts the cell wall and an elliptic cylindrical map projection might be more adequate. Furthermore, there is more noise in the absorption than in phase-contrast based tomograms, which makes analysis more difficult. Therefore, I suggest using phase-contrast based tomographic microscopy. Nevertheless, the analysis shows pits and cell wall alterations that might be induced by fungal activity, because the pattern of the damages were similar to those found in semi-thin light microscopy sections of incubated wood samples by Lehringer et al. [99]. I found that most of the cell wall alterations were located in the vicinity of bordered pits, and that the size-distribution in Fig. 3.4(c) shows a concentration of pixels with low attenuation to large CWE's such as cell wall alterations. This result corresponds with the findings of Lehringer et al. [99] and according to his classification system the present method is able to classify the cell wall and bordered pits (indicated by L in Fig. 3.3(a) and (b)) as 'strongly degraded'.

Despite the inherent structure of wood, fungi degrade woody tissues, and decay types fall into three categories according to their mode of degradation of the woody cell walls. Traditionally, wood decomposition by fungi is usually classified into three categories based on micro-morphological and chemical characteristics of decay, resulting in different patterns of degradation of the cell wall (Tab. 2.5): soft rot, brown rot and white rot, the latter subdivided into simultaneous rot and selective delignification as caused by e.g. *P. vitreus* [172]. Finally, the presented method has the potential to identify and quantify those cell wall alterations caused by different decay types and additionally other objects within wood such as bordered pits, intrinsic defects or hyphae by comparing the wood sample before and after fungal incubation.

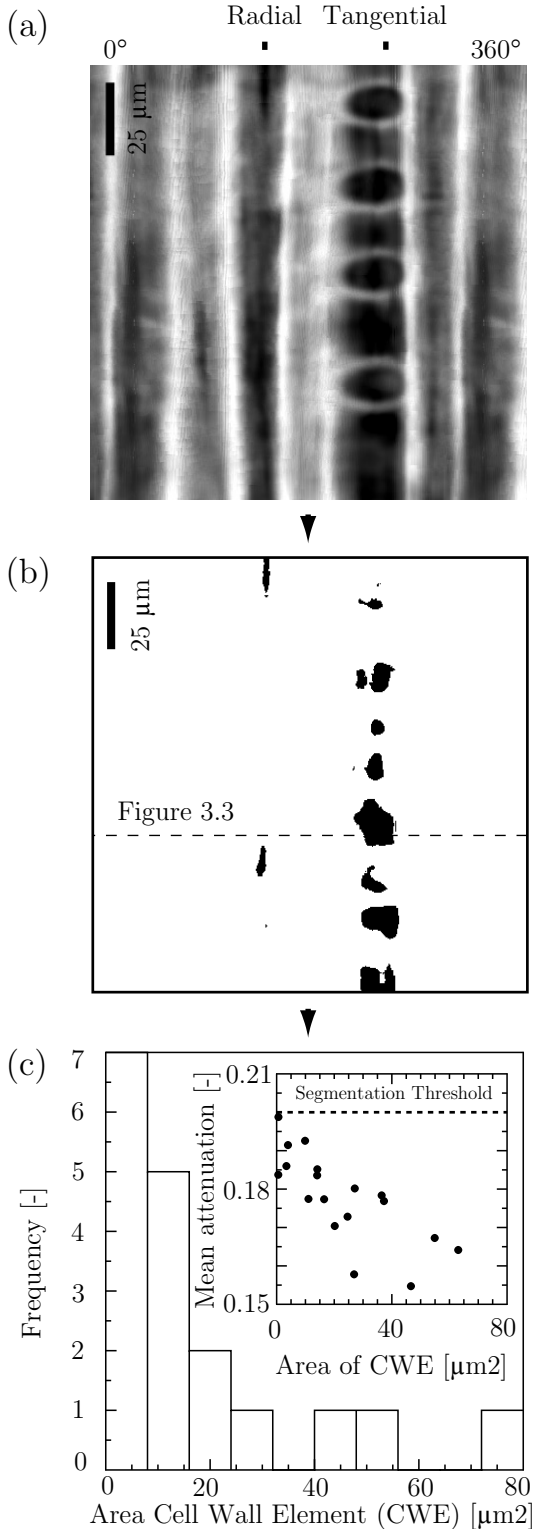

Figure 3.4: Quantification of cell wall elements (CWE). (a) *Dark colors* in the tracheidal 2D-map correspond to a low attenuation of the beam and therefore to a low density of the cell wall. The pits and cell wall alterations induced by the white-rot fungus *Physisporinus vitreus* are clearly visible. (b) Identification of the CWE by construction a threshold based binary mask of the tracheidal 2D-map. The tomogram of Fig. 3.1 corresponds to the *marked row*. (c) An automated segmentation of CWE allows analyzing e.g. their size-distribution. The inset shows the area of the CWE plotted against their mean attenuation.

3.1.3 Summary

I presented a method to analyze and quantify microscopic CWE such as pits, intrinsic defects and cell wall alterations induced by *P. vitreus*. The analysis focused on Norway spruce tracheids degraded by the white-rot fungus *P. vitreus*. The CWE were clearly visible and it was possible to segment and determine the distribution of the CWE size and orientation.

I found that most of the cell wall alterations were located in the vicinity of the bordered pits and the computed size-distribution shows a concentration of pixels with low attenuation to large CWE such as cell wall alterations. However, in addition to this classical wood anatomical method, for the first time this approach allowed to compute the properties (e.g. area, orientation and size-distribution) of cell wall elements of each tracheid of a specimen, which is essential for linking the influence of microscopic cell wall elements to macroscopic system properties such as wood strength or permeability.

Therefore, in the future it is of interest to systematically measure the fungal activity of *P. vitreus* in Norway spruce samples for different incubation periods and model the evolution of its impact to the cell wall structure. The obtained models are essential to simulate the permeability changes of infected wood in order to optimize the choice of pellet concentration and reaction times that are required to induce a certain degree of wood permeability by *P. vitreus*. Furthermore, the presented method facilitates the development and calibration of mathematical models to optimize the impact of wood decay-fungi for biotechnological applications in pure and applied wood sciences.

3.2 Three-dimensional distribution of bordered pits

Pits regulate the transport of water and nutrients in vascular plants. The distribution of pits within the xylem is important to understand and model various biological and physical processes in trees, as well as for technological applications of wood. The present section characterises and quantifies the distribution of pits within a growth ring of Norway spruce using high-resolution synchrotron tomographic microscopy. Based on digital image processing an automated evaluation

of the pit's position, the inter-pit distance, their orientation and size in early-, transition and latewood is possible. The provided full 3D anatomical picture of Norway spruce wood supports the development mathematical models in various fields.

3.2.1 Introduction

Norway spruce is a softwood with complex cellular and hierarchical structure. The orientation of wood is usually identified as longitudinal (along the trunk), radial (from the pith to the bark) and tangential (perpendicular to the radial direction) as shown in Fig. 2.2. The stem consists of growth rings formed mainly of two cell types (Sec. 2.1.1). The lumens, which are the voids within the cells, are connected by valve-like structures called pits (Fig. 2.6). The knowledge about the distribution of the pits is important to understand and model various biological and physical processes such as transport of nutrients and water [29], fungal growth [69, 55], shrinking and swelling of wood [41], vulnerability to cavitations [104] or embolism [72] as well as for technological applications such as drying and impregnation of spruce wood [152] and pulping ([176] and references therein). The 3D distribution of pits in Norway spruce is still not fully characterised, especially the inter-pit distance of the bordered pits in the overlapping zones of the tracheids as a function of the tracheids position within a growth ring.

The 3D distribution of these microscopical objects on an mesoscopic length scale of a growth ring poses a serious challenge for their experimental evaluation since the experimental equipment must provide both high resolution on a sub-micrometer scale and a large field of view on the millimetre scale.

In the 20th century light-, laser- or electron-microscopy were the methods of choice to fullfill this high performance. Usually the wood samples were microtomed into thin sections and analysed by hand (see Sec. 2.3.1 for a short review). Based on such studies it is possible to determine the permeability of wood [33, 143] and describe transport processes in more detail [173, 29]. However, these are all destructive methods providing only two-dimensional information about anatomical features. Trtik et al. [193] demonstrated that by using high resolution tomographic microscopy even the detection of the torus is possible. Such high resolution tomographic microscopy provides full 3D analysis of wood anatomy such as the vessel

network [195] or the pits [117] and in combination with image processing method automated quantification of anatomical features is possible [57, 23]. Such quantitative methods provide full 3D anatomical information and allow to analyse the structure of wood of a large number of samples across different species as well as to develop mathematical models in a multitude of fields.

3.2.2 Materials and methods

Wood

Defect-free heartwood is prepared of a Norway spruce tree grown in Switzerland. There are two types of samples both fabricated using a microtome: The large samples have a dimension of approximately 400 µm (radial) × 400 mm (tangential) × 6 mm (longitudinal), whereas the small ones are approximately 2000 µm (radial) × 2000 µm (tangential) × 6mm (longitudinal). Before the tomographic experiment the samples were stored for two weeks at 22°C and 50% relative humidity.

Synchrotron tomographic microscopy

The tomographic experiments were performed at the TOMCAT beam line line at the synchrotron radiation facility SLS at the PSI in Villigen (Switzerland). The PSI setup enables measurements both in absorbtion and phase-constrast mode, whereby the latter is preferred for low absorbing material such as wood. The large samples are measured in absorption mode with a resolution of 1.85 × 1.85 µm per VOXEL, whereas the small samples are measured in phase-contrast mode providing a resolution of 0.37 × 0.37 µm per VOXEL. A climatic chamber is used to control the RH at 70%. Generally, the same technical equipment and measurement setup is used as described in Fuhr et al. [57].

Detection of the pits

Fuhr et al. [57] proposed a method for the automated quantification of Norway spruce cell wall elements such as pits, intrinsic defects, hyphae or cell wall alterations (Sec. 3.1). The algorithm makes use of the characteristic elongated shape of the tracheids by mapping these 3D cylindrical objects to a 2D image (i.e. tracheidal 2D-map) using cylindrical projection (Fig. 3.1(d)). Based on these final grey-scale images, in which each pixel represents the density of the cell wall by a certain angle, a segmentation of the pits is possible (Fig. 3.5(b)) and therefore the calculation of their properties, i.e. 3D position, orientation, frequency, size, shape and intensity.

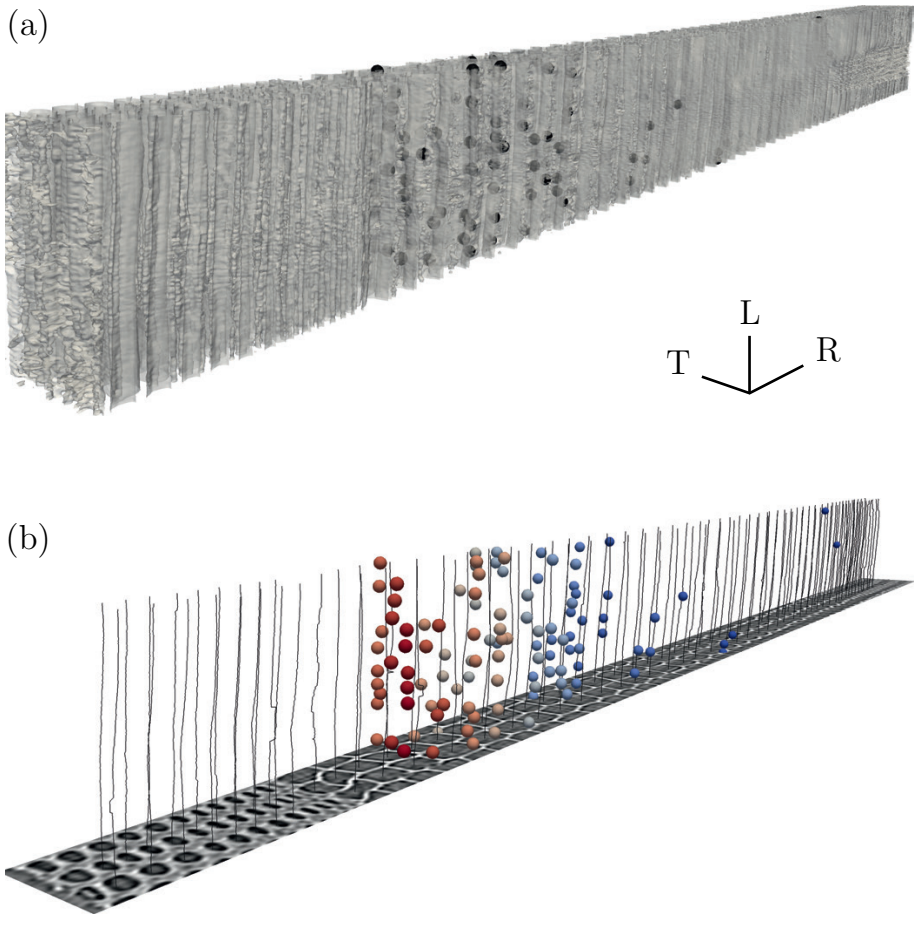

Figure 3.5: The distribution of bordered pits within a Norway spruce growth ring. The size of the region of interest is approximately 0.2 × 0.1 × 2 mm and the resolution of the tomograms are 1.85 × 1.85 × 1.85 µm. Quantitative data is given in Fig. 3.6.

3.2.3 Results and discussion

Fig. 3.5 visualizes the distribution of bordered pits within a Norway spruce growth ring. The growth ring is approximately 2 mm width, whereby the ROI of Fig. 3.5 has a size of approximately 0.2 × 0.1 × 2 mm. All lumens are scanned by the algorithm and 109 bordered pits were detected. However, an automated segmentation of the bordered pits was not possible, because absorbtion based tomographic microscopy is used at this resolution (Sec. 3.1.1).

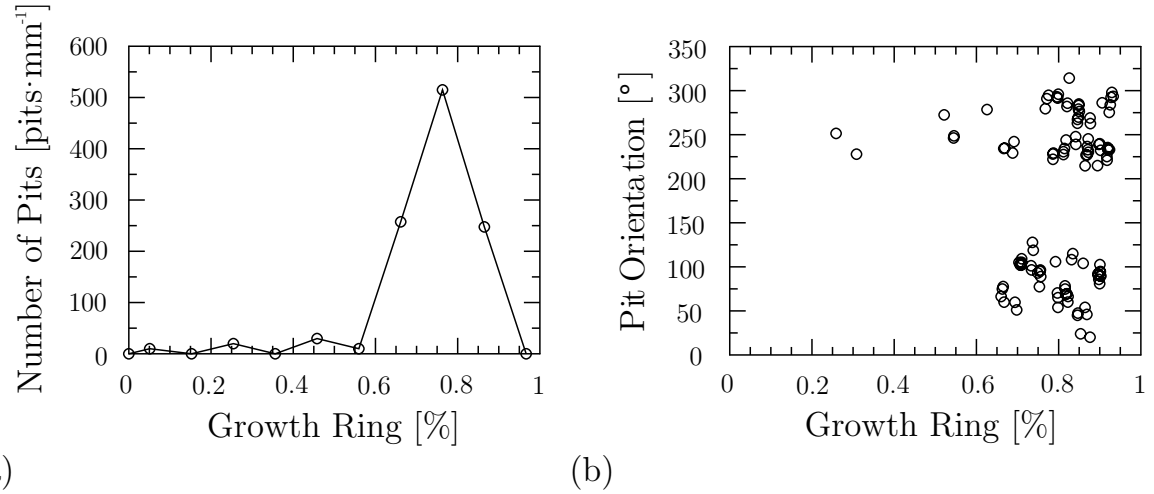

Figure 3.6: Distribution of bordered pits within the growth ring of Fig. 3.5. (a) Most of the bordered pits occur in the early-wood and (b) on the radial cell walls, i.e. $\sim 90°$ and $\sim 270°$. 0° and 180° correspond to the radial direction (R) and 90° and 270° to the tangential direction (T) in Fig. 3.5.

Fig. 3.6(a) and Fig. 3.6(b) show the distribution of the bordered pits and their orientation within the growth ring of Fig. 3.5. Most of the bordered pits occur on the radial cell walls within the transition wood, whereas no bordered pits on tangential cell walls are found as reported by Sirviö & Kärenlampi [176]. However, the analyzed sample is relatively small and more qualitative and quantitative data are needed.

Fig. 3.7 shows bordered pits in the overlapping area of selected tracheids. The ROI has a size of approximately 100 × 100 × 100 µm and a resolution of 0.37 μm^3 per VOXEL. The pit density is approximately 40 to 50 pits $\cdot\, mm^{-1}$, which is

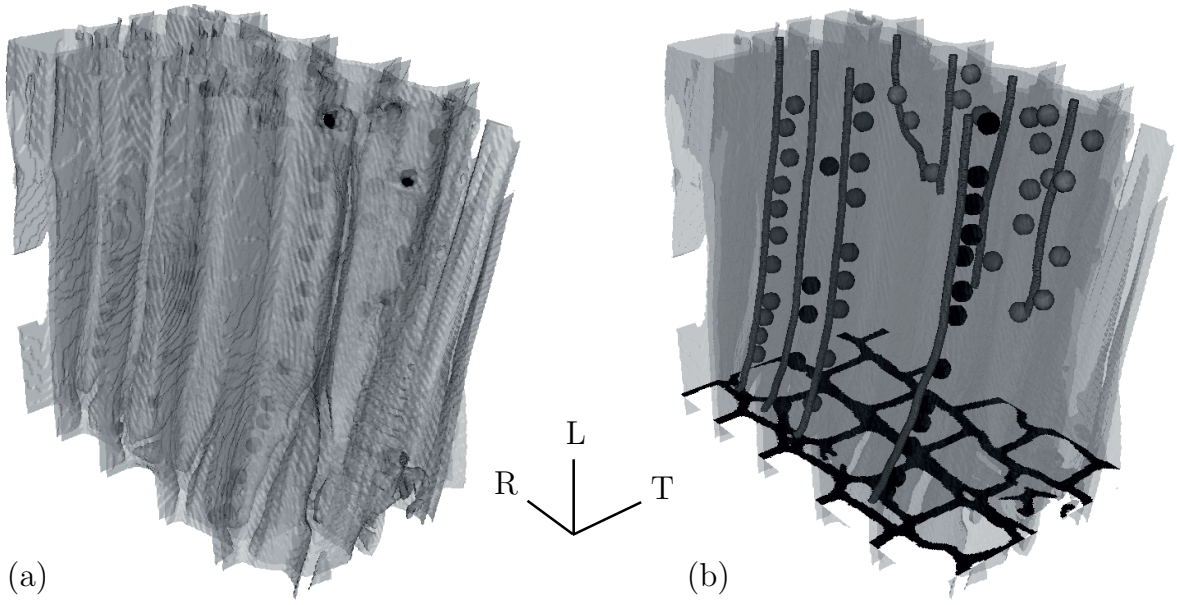

Figure 3.7: Bordered pits in the overlapping region of selected tracheids. (a) The presented region of interest has a size of approximately 100 × 100 × 100 µm. The wood is visualize and rendered via isosurfaces. (b) shows the bordered pits (black) and the corresponding lumens (grey tubes).

in good agreement with the findings of Sirviö & Kärenlampi [176].

3.2.4 Summary

The present section provides a full 3D anatomical picture of the distribution of pits in Norway spruce wood. The findings agree with the results of previous works in this field [176, 22], but this section shows the distribution of the bordered pits both in early- and latewood. Furthermore, I studied the bordered pits in overlapping area of the tracheids. The presented algorithm uses, with the exception of one step, only 2D morphological image processing operations. The proposed method is fast, stable and enables processing very large tomographic images.

The developed framework based on high-resolution tomographic microscopy in conjunction with digital image processing offers an automated analysis of the pits. However, high-resolution tomographic methods do not substitute classical microscopy such as LM, REM or CLSM (Sec. 2.3) since they do not provide information about the chemical composition of the cell wall and objects with low contrast such as hyphae. Therefore a combination of different microscopy and

staining techniques allows analysing e.g. both fungal growth and impact in wood by using CLSM in combination with high-resolution tomography [187].

Therefore, in future works it is proposed to systematically analyze specimens before and after fungal incubation. By comparing the 2D tracheidal maps of each tracheid in a sample a full three-dimensional picture of the impact of wood-decay fungi is possible. Such information of the fungal impact on the cell walls enables calculating the permeability of a specimen using a hydraulic permeability model as presented in Ch. 5.

4 Modelling the hyphal growth and impact of *P. vitreus*

4.1 Fungal growth model

4.1.1 Introduction

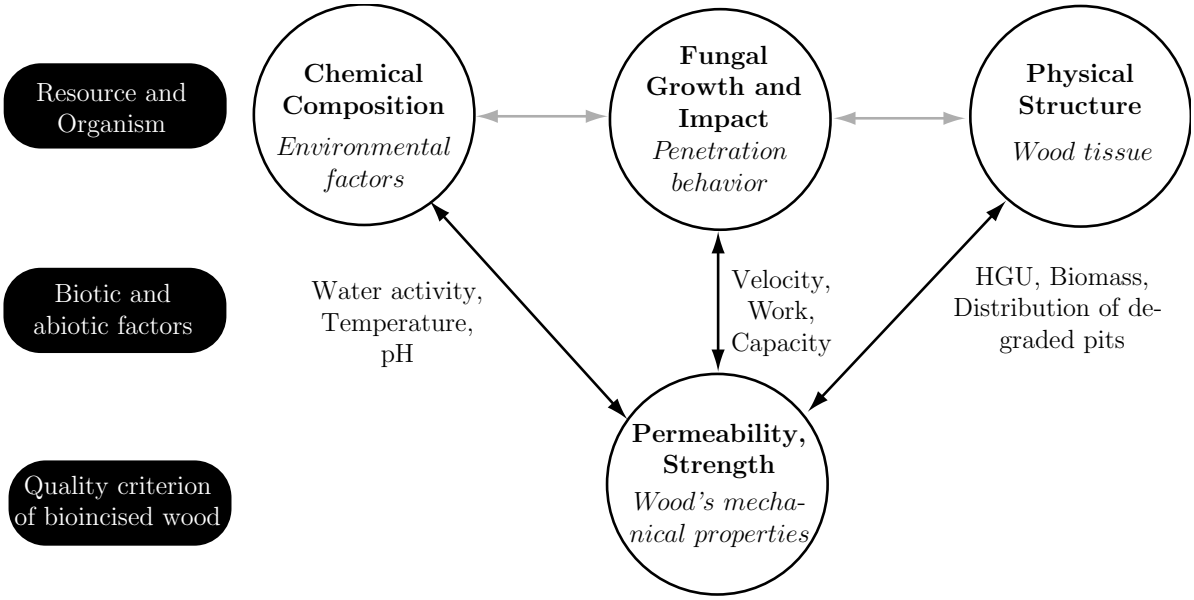

Figure 4.1: Resource, organism and biotic and abiotic factors influence the quality of bioincised wood. It is proposed to study the optimization of the biotechnological process bioincising by means of mathematical models, because of the complexity of the system (fungus-wood). Each subject is presented in a chapter, i.e. the chemical composition (Sec. 4.2), fungal growth and impact (Sec. 4.3) and the physical structure (Sec. 4.4).

It is proposed to study the biotechnological process bioincising by means of a mathematical model, because many factors affect the growth and impact of *P.*

vitreus in Norway spruce in such a complex way (Fig. 4.1) that an evaluation of the optimal incubation conditions is very expensive or even not possible using only laboratory experiments. The primary goal of a modelling framework is to analyze the influence of biotic and abiotic factors on the wood's permeability, which in combination with the wood's strength is the quality criterion of bioincised wood (i.e. higher permeability results in greater treatability of the wood). Therefore, the chemical composition (i.e. environmental factors such as the water activity, temperature and type of medium) and the physical structure (i.e. the distribution of tracheids and pits) of the resource determine the penetration behaviour of a wood-decay fungus. Each category is presented in this chapter: the chemical composition (Sec. 4.2), fungal growth and impact (Sec. 4.3) and the physical structure (Sec. 4.4).

The interaction between fungus and wood is very complex and it is the modeller's task to identify and abstract the relevant mechanisms into a model, whereby the challenge is to represent the reality by a minimum of parameters.

4.1.2 Description of the model

The main focus of the FGM is the identification and investigation of key processes of hyphal growth (e.g. uptake of nutrients) and the resulting increase in wood permeability. In order to investigate these, a model of the microscopic level is developed, focussing on the wood's structure and nutrients (i.e. the substrate) and the tree-like network of the fungus (i.e. the mycelium). Generally, the FGM reduces the enormously complex growth of *P. vitreus* to a pit-to-pit growth of individual hyphae: starting from an initial state $m = 0$ at each iteration step $m \in \mathbb{N}$ the mycelium may be extended by one edge. This approach uses an adaptive time increment, which enables simulation of the growth of wood-decay fungi from the microscopic (mm) to the macroscopic scale (cm).

I used a 3D FGM because of the distinct properties of Norway spruce wood in the longitudinal, radial, and tangential directions. The interaction of a fungus with the underlying substrate is enormously complex because of the many feedback mechanisms. The aim of the model is to reduce a complex (biological) system to the essential key processes governing the growth of the fungus. It is considered that a model that includes polarization, degradation, transport, branching,

growth costs and direction of growth will describe the growth of *P. vitreus* in wood sufficiently for my purpose.

Resource (Wood)

Norway spruce is a softwood consisting mainly of two cell types. Tracheids are the main cells (90 - 95%) and the rest are parenchymal cells (Sec. 2.1.1). During its primary stage of growth *P. vitreus* degrades the lignified pit membranes of Norway spruce heartwood [168]. The FGM reduces the complex structure of the wood to a network of tracheids (cell walls) connected by bordered pits (nutrient source). Rays and other types of cell wall breaches, such as pinoid pits, are not considered in the model.

The nutrient source is what fungal enzymes act upon. The model assumes that all the essential substances for fungal growth, e.g. lignin and water, are concentrated in the membranes of bordered pits. The fungus degrades the pit membranes by extracellular digestion and the pit membranes are modelled as points with the attributes

$$\begin{array}{lll} R_j & j = & (1...N_p) \\ F_j^{(m)} & \in & [0, \nu] \end{array} \tag{4.1}$$

where R_j denotes the coordinates of an arbitrary nutrient point (j), N_P is the number of nutrient points in the system and the variable $F_j^{(m)}$ describes the available amount of nutrients at point (j) at iteration step m; ν denotes the initial $(m = 0)$ amount of nutrient at point (j). By degrading the lignified pit membrane *P. vitreus* opens the closed connection between two adjacent tracheids, which allows the fungus to exploit the wood and capture the resource. Thereby, the fungus increases the wood's permeability, which is observable by increasing holes in the tori of the pits as shown in Fig. 2.11. Bardage & Daniel [5] tested several wood-decay fungi and found that all of them are able to penetrate into capillaries with a radius of more than 0.6 mm within 15 d, while none of them has the capacity to grow through capillaries with a radius of less than 0.1 mm. Therefore I

introduce an opening threshold into the model describing the minimal radius of a capillary (i.e. hole in the torus), which is prerequisite for a fungus to growth from one pore to another. The relation between the amount of nutrients at point (j) and the radius of a hole in the torus is unknown, and we simply assume that the fungus is able to grow through the degraded torus into an adjacent tracheid if

$$F_j^{(m)} < \kappa \tag{4.2}$$

where $\kappa \in [0, \nu]$ denotes a specific opening threshold.

Cell walls are the substratum on which the hyphae grow. During the primary growth phase I assume that extracellular enzymes secreted by hyphae do not interact with the cell walls. Hyphal degradation of cell walls commences mainly during the secondary stage. In the present model only the primary stage of hyphal growth is taken into account. Cell walls are additional boundary conditions within the system: they determine the distance between the pit membranes and limit the accessible set of pit membranes for the fungus.

Fig. 4.2 shows the model wood composed of cell walls and nutrient sources. The tracheids are polyhedrons with six faces. In the model, all tracheids have the same dimension in tangential w_2, as well as in the longitudinal w_3 directions. In order to model a growth ring, the tracheid width, w_1, differs for early-, transition-, and latewood. The pits are randomly uniformly distributed along the cell walls according to specific pit densities that depend on the orientation of the underlying cell wall (i.e. tangential or radial pitting) and the position of the cell wall axis within the growth ring (early- and latewood pitting). In order to model overlapping tracheids pits are also located at the tracheid end faces. Differences in size and shape between early- and latewood pits and parenchyma cells (rays) are not considered in this model.

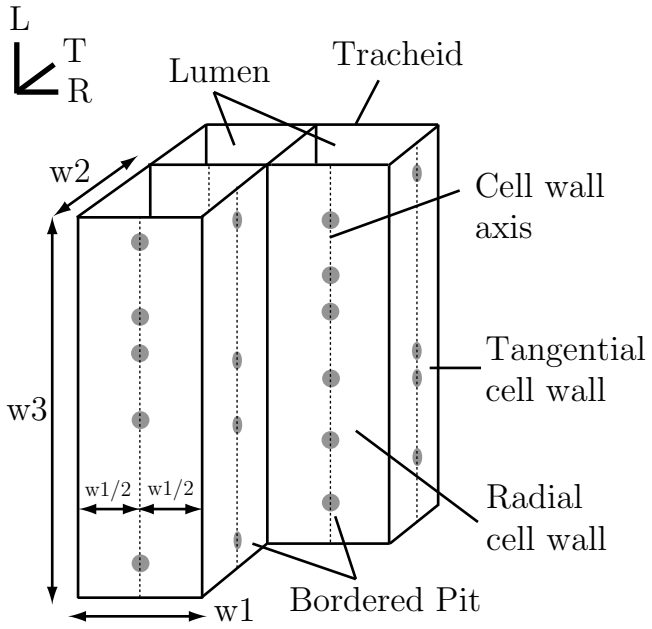

Figure 4.2: Model of Norway spruce wood. The model reduces the complex wood structure to a network of tracheids connected solely by bordered pits. The pits are randomly uniformly distributed with density ρ along the cell wall axis (dotted line), depending on the orientation of the underlying cell wall (tangential or radial pitting) and the position of the cell wall in the growth ring (early- and latewood pitting). Every tracheid consists of six cell walls and has a width w_1, a height w_2, and a length w_3. In order to model a growth ring, the tracheid width w_1 for early-, transition-, and latewood differs.

Mycelium (fungus)

An aggregation of edges and nodes form the mycelium. The edges connect the nodes and represent the filaments, which are the framework of the mycelium. The nodes are at the sites of the pits. Thus,

$$\begin{array}{lcll} r_i & \in & \bigcup_i R_i & \\ f_i^{(m)} & \geq & 0 & i = (1...N_k^{(m)}), \\ b_i & \geq & 0 & \end{array} \tag{4.3}$$

where $N_K^{(m)}$ denotes the number of nodes in the system at iteration step m, r_i

represents the coordinates of node (i); R is a vector containing the coordinates of the pits; and $f_i\ (m)$ is the amount of nutrient at node (i). The variable b_i denotes the iteration step at which node (i) is added to the mycelium. The consumption of nutrients is irreversible. The nodes are connected by edges. The adjacency matrix of the network has the order $(N_K^{(m)} \times N_K^{(m)})$ and is defined by Eq. 2.4. The orientation of a node $c_i^{(m)}$ is given by

$$c_i^{(m)} = \sum_{n=1}^{N_K^{(m)}} \mathcal{H}(b_i - b_n) \cdot a_{in}^{(m)} \cdot \frac{(r_i - r_n)}{\|r_i - r_n\|}. \tag{4.4}$$

The total hyphal length of the mycelium at iteration step (m) is given by summing Eq. 2.6 over i. $\mathcal{H}(x)$ is the Heaviside step function.

There is no restriction concerning the crossing of edges. The model omits autolysis and growth is irreversible. Fig. 4.3 shows the network consisting of edges and nodes. The model assumes that all fungal activity such as the uptake of nutrients and branching takes place at the location of the bordered pits. This restriction is a simplification, but the 'backbone' of the mycelium is determined by the location of the pits, which are the weakest connections between two tracheids and therefore the main pathways of the fungus in its first stage of growth (Fig. 2.6(b)). The key processes (i.e. polarization of growth, hyphal growth, uptake and concentration of nutrients and branching (lateral and apical)) describe the dynamics of this network and the growing mycelium. In order to model the growing fungus at a later stage of growth one has also to consider processes such as branching between the pits, autolysis and cell wall degradation (i.e. cell wall thinning and bore holes).

For filamentous fungi the dynamics of the mycelium is dominated by the extension of the filaments at the tips. This apex-located building up of cell walls, called polarization of growth, distinguishes filamentous fungi and is a key aspect of their morphogenesis [189]. The hyphal tip growth is supported by a Spitzenkörper (Sec. 2.2.1). These sub-apical phase-dark structures found in higher fungi play an important role in the growth and orientation of the hyphal tip [76]. The Spitzenkörper seems to work as a switching station between the incoming vesicles transporting components for the cell wall and the synthesis of the proteins

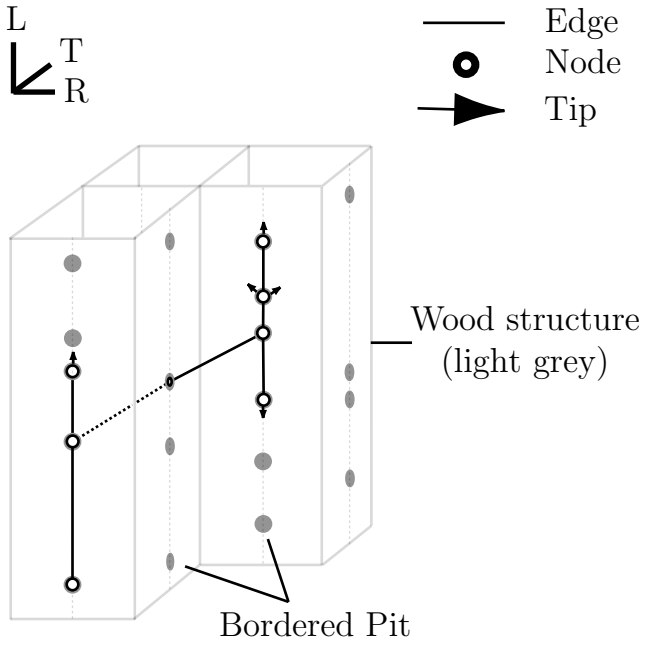

Figure 4.3: Model of *Physisporinus vitreus*. An aggregation of edges and nodes forms the mycelium. The position of the nodes is restricted to the bordered pits and the edges connect the nodes in free space. The pits are initially closed and impenetrable for the fungus. It is assumed that the fungus has to degrade a certain amount of nutrient from the pit in order to open a large enough capillary in the torus to growth from one lumen to another (Fig. 2.11 and Eq. 4.2). Tips denote polarized nodes. Branching occurs if the concentration of nutrients at a node exceeds a specific threshold.

comprising the cell wall. In higher fungi, hyphal morphogenesis seems to be inextricably linked with the existence of a Spitzenkörper. In order to simulate the dynamics of mycelium I introduced the concept of polarization and tip into the model. The continuous and simultaneous hyphal growth of every polarized fungal cell (i.e. tip) is modelled by a sequential growth algorithm (i.e. the FGM). Starting from an initial state $m = 0$ at each iteration step $m \in \mathbb{N}$ *one* active node (polarization $p > 0$) is chosen with a probability P, using uniformly distributed random numbers, and the mycelium may be extended by *one* edge. The extension of *one* hypha means that we go from one configuration of the mycelium to another. After m iteration steps there are many different configurations possible, depending on the set of random numbers, and one should sufficiently average over different realizations. Therefore, the probability P describes the change to go from one configuration to another by moving a specific hypha, while the complementary event $(1 - P)$ is the probability to reach other configurations. The probability P

of adding an edge to node (i) at iteration step m is

$$P_i^{(m)} = \frac{p_i^{(m)}}{\sum_{n=1}^{N_K^{(m)}} p_n^{(m)}}. \tag{4.5}$$

The polarization $p_n^{(m)}$ of an arbitrary node (i) of the mycelium is given by

$$p_i^{(m)} = \mathcal{H}(s_i^{(m)} - 1) \cdot f_i^{(m)}, \tag{4.6}$$

where $s_i^{(m)}$ is the number of tips at node (i). A node is defined as polarized if $p_i > 0$. Tips arise from branching and the number $s_i^{(m)}$ of tips at node (i) is given by

$$s_i^{(m)} = max\left\{(si^{(m)} - 1), \left[\frac{f_i^{(m)}}{\beta_i^{(m)}}\right]\right\} - \sum_{(n)\neq(i)}^{N_K^{(m)}} a_{in}^{(m)} \delta_{mb_n}, \tag{4.7}$$

$$\beta_i^{(m)} = \begin{cases} \beta_t & \text{for} \quad q_i^{(m)} = 1 \\ \beta_s & \text{for} \quad q_i^{(m)} > 1 \end{cases} \tag{4.8}$$

where δ_{ij} is the Kronecker delta and $[\cdot]$ is the entire function. The total number of tips in the system at iteration step m is calculated by integrating Eq. 4.7 over i. $b_i^{(m)}$ introduces a specific branching threshold that depends on the degree of node (i), i.e. apical $(q_i^{(m)} = 1)$ or lateral branching $(q_i^{(m)} > 1)$. If the concentration of nutrients $f_i^{(m)}$ on a link node (lateral) or tip node (apical) exceeds the concentration of $\beta_t \cdot \nu \cdot (s_i^{(m)} + 1)$, then branching occurs and the number of tips is incremented by one. β_t or β_s are specific thresholds for apical $(q_i^{(m)} = 1)$ or lateral branching $(q_i^{(m)} > 1)$. The tips are precursors to branching and they exist for about $N_S^{(m)}$ iteration steps at a node, where $N_S^{(m)}$ is the total number of tips in the system. There is no restriction about the total number of tips per node, but we observe a maximal number of two tips per node.

$$dt^{(m)} = \frac{\lambda}{\mu \cdot N_S^{(m)}}, \tag{4.9}$$

where λ is the mean edge length and μ is the mean hyphal growth rate, which is equivalent to the averaged velocity of hyphae measured from laboratory experiments. Therefore, the algorithm of the FGM has to run $N_S^{(m)}$ iteration steps to simulate the simultaneous extension of the mycelium at $N_S^{(m)}$ polarized ($p_i > 0$) nodes. The real time t is calculated by integrating Eq. 4.9 over m.

The hyphal growth rate is defined as the growth velocity of a single hypha and the mean hyphal growth rate as the averaged growth velocity of several hyphae at a specific region of a colony (e.g. the growth front). The mean hyphal growth rate can be evaluated from laboratory experiments, in this case the radial expansion of a colony on MEA at 22°C and pH 5 for different levels of water activity (a_w). Schubert et al. [160] found that, apart from nutrients and oxygen supply, pH and a_w play an important role in substrate colonization. On basic MEA medium the optimal conditions for growth of *P. vitreus* are $a_w = 0.998$, 20°C, and pH 5. This experiments on MEA medium may not represent the hyphal growth rate in situ, but experiments with *Trichoderma atroviride* [162] using LNA of a similar nutrient composition such as wood [182] show that the growth rates on LNA medium are about 25% slower compared to MEA medium an effect, which can be observed as well in growing colonies of *P. vitreus*. The used growth rates based on MEA experiments should be acceptable for the present purpose. To reduce the FGM to its essential processes it is assumed that changes in a_w, temperature, and pH only affect the mean hyphal growth rate μ. Effects of the substrate (e.g. swelling and shrinking of wood) are omitted and assume that the hyphal growth rate is the same in the whole colony from the front to the fungal inoculum.

Uptake and concentration of nutrients takes place at the nodes. The evolution equations for the nutrient concentration of a node (i) and a pit (j) after m iteration steps are defined by Eqs. 4.10 - 4.15. The terms Γ_i and Λ_i describe transport processes, while Δ_{ij} and Ω_i are the degradation rate and the cost of growth, respectively

$$F_j^{(m)} = F_j^{(m-1)} - \sum_{i=1}^{N_K^{(m)}} \Delta_{ij}^{(m,b_i)} \tag{4.10}$$

$$\Delta_{ij}^{(m,b_i)} = \begin{cases} 0 & \text{for} \quad m < b_i \\ \alpha_I & \text{for} \quad r_i = R_j, m = b_i \\ \dot{\alpha}_C & \text{for} \quad r < R_i, m > b_i \end{cases} \tag{4.11}$$

$$f_i^{(m)} = \mathcal{H}(m - b_i - 1) \cdot f_i^{(m-1)} + \sum_{j=1}^{N_P^{(m)}} \Delta_{ij}^{(m,b_i)} + \Gamma_i^{(m,b_i)} - \Lambda_i^{(m)} - \Omega_i^{(m,b_i)} \tag{4.12}$$

$$\Gamma_i^{(m,b_i)} = \delta_{mb_i} \left(\sum_{(n,l)\neq(i,i)}^{N_K^{(m)}} a_{in}^{(m)} a_{nl}^{(m)} \frac{f_l^{(m-1)}}{s_l^{(m-1)} + 1} + \sum_{(n)\neq(i)}^{N_K^{(m)}} a_{in}^{(m)} \frac{f_n^{(m-1)}}{s_n^{(m-1)}} \right) \tag{4.13}$$

$$\Lambda_i^{(m)} = \left(\sum_{(n,l)\neq(i,i)}^{N_K^{(m)}} \frac{a_{in}^{(m)} a_{nl}^{(m)}}{s_l^{(m-1)} + 1} \delta_{mb_l} + \sum_{(n)\neq(i)}^{N_K^{(m)}} \frac{a_{in}^{(m)}}{s_i^{(m-1)}} \right) f_i^{(m-1)} \tag{4.14}$$

$$\Omega_i^{(m,b_i)} = \delta_{mb_l} \cdot \epsilon \cdot l_i^{(b_i)} \tag{4.15}$$

α_I and $\dot{\alpha}_c$ are the initial and continuous degradation rate, respectively, and ϵ is the growth costs.

Wood-decay fungi are aerobic organisms producing CO_2, water and energy from wood by respiration. They break lignin by oxidoreductase and the degradation of cellulose and hemicelluloses is predominantly by hydrolases [159]. *P. vitreus*

secretes ectoenzymes, such as laccase, to metabolize lignin. In my model the degradation rate $\Delta_{ij}^{(m,b_i)}$ represents a more mechanistic view of nutrient uptake by the fungus; that is, if a hypha reaches a pit the transport distance of nutrients to the hyphal tip is very short. Thus, in this initial phase we assume that a hyphal tip accumulates specific amounts of nutrients α_I and in a second phase the fungus consumes the nutrients by a constant rate $\dot{\alpha}_c$ (Eq. 4.15).

Transport mechanisms are essential for the growth of filamentous fungi and their hyphae in a mycelial network. The mechanisms of nutrient translocation in fungi have not yet been characterized in detail, but a mixture of mass flow, diffusion, cytoplasmic streaming and specific vesicular transport is observed. To encompass these complex biological processes I introduce simple mechanisms into the model, described by $\Gamma_i^{(m,b_i)}$ and $\Lambda_i^{(m)}$ in Eq. 4.12. This mechanism is inspired by the active translocation of nutrients in the vicinity of tips by bulk flow [66]. The model does not consider anastomosis or diffusion of nutrients because transport processes in mycelia networks of wood-decay fungi are completely unexplored *in situ* and therefore an experimental verification of diffusion in a model for wood-decay fungi is not possible up to now. However, the consideration of diffusion and anastomosis in lattice-free models would be possible as shown by Carver & Boswell [28].

It is assumed that a specific hyphal length supports a tip node. The supporting length corresponds to the adjacent nodes, as well as to the neighbouring adjacent nodes described by terms 1 and 2 in Eqs. 4.13 and 4.14. If the mycelium is extended by one edge at node n, the portion of f_n/s_n nutrients from node n and $f_n/(s_n+1)$ nutrients from the neighbouring adjacent nodes of node n are transferred to the new tip node, where f_n is the amount of nutrients and s_n are the number of tips at node n. At each iteration step m the amount of nutrients transferred to the new node (Eq. 4.13) is equal to the amount of nutrients subtracted from the neighbouring adjacent nodes (Eq. 4.13), thus one has $\sum_{i=1}^{N_K} \Gamma_i^{(m,b_i)} - \Lambda_i^{(m)} = 0$.

The direction of hyphal growth depends on the distance and orientation of the node to the reachable pits. For a hyphal node, all pits within the same tracheids, as well as the pits of adjacent tracheids, can be reached if the pit membrane at the underlying hyphal node is open, that is, degraded by the fungus (Eq. 4.15). After choosing a node (i) according to its polarization every pit (j) fulfilling the

conditions

$$\cos\Theta \leq \frac{c_i \cdot (r_i - r_j)}{\|c_i\| \|r_i - r_j\|} \quad \text{and} \quad \xi \leq \|r_i - r_j\| \tag{4.16}$$

is chosen with the same probability using uniformly distributed random numbers. The model parameters ξ and Θ describe the direction of growth. At first glance, this approach appears too simple, because of the predominantly forward motion of a hypha [154]. However, wood does in fact canalize hyphal growth, because of the directed distribution of the pits and cell walls, which restricts the available nutrients.

Fungi require nutrients in order to elongate their hyphal cells. The growth costs or nutrients used to synthesize a specific number of hyphal cell walls depend linearly on the length of a new edge (Eq. 4.15). The concentration of nutrients $f_n^{(m)}$ in the adjacent node n is then reduced by $\Omega_i^{(m,b_i)}$. The mycelium is extended by one edge if $f_n^{(m)}$ of the nutrients in the adjacent node n is larger than $\Omega_n^{(m,b_i)}$. If $f_n^{(m)} < \Omega_n^{(m,b_i)}$, growth ceases and no edge will be added to node n.

4.1.3 Simulation

The FGM is a sequential algorithm consisting mainly of three stages. At the beginning, the model is initialized and the boundary conditions are set. The simulation starts at iteration step $m = 0$ by defining the initial state of the mycelium. Typically, the mycelium simply consists of nodes placed with a density of n_k^0 on the surface of the wood specimen. These starting nodes, called pellets, imitate the *in situ* infection process, which is normally peformed by placing the wood specimen on a nutrient medium, e.g. a 'feeder block' of Scots pines (*Pinus sylvestris*) or LNA, previously colonized with the fungus. The pellet density n_k^0 is given by the density of the mycelium on the nutrient medium. The starting nodes have a node degree $q_i = 0$, an initial number of tips $s_i = n_s^0$, nutrient concentration $f_i^0 = n_n^0$ and orientation $c_i^0 = n_c^0$. n_s^0, n_n^0 and n_c^0 depend on the incubation conditions. Next, the evolution of the mycelium starts by executing the FGM for as long as the simulation's end is not reached and consists of the following sequential processes. First,

a polarized node ($p_i > 0$) of the mycelium is chosen randomly using uniformly distributed random numbers according to Eqs. 4.5 and 4.6 (polarization). The mycelium is extended by one edge (growth) if pits are available in the vicinity of the chosen node (Eq. 4.16) and the nutrient source is larger than the growing cost (Eq. 4.15) of extending the mycelium to the next pit. Next, the real time increment is calculated according to Eq. 4.9 and all pits underlying a node are degraded according to Eq. 4.10 (uptake and concentration). Subsequently, all nodes are checked if the condition for branching is fulfilled (branching). Finally, it is checked if the simulation's end has been reached and if so, the macroscopic variables are estimated (e.g. the distribution of degraded pits).

4.2 Growth on Petri dish

4.2.1 Introduction

Microorganisms such as wood-decay fungi regulate their metabolism in response to changing environmental conditions. Water activity, temperature and pH are key factors in the growth behavior and development of the fungal mycelium [147]. Understanding the influence of these abiotic factors is relevant for biotechnological applications of wood-decay fungi in particular, e.g. the basidiomycetes *P. vitreus* and *Neolentinus lepideus* in bioincising [165, 98] or bioremediation [115, 122], as well as the morphogenesis of filamentous fungi in general.

Mathematical models in combination with laboratory experiments can investigate in detail the growth behavior of the fungus to enable optimization of biotechnological processes under defined conditions. Filamentous fungi form a complex, tree-like structure termed the mycelium in order to explore their environment. By considering the mycelium as a network, common network measures, such as radial growth rate and the hyphal growth unit, can be applied to study fungal colonies [51].

Recent developments in discrete modelling approaches, in which hyphae are considered as discrete structures, have enabled successful simulation of fungal growth in heterogeneous [21, 18] or even complex physically and chemically structured wood-like environments ([55] and Sec. 4.1). This class of models is not a substitu-

tion for classic modelling approaches such as Response surface (RS) methodology or Radial basis function (RBF) [133, 134, 11, 162, 163, 160, 164], but rather a complementary method of further investigating aspects of hyphal growth at the level of a single colony [31].

The present section investigates environmental effects on the growth of colonies of *P. vitreus* by using a lattice-free discrete modelling approach in which hyphae and nutrients are considered as discrete structures.

4.2.2 Materials and methods

Hyphal growth model

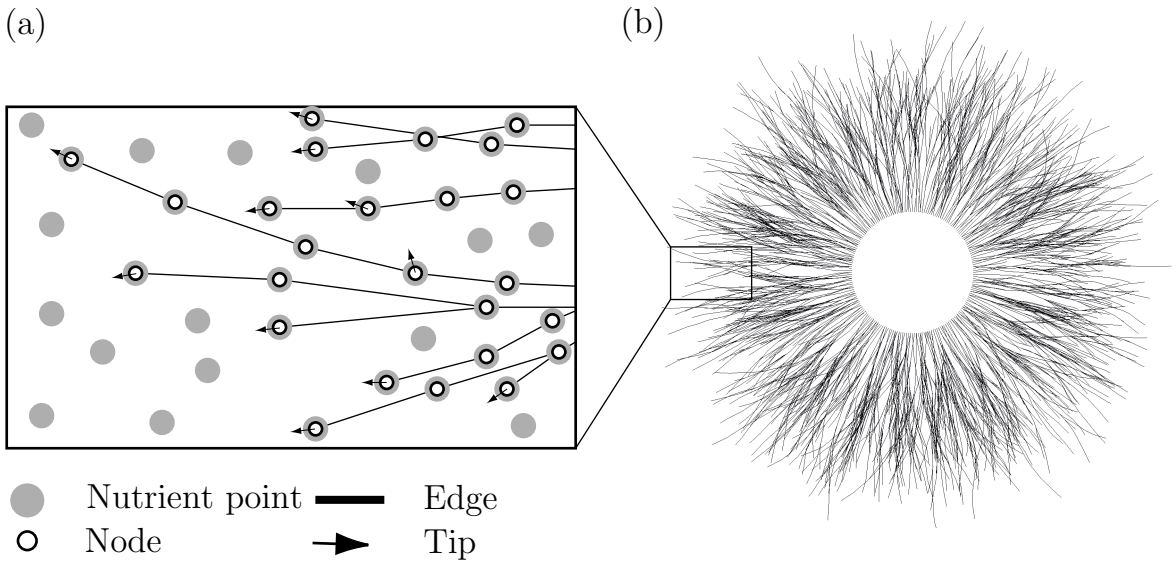

Figure 4.4: Fungal growth model (FGM), which considers hyphae and nutrients as discrete objects. (a) Hyphae are root-like branching structures of the filamentous fungus are represented in the model by edges and nodes. (b) Starting from the initial nodes, the growth of the fungal colony is determined by key processes such as the polarization, branching, uptake and concentration of nutrients and their transport. Details of the model's construction can be found in Sec. 4.1.

In order to analyze the growth of filamentous fungi in a homogeneous environment (e.g. 2% MEA), a 2D version of the hyphal growth model introduced by Fuhr

et al. [55] is used, Sec. 4.1 and Fig. 4.4). The substrate consists of Poisson-distributed nutrient points with ν initial amount of nutrients (Fig. 4.5). Therefore, the probability P of finding k nutrient points in a specific area is given by

$$P(k) = \frac{\omega^k}{k!} e^{\omega}, \tag{4.17}$$

where $\omega > 0$ is a scale parameter of the distribution. The present concept does not consider the diffusion of nutrients. This simplification is acceptable, because the agar of the Petri dish (0.5 mm) is approximately 500 times thicker than the diameter of the hyphae (1 µm) and a lack of nutrient may occur after a long time.

The simulation begins by placing n_k^0 starting nodes, called pellets, with an initial nutrient concentration n_n^0 on a circle with diameter n_d^0 millimeters in the center of a two-dimensional surface $L \times L$. The initial nodes have tips with an orientation normal to the circle's surface. At every iteration step m of the algorithm, the mycelium is extended by one edge of length l_i at node (i) if the nutrient concentration $f_i^{(m)}$ is larger than the required amount of nutrients $\Omega_i^{(m)}$ to maintain and extend a hypha. The simulation ends when all nutrients are depleted or a specific number of time steps is reached.

The maintenance and extension of a hyphal cell involves many physical and biochemical processes, such as mobilization of the nutrients bound up in the tissue (i.e. agar or wood cell walls) into a soluble form by specific enzymes and mediators for uptake, conversion, transport, storage and synthesis to cell wall and other metabolic products. The speed and efficiency of these processes depend on environmental factors and are regulated by the fungus. To encompass the energy consumption of these complex biological processes, we introduced a simple mechanism, called growth costs, into the model. Inspired by the Arrhenius equation [105], the growth costs may be given by the power law

$$\Omega_i^{(m)} = \left(a \cdot \frac{l_i^{(m)}}{\xi} \right)^b \cdot \nu \tag{4.18}$$

where a and b are adjustable factors that depend on water activity and temperature, respectively. ξ is the growth cut-off length and ν is the initial amount of nutrients at each nutrient point [55]. The scaling behavior of the adjustable factors can be estimated by comparing the simulation with laboratory experiments. Typical model parameters are given in Tab. 4.1.

	Parameter	**Value**	**Units**
Substrate			
Box size $L \times L$	L	90	mm
Number of nutrient points	N_p	$1.6 \cdot 10^7$	-
Poissonian distribution ($interval = 2 \cdot \xi$)	ω	2733	-
Fungus			
Mean hyphal growth rate	μ	2.6	mm/day
Mean edge length	λ	$2/3 \cdot \xi$	mm
Growth cut-off length	ξ	10	mm
Growth cut-off angle	θ	0.44	$^\circ$
Growth costs (Eq. 2)	$[a, b]$	[1, 1.5]	-
Pit initial nutrient (*)	ν	1	-
Pit initial degration rate	α_1	$\nu/20$	-
Pit degration rate	α_c	$0.45 \cdot \nu$	1/day
Apical branching threshold	β_t	$0.6 \cdot \nu$	-
Lateral branching threshold	β_s	$0.35 \cdot \nu$	-
Simulation			
Initial number of pellets	n_k^0	200	-
Inital number of pits	n_s^0	1	-
Initial nutrient concentration	n_n^0	$3/2 \cdot \beta_t$	mol
Diameter of inoculum	n_d^0	2	mm

Table 4.1: Typical model parameters used in the present study of *Physisporinus vitreus*. (*) Unit for the nutrients is not defined.

Experimental design

LM is used to calibrate and verify the hyphal growth model. *P. vitreus* EMPA 642 was cultivated on a cellophane-covered Petri dish moistened with 2% MEA. The fungus starts from an inoculum with a diameter of approximately 2 mm. The experiments were performed using a Zeiss 200M (10, 0.5 NA Fluar objective) and wide-field microscopy (WFM) at room temperature and pH 6. The growing colony was observed over a time span of 2.5 hours by taking single images of 1024×1024 pixels (48-bit RGB color) with a resolution of approximately 0.78 µm/pixel. A 3×4 grid of single images was used to construct a mosaic image of 2077×4095 pixels. The stitching of the single images into a mosaic image was performed with the AxioVision software package. The mosaic images were taken with a camera (AxioCamMR3) at intervals of 15 minutes. A radial growth rate of the fungal colony of approximately 2 mm/day is observed, which corresponds to a water activity level of the environment of approximately 0.990 [163].

4.2.3 Results

The combined abiotic factors, temperature, pH and water activity, significantly influence the growth behavior and development of the wood-decay fungus *P. vitreus* [160, 163]. In order to investigate and discuss the underlying mechanism of the growth behavior of the fungus, I calibrated the FGM as the first step in my study (Sec. 4.2.3) by comparing the microscopic growth pattern of the colony *in vitro* and *in silico*. The obtained parameter set can be used to estimate the parameters a and b of Eq. 4.18 by comparing the simulation with the laboratory experiments of Schubert et al. [163] (Sec. 4.2.3). Knowledge of the scaling behavior of these parameters may be useful for simulating the fungus growing in complex structured environments such as wood where the activity of the fungus (i.e. degradation of bordered pits or the creation of bore holes and cavities) changes the local environmental conditions (e.g. the water activity level in a lumen).

Growth pattern

Fig. 4.5(a) shows the growth front of *P. vitreus* measured with WFM and Fig. 4.5(b) shows the corresponding simulation using the parameter set given in Tab. 4.1. The growth fronts of the colonies expanded at room temperature with an approximate radial growth rate G_r of 2 mm/day, which corresponds to a water activity level of 0.990. The hyphal length of the mycelium, the number of active tips and the HGU of the colony front is measured over a time span of 150 minutes (box inset of Fig. 4.5) and the results are presented in Tab. 4.2. Only the front of the colony is considered because identifying the active tips in the core region of the fungal colony is difficult when there are many overlapping layers of mycelium.

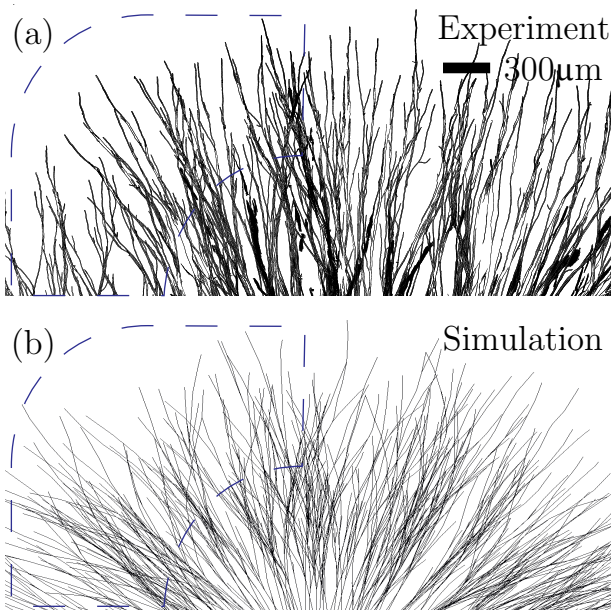

Figure 4.5: Model calibration. In order to calibrate the fungal growth model (FGM), we compared the simulation with laboratory experiments of cultivating *Physisporinus vitreus* on 2% malt extract agar and observing the fungus for 150 minutes using wide-field microscopy. The qualitative comparison of the growth front (a) *in vitro* and (b) *in silico* using the FGM with the parameter set given in Tab. 4.1 showed good agreement. Quantitative comparisons of the total hyphal length of the mycelium, the number of active tips and the hyphal growth unit within the box are given in Tab. 4.2.

	Symbol [unit]	Experiment	Model
Total hyphal length	L_m [mm]	90	96
Number of active tips	N_t [-]	210(±50)	230
Hyphal growth unit	HGU = L_m/N_t [µm]	428(±90)	417
Radial growth rate	G_r [mm/day]	2	2.05

Table 4.2: Quantitative comparison of the experimental and simulation results shown in Fig. 4.5. The evolution of the mycelium is measured *in vivo* over a time span of 150 minutes at a temperature of approximately 20°C, pH 6 and a water activity level of 0.990. These experimental conditions correspond to the fungal growth model using the parameters given in Tab. 4.1.

Radial growth rate

Fig. 4.6 shows the experimental [163] and corresponding simulated radial growth rates measured at different temperatures and evaluated for four levels of water activity: 0.998, 0.990 and 0.982. The simulation using the FGM was performed by fitting the model parameters a and b to water activity and temperature T, respectively. I used a = (0, 0.3, 0.8, 1.2) for the water activity levels (1, 0.998, 0.990, 0.982) and b as a parameter of temperature was defined as

$$b = \tfrac{T-7}{5.75} \quad \text{for} \quad b \in [0, 4]. \tag{4.19}$$

The model shows that G_r increases with higher water activity levels and decreases with lower temperatures. For $a = 0$, the growth costs of the fungus vanish and the maximal growth rate of 4.5 mm/day is observed.

However, the model parameters a can be estimated as function of water activity (a_w) as shown in Fig. 4.8 by

$$a(a_w) = -1.7 \cdot a_w^{65} + 1.7 \tag{4.20}$$

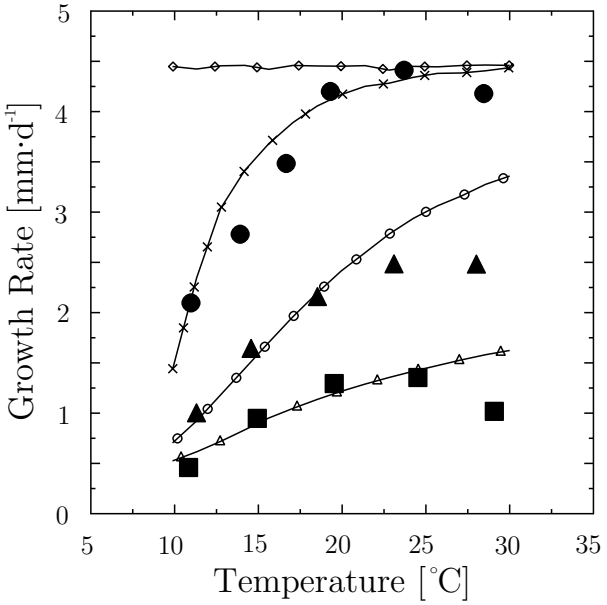

Figure 4.6: Effect of the environment *in vitro* and *in silico*. Response of the fungus to different water activity levels and temperatures at pH 5 are shown. The filled symbols are the laboratory experiments of Schubert et al. [163]; the water activity levels are 0.998 (circle), 0.990 (triangle) and 0.982 (square). The solid lines with the empty symbols are the corresponding simulation of the FGM using $a = (0.0,$ 0.3, 0.8, 1.2) and values of b in the interval [0.2, 4.0]. Each solid line represents the average over 10 realizations and the uncertainty of the data points is within the range of the symbols.

The model parameter a increases with decreasing water activity levels, while the parameter b depends linearly on temperature (Eq. 4.19). Thus, the growth costs are given by combining Eqs. 4.18, 4.19 and 4.20 as

$$\Omega_i^{(m)}(a_w, T) = \left\{ (-1.7 \cdot a_w^{65} + 1.7) \cdot \frac{l_i^{(m)}}{\xi} \right\}^{\frac{T-9}{5}} \cdot \nu \tag{4.21}$$

4.2.4 Discussion

The growth pattern of the fungus *in vitro* and *in silico* shows a good qualitative (Fig. 4.5) and quantitative (Tab. 4.2) agreement. The difference between model and experiment is for all quantities smaller than 10%, but the error of the ex-

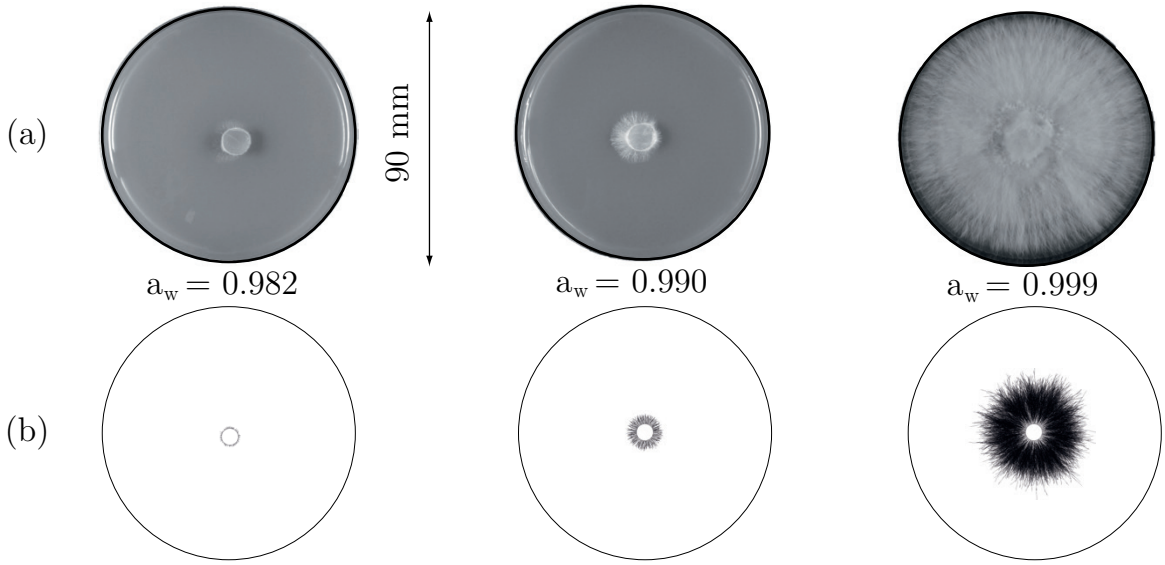

Figure 4.7: Growth pattern. (a) Morphology of Physisporinus vitreus at water activity levels of 0.982, 0.990 and 0.998 from left to right at temperature T = 20°C and pH = 6. (b) The corresponding simulations show the fungal colony after approximately 24 hours of growth using $a = (0, 0.8, 1.2)$ and $b = 2$.

periment is quite large, i.e. approximately 25% and 20% for the number of active tips and the hyphal growth unit respectively (Tab. 4.2). *P. vitreus* has a hyphal growth unit of approximately 420 µm. This estimation is on the upper limit since Trinci et al. [192] measured values between 80 µm (i.e. *Neurospora crassa*) and 320 µm (i.e. *Mucor hiemalis*) under similar conditions. Moreover, we observed that hyphae on the colony front (i.e. the leading hyphae) grew much faster than hyphae in the older part of the mycelium (i.e. primary or secondary hyphae). Such behavior has been reported for many species [27]. The ratio of the velocities of these classes of hyphae is approximately 5/1. This effect may be represented in the FGM as a lack of nutrients in the core of the colony.

The radial growth rate of *P. vitreus* is mainly effected by the water activity and temperature [163] as shown in Fig. 4.6. Thereby the underlying dynamics of the FGM is driven by the power law of Eq. 4.18. Close to the growth/no growth interface, which is above $a = 2.5$, the FGM shows a poor accuracy, which was also observed by Schubert et al. [163] using RS. In addition, above approximately $a = 6.4$ there was no growth observable within a day, because the growth costs, even for small hyphal lengths (i.e. ~ 0.16), are higher than the available nutrients at a nutrient point. At between 10°C and 25°C the model shows a good agreement

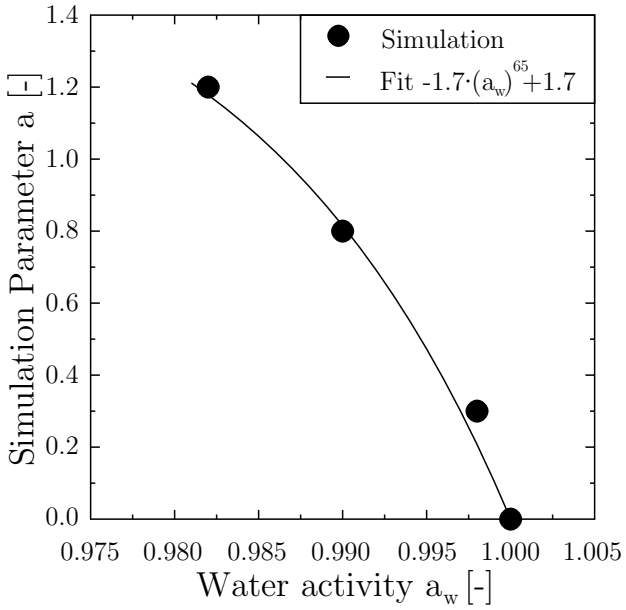

Figure 4.8: Parameter estimation. The model parameter a decreases with increasing water activity level.

with quantitative (Fig. 4.5) and qualitative laboratory experiments (Figs 2 and 4). *P. vitreus* may have its optimum temperature for growth at 25°C, which can be explained by the existence of an ecological niche for this species at this temperature, and hyphal growth may be regulated by the fungus. The effect of such regulation above 25°C was not incorporated in my model.

Furthermore, other approaches may perform better in predicting specific growth rates. For example, using a RBF neural network, Schubert et al. [163] found that the growth of *P. vitreus* mainly depends on the water activity level (0.950 - 0.998) and temperature (10 - 30°C), while pH (4 - 6) affected the growth rate to a lesser extent. Despite this success, RBF is unable to explain the underlying mechanistic rules concerning the basic architecture and dynamics of fungal networks on the scale of a single colony, e.g. either on Petri dishes or in wood. In such a situation, discrete modelling approaches such as the FGM are the methods of choice.

The influence of wood-decay fungi on the microclimate of their substrate is not well known, because wood is an opaque material and experimental observation of the living fungus on a microscopic scale is difficult. Laser scanning microscopy or synchrotron radiation tomography are experimental tools for the non-destructive, three-dimensional investigation of the interaction between wood and fungus [55, 187, 58], but they are very time- and cost-intensive and often the size of the

specimens is limited. The present framework, which is a combination of laboratory experiments and FGM, offers the possibility of investigating complex interactions by measuring the growth *in vitro* (on Petri dishes) and simulating the fungus growing in wood-like substrates, whereby the response of each single hypha to its microclimate in a lumen (i.e. water activity and temperature) is taken into account by the growth costs (Eq. 4.18). I have to remember that Petri dishes are not the natural habitat of wood-decay fungi, but their response to environmental factors may happen in a wood in a similar way. However, the FGM is able to simulate the growth and impact of wood-decay fungi both on Petri dishes and in wood (Sec. 4.4). Thus, for the first time, an investigation of environmental factors on the growth of wood-decay fungi on the colony scale in different environments (i.e. wood and Petri dishes) by the same model is possible.

4.2.5 Summary

The present section analyzed the combined effect of temperature, pH and water activity on the radial growth rate of *P. vitreus* in a homogeneous environment using a two-dimensional hyphal growth model that considers both hyphae and nutrients as discrete structures. The simulations show good qualitative and quantitative agreement with the experimental results.

It is shown that the combined effect of temperature, pH and water activity on the radial growth rate of a fungal colony may be explained by growth costs for hyphal expansion at the microscopic level, as described by the power law of Eq. 4.21. The presented model is limited to a temperature range between 5°C and 25°C and a water activity between 0.982 and 1, which are generally known boundaries of many basidiomycetes. The results have significance for the biotechnological application of *P. vitreus* in processes such as bioincising [170], as well as for the study of filamentous fungi in general. The concept of growth costs, which includes the energy consumption of processes such as the mobilization of nutrients, their uptake, conversion, transport, storage and synthesis to cell wall and other metabolic products, can be used as a tool to simulate the growing fungus in a heterogeneous environment with a distinct microclimate (e.g. a porous substrate such as wood). In such a simulation, the response of each single hypha to its microclimate is taken into account by the growth costs (Eq. 4.21). Therefore,

future studies will focus on modelling the growth of *P. vitreus* in heterogeneous and physically structured two-dimensional wood-like environments.

4.3 Penetration capacity

4.3.1 Introduction

The primary goal of a modelling framework for the optimization of bioincising is to analyse the influence of biotic and abiotic factors on the wood's permeability, which is in combination with the wood's strength the quality criterion of bioincised wood (i.e. a higher permeability results in a higher treatability of the wood). Thereby, the chemical composition (i.e. environmental factors such as the water activity, temperature and type of medium) and the physical structure (i.e. the distribution of tracheids and pits) of the resource determine the penetration behaviour of a wood-decay fungus as shown in Fig. 4.1. Using the FGM previous studies analyzed the metabolism of *P. vitreus* [58] and the effect of the wood tissue on its growth [55], whereas the penetration behaviour was not studied in detail up to now (Fig. 4.1). Thus, the focus of this section is to study the rule of the bordered pits in order to obtain a complete modelling framework covering all relevant effects for the optimization of the permeability of bioincised wood samples.

The degradation of the bordered pit membranes in their first stage of growth seems to be a common strategy of wood-decay fungi to colonize softwoods [110, 37, 70, 69, 169], because the size, structure and distribution of bordered pits is a significant factor for the accessibility of wood tissue both for fluids and fungal hyphae [147]. The time required by a hypha to penetrate through a bordered pit either by the support of pressure or enzymes (i.e. pit penetration time) obviously influences the ability of the mycelium to colonize a refractory wood such as Norway spruce heartwood. Understanding the penetration behavior of wood-decay fungi is of interest for their biotechnological use, e.g. the white-rot fungus *P. vitreus* can be used to improve the permeability of refractory wood species [170, 98], as well as for the study of wood-decay fungi in general.

The material is presented in three parts. In a first step we discuss the growth

pattern of *P. vitreus* using the FGM and laboratory experiments (Figs. 4.22 and 4.25). In a second step we use an analytical model to analyze the penetration velocity of *P. vitreus*, in order to quantify the key factors determining the growth and expansion of the mycelium in wood modeled by the FGM (Fig. 4.13). Moreover, such an analytical model enables us to discuss various mode of pit penetration by *P. vitreus*, i.e. pit penetration by pressure or enzymes (Tab. 4.4). However, the analytical model does not provide information about impact of *P. vitreus* to the wood tissue, e.g. the distribution of degraded pits, and therefore the FGM is finally to discuss the penetration work and the penetration capacity of *P. vitreus* (Figs. 4.14(a) and 4.14(b)).

4.3.2 Materials and methods

Specimen material

The white-rot basidiomycete *P. vitreus* EMPA 642 was cultivated in 9 cm Petri dishes on 2% MEA at 23°C and 70% RH. After 2 weeks defect free and sterilized (121°C, 20 min and 200 kPa vapour pressure) Norway spruce samples are with a size of approximately 10 mm (longitudinal) × 2 mm (radial) and 10 mm (tangential) are placed on the mycelium. The faces of the samples, with the exception of one radial tangential face, were sealed with a topcoat (Nuvovern ACR Emaillack, Walter Mäder AG, Killwangen, Switzerland) by brushing, so that the *P. vitreus* colonized the wood via the unsealed side in longitudinal direction (Fig. 4.9(a)).

Light microscopy

After 10 days of incubation at 23°C and 70% RH I cut thin sections of approximately 30 µm thickness from the wood samples using a microtome as shown in Fig. 4.9(b). I stain the fungus with lactophenol blue, take mosaic images with a pixel size of approximately 0.65 µm × 0.65 µm using a Zeiss LSM 510-NLO (Fig. 4.9(c)) and analyze the images by digital image processing (Fig. 4.9(d)).

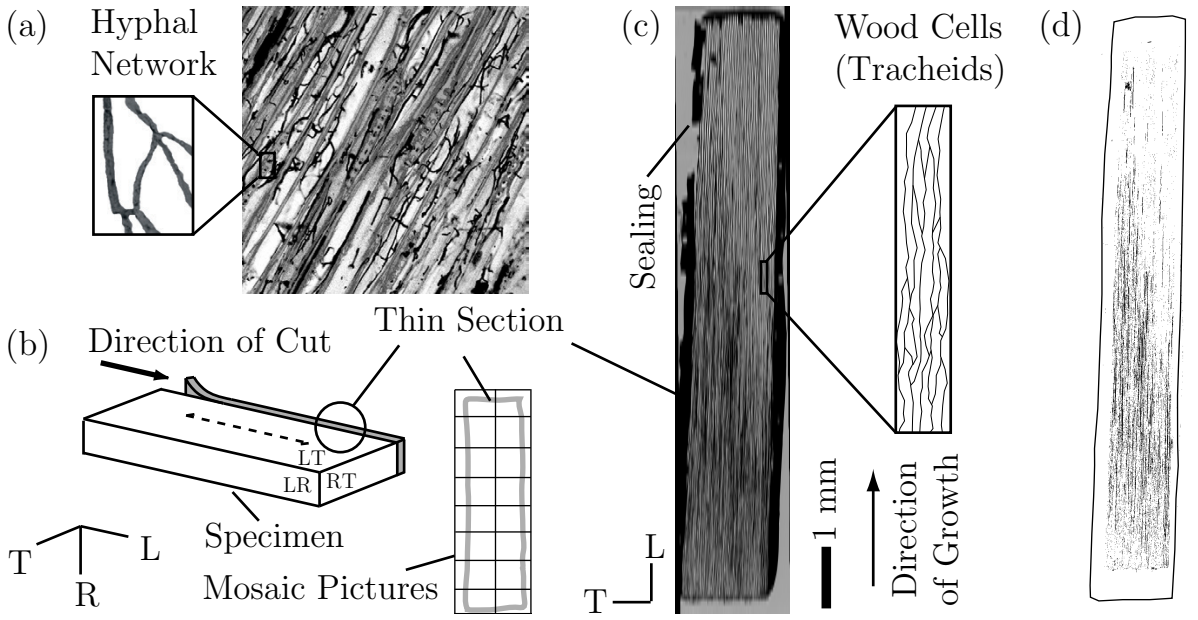

Figure 4.9: Light Microcopy: (a) Wood-decay fungi exploit a wood tissue by forming a network (mycelium) consisting of filaments (hyphae), which are visible under the light microscopy. (b) Mosaic pictures of (c) thin sections enable the analyzation of the mycelium's morphology by image processing (d).

Hyphal growth model

Inspired by the approach of Comstock [32] and Siau [173] I model the Norway spruce tracheids as elongated rectangles with tapered ends. The shape of the tracheids is determined by their length l_L, width l_T and the length of the overlapping zone l_O (Fig. 4.10(a)) where most of the bordered pits are located [176]. These pits play an important role in the growth strategy of many wood-decay fungi [110, 37, 70, 69, 169], because they are the shortest path for a wood-decay fungus in longitudinal direction as shown by the dotted line in Fig. 4.10(a). The nutrient points are randomly uniformly distributed along the cell walls of the tracheids with the density ρ mm^{-1}.

The simulation starts by placing n_k^0 starting nodes, called pellets, with an initial nutrient concentration n_n^0 on the longitudinal face of the wood specimen (Fig 4.10(a)). All pits are initially closed (i.e. $F_j > \kappa$). Typical model parameters used throughout this section are given in Tab. 4.3. The unit of the resource which sustains fungal growth, called pit nutrient, is given in micrometer (µm), because I prefer to express the fungal activity (Eq. 4.31) with a measure, which is observable

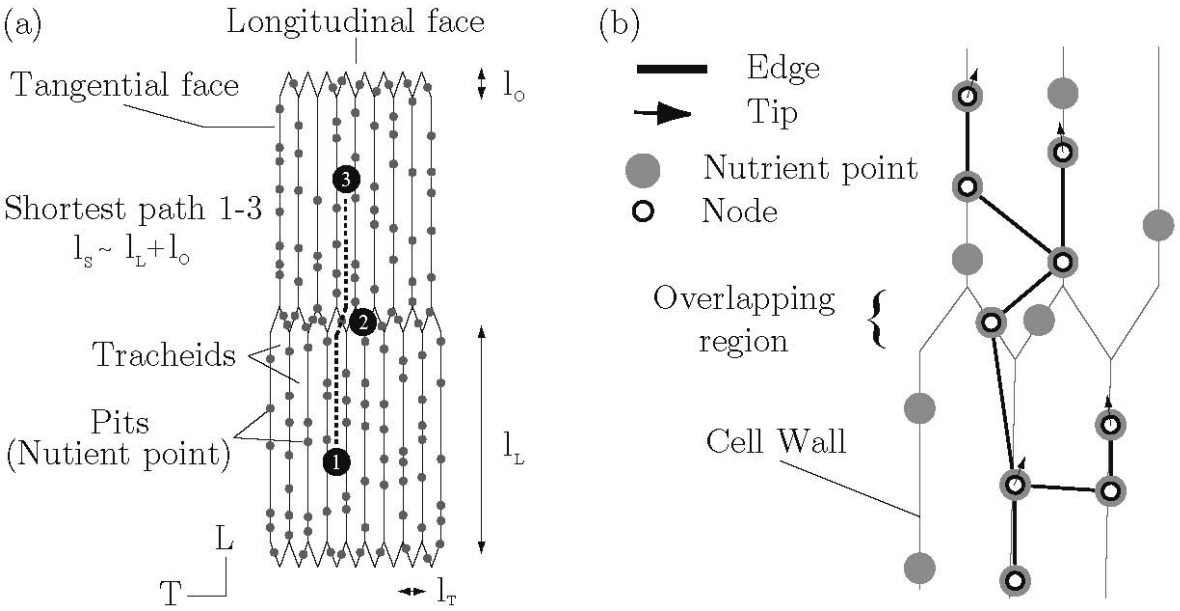

Figure 4.10: Model description. (a) A longitudinal-tangential section of Norway spruce wood is characterized by the cellular structure of the tracheids. The principal directions of wood are usually termed as longitudinal, radial and tangential, denoted by the letters L, R and T. The pits are the substrate for the fungus (i.e. nutrient points) and distributed with a density ρ on the substratum of the fungus (i.e. tracheid cell walls) by using uniform random numbers. (b) The mycelium is modeled as an assemblage of edges, nodes and tips. The evolution of the mycelium is characterized by a pit-to-pit growth of the fungus. Details about the model construction can be found in Sec. 4.1 and in Fuhr et al. [55].

in laboratory experiments, e.g. holes in the torus of the bordered pits (directly) or a permeability (indirectly).

Analytical growth model

The shortest time T_s of a hypha to growth in longitudinal direction from a tracheid into an adjacent one, indicated in Fig. 4.10(a) by the dotted line, may be given by

$$T_S^{1-3} = \frac{l_S}{2 \cdot \mu_{12}} + \frac{l_S}{2 \cdot \mu_{23}} + \tau, \tag{4.22}$$

	Parameter	Value	Units
Wood			
Tracheids	$[l_L, l_T, l_O]$	[2.5, 0.08, 0.04]	mm
Number of nutrient points	ρ	40	$l \cdot \mathrm{d}^{-1}$
Diameter of bordered pit	D	10	µm
Fungus			
Mean hyphal growth rate	μ	1	$l \cdot \mathrm{d}^{-1}$
Mean edge length	λ	$2/3 \cdot \xi$	l
Growth cut-off length	ξ	0.125	l
Growth cut-off angle	θ	90	$^\circ$
Growth costs (Eq. 2)	$[a, b]$	[0, 0]	-
Pit initial nutrient $(\cdot)$	ν	D	-
Pit initial degration rate	α_I	0	-
Pit degration rate	α_c	4	$\mu\mathrm{m} \cdot \mathrm{d}^{-1}$
Apical branching threshold	β_t	$0.6 \cdot \nu$	-
Lateral branching threshold	β_s	$0.35 \cdot \nu$	-
Simulation			
Initial number of pellets	n_k^0	60	-
Inital number of pits	n_s^0	1	-
Initial nutrient concentration	n_n^0	$3/2 \cdot \beta_t$	-

Table 4.3: Typical model parameters used in the present section.

where μ_{ij} is the growth velocity of a hyphae (i.e hyphal growth rate) within a tracheid, l_S is the length of the shortest path and τ is the pit penetration time, i.e. the time of a hypha to growth through a bordered pit. Generally, there are two modes of pit penetration by a hypha. In the first case the torus is eroded by enzymes, e.g. *P. vitreus* [81], whereas in the second case a hypha breaks through the torus by mechanical pressure, e.g. blue stain fungi [110], which is typically indicated by cracks in the torus.

For the first case we may write for the pit penetration time

$$\tau^{(1)} = \frac{D \cdot \kappa}{\dot{\alpha}_c}, \tag{4.23}$$

where D is the diameter of a bordered pit and $\kappa \in [0, 1]$ is an opening threshold. Thus, $D \cdot \kappa$ is the diameter of a hole, which is prerequisite for a vegetative hypha to penetrate through the torus. $\dot{\alpha}_c$ is the pit degradation rate, given in $\mu m \cdot d^{-1}$, to dissolve the torus. The upper case number indicates the mode of pit penetration.

For the second case, the pit penetration by pressure, It is assumed that the fungus bores a hole in the torus by a constant rate $\dot{\alpha}_p$, i.e. the diameter of a hole in the torus after t days is given by

$$\delta(t) = \dot{\alpha}_p \cdot t. \tag{4.24}$$

Bardage & Daniel [5] found that the ability of fungi to penetrate micropores depends on time, i.e. smaller pores cause longer penetration times. They reported penetration times between 1 and 10 days for micropores of size 0.6 - 0.2 µm, whereby no fungus was able to penetrate micropores smaller than 0.2 µm within 15 days (Fig. 4.11). Based on these experiments, it is assumed that the relation between the diameter of a hole d and the penetration time t is roughly given by the power law

$$\frac{t}{t_{max}} = \beta_1 \left(\frac{d}{d_{max}} \right)^{\beta_2} \tag{4.25}$$

using $t_{max} = 10$ d and $d_{max} = 0.6$ µm as shown in Fig. 4.11. Therefore, the diameter of a hole after $\tau^{(2)}$ days (Eq. 4.24) is equal to a hole, which is prerequisite for penetration after $\tau^{(2)}$ days (Eq. 4.24 solved for d), i.e.

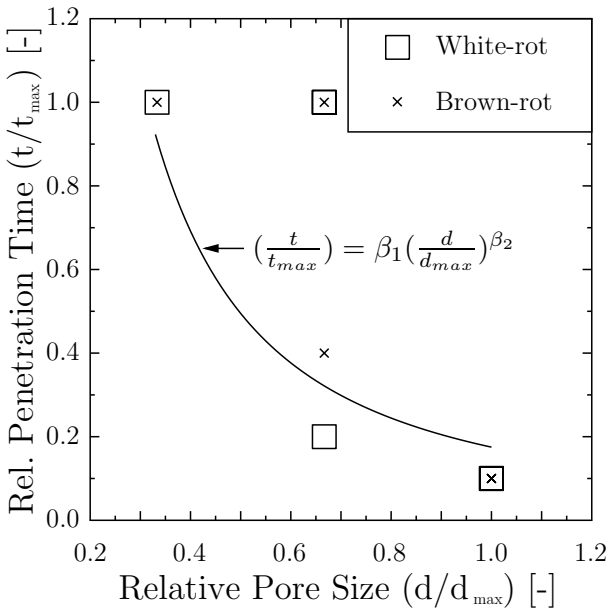

Figure 4.11: Penetration Time: Pore size plotted versus penetration time of wood-decay fungi using $d_{max} = 0.6$ µm and $t_{max} = 10$ days. The solid line represents $\beta_1 = 0.175$ and $\beta_2 = -1.5$. Experimental data reproduced after Bardage&Daniel[5].

$$\dot{\alpha}_p \cdot \tau^{(2)} = d_{max} \cdot \left[\frac{1}{\beta_1} \left(\frac{\tau^{(2)}}{t_{max}} \right) \right]. \tag{4.26}$$

Solving Eq. 4.13 for the penetration time $\tau^{(2)}$ gives

$$\tau^{(2)} = \left[\frac{d_{max}}{\dot{\alpha}_p} \left(\frac{1}{\beta_1 \cdot t_{max}} \right) \right]^{\frac{1}{1-\beta_2}}. \tag{4.27}$$

Penetration velocity, work and capacity

For biotechnological applications of wood-decay fungi it is important to understand their capability to penetrate into a specific direction of a wood tissue by a certain amount of time. Therefore, the penetration velocity of a fungus (or hypha) is defined as

$$v_f = \frac{\text{Penetration depth}}{\text{Time}}. \tag{4.28}$$

Furthermore, the penetration work of a fungus is defined as

$$W_Q = \text{Quantity} \cdot \text{Penetration Depth}, \tag{4.29}$$

where the subscript letter Q denotes denotes a quantity of interest, e.g. the total hyphal length of the mycelium, the total number of open pits or the mass loss of the wood. In addition, I propose the penetration capacity of a fungus as

$$\Pi_Q = \frac{\text{Penetration Work}}{\text{Time}}. \tag{4.30}$$

Obviously, the penetration capacity of a fungus strongly depends on factors such as temperature, water activity and pH, the microclimate and the presence of wood preservatives etc., since wood decay-fungi are sensitive to their environment. The scalar Π_Q may figure as a measure for the efficiency of a specific fungus to colonize a certain wood tissue.

For simplicity, throughout this work, the terms 'penetration work' and 'penetration capacity' are used for the specific penetration work and penetration capacity using the total amount of degraded pit nutrients as quantity of interest.

4.3.3 Results

Growth pattern

After 10 days of incubation it is observed that the fungus starting from the unsealed longitudinal face penetrated approximately 10 mm into the wood sample (Fig. 4.9(d)). This corresponds to a penetration velocity of approximately 1

$\mathrm{mm} \cdot \mathrm{d}^{-1}$. The morphology of the growth front is characterized by hyphae growing at different rates (i.e. leading hyphae). The density of the mycelium at the unsealed end is much higher than on the growth front. We measure that a hypha crosses 3-4 tapered ends from the unsealed to the opposite face.

Fig. 4.12 shows the evolution of the mycelium over a time span of 36 hours for κ = 0.5 and 1.0 (see Eq. 4.2) using the model parameters of Tab. 4.3. The system consists of 20 tracheids with totally 1070 pits. The fungus starts growing form the left longitudinal face and fixed boundaries are imposed to all faces. For κ = 1.0 the fungus grows without any resistance by the pit membranes and after approximately 32 hours the first hypha reaches the longitudinal face on the right side, whereas the fungus requires in the second case (i.e. $\kappa = 0.5$) approximately 42 hours for the same distance. The total hyphal length of the mycelium is approximately 130 mm for both conditions, whereas the number of tips is about 350 and 500 for $\kappa = 1.0$ and 0.5 respectively. In addition, the model shows that for $\kappa = 0.5$ *P. vitreus* requires about 15% more nutrients in order to reach the right longitudinal face.

Penetration velocity

Fig. 4.13 shows the velocity of the mycelium v_f (Eq. 4.28) evaluated for hyphal growth rates between 0.5 and 5 $\mu\mathrm{m} \cdot \mathrm{d}^{-1}$ and pit degradation rates between 0.5 and 4 $\mu\mathrm{m} \cdot \mathrm{d}^{-1}$ (Eq. 4.23) using the model parameters of Tab. 4.3 and the tracheid framework of Fig. 4.10(a). The system consists of 2 (longitudinal) $\times$ 10 (tangential) tracheids and fixed boundaries are imposed to all faces. The fungus starts growing from the lower longitudinal face and the velocity is evaluated by measuring the time of the mycelium between the points 1 and 3.

It is observed that the higher hyphal growth rates μ and higher pit degradation rates $\dot{\alpha}_c$ result in higher growth velocities v_f of the mycelium. According to Eq. 4.22 and 4.28 the velocity of the mycelium is given by

$$v_f = \frac{L_S}{T_{13}} = \frac{L_S}{\frac{L_S}{2}(\frac{1}{\mu_{12}} + \frac{1}{\mu_{23}}) + \tau}. \tag{4.31}$$

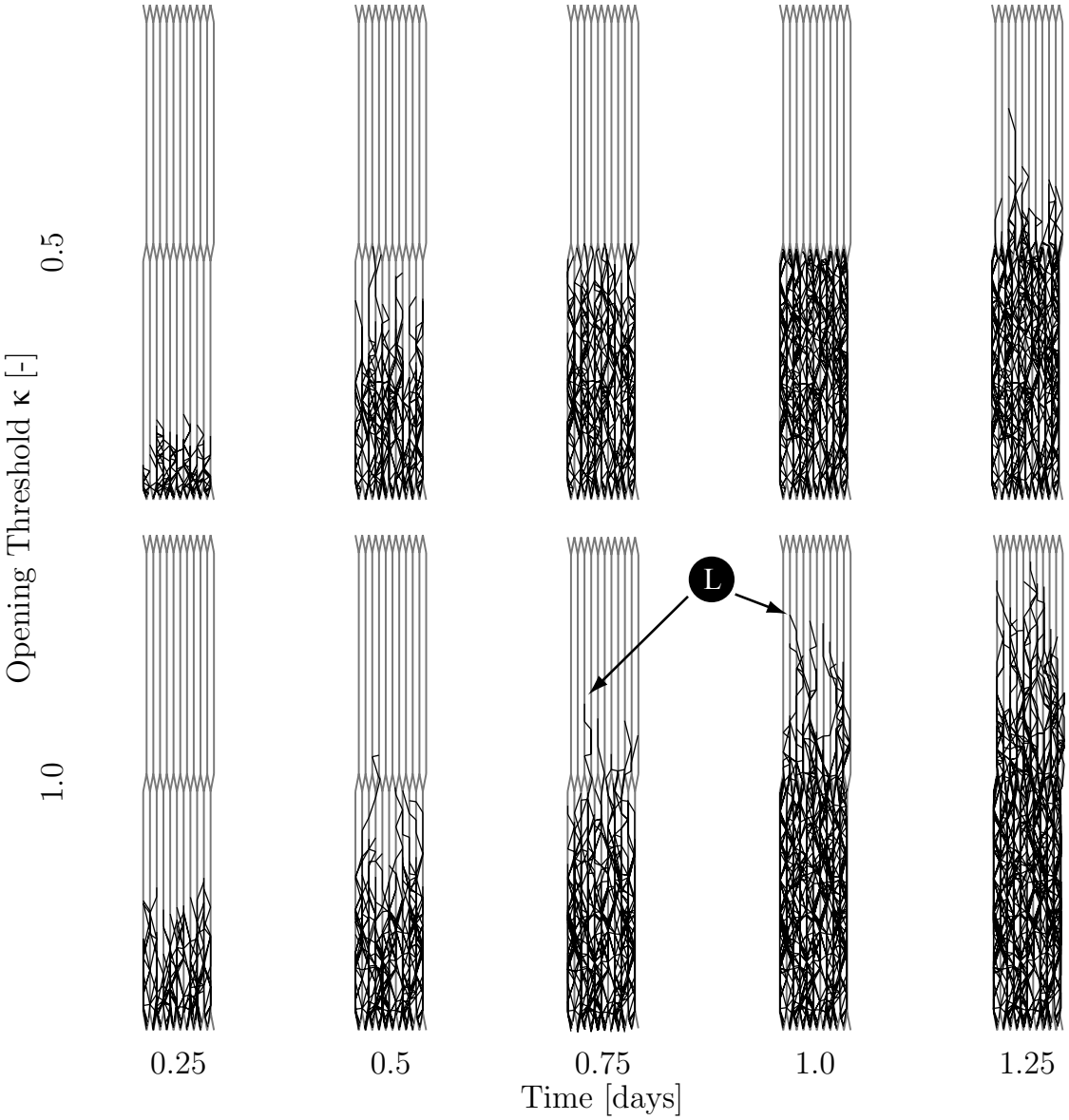

Figure 4.12: Growth pattern. The evolution of the mycelium starts from the left longitudinal face by using the model parameters given in Tab. 4.3. Fixed boundaries are imposed to all faces. The fungus reaches the right longitudinal face after approximately 32 and 42 hours for $\kappa = 1.0$ and 0.5 (Eq. 4.2) respectively. The letter L denotes leading hyphae.

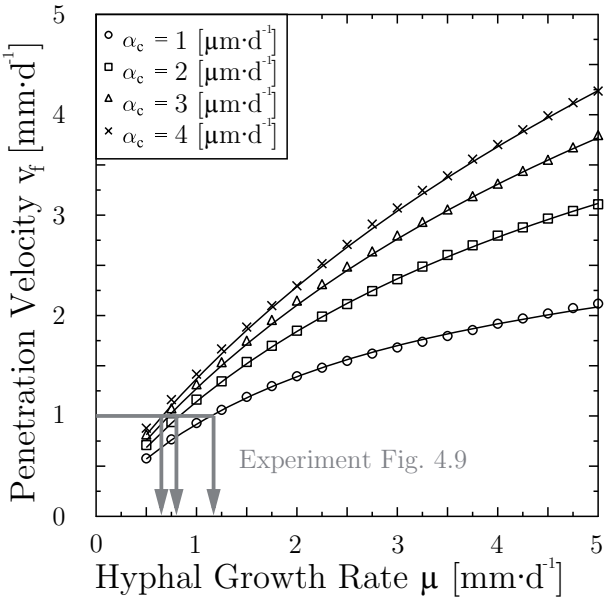

Figure 4.13: Penetration velocity. The hyphal growth rate μ plotted versus the growth velocity (Eq. 4.28). The symbols represent simulations for $\dot{\alpha}_c = 1$, 2, 3 and 4 $\mu\mathrm{m} \cdot \mathrm{d}^{-1}$ using the parameters of Tab. 4.3 and the tracheid framework of Fig. 4.10(a). The solid lines are the corresponding analytical models (Eq. 4.31) using Eq. 4.32 - 4.35 and $N_t = 2.65$, $p = 0.5$ and $q = 3$. Each symbol represents the average over 1000 realizations and the uncertainty of the data points is within the range of the symbols.

I assume that the hyphal growth rate of the leading hypha (Fig. 4.10) before (μ_{12}) and after (μ_{23}) the overlapping area are faster than the rest of the mycelium by a factor μ^* and $q \cdot \mu^*$ respectively. In addition, the penetration time depends on the number of nodes per pit N_t, i.e. the more nodes per pit the higher the pit degradation. We may write for the pit penetration time τ, the hyphal growth rate μ_{12} and μ_{23} and the factor μ^*

$$\tau = \frac{\tau^{(1)}}{N_t} = \frac{D \cdot \kappa}{N_t \cdot \dot{\alpha}_c}, \tag{4.32}$$

$$\mu_{12} = \mu + \mu^*, \tag{4.33}$$

$$\mu_{23} = \mu + q \cdot \mu^*, \tag{4.34}$$

$$\mu^* = N_t \cdot \dot{\alpha}_c \cdot \left(\mu \cdot \frac{\tau}{L_S} \right)^p. \tag{4.35}$$

The solid lines in Fig. 4.13 show Eq. 4.31 using Eq. 4.32 - 4.35 and $N_t = 2.65$, $q = 3$ and $p = 0.5$. The velocity of 1 $\mathrm{mm \cdot d^{-1}}$ measured from the experiment of Fig. 4.9(d) corresponds approximately to hyphal growth rates μ ($\dot{\alpha}_c$) = 0.66 (4), 0.73 (3), 0.84 (2) and 1.14 (1) $\mathrm{mm \cdot d^{-1}}$. The pit degradation rates $\dot{\alpha}_c$ = 1, 2, 3 and 4 $\mathrm{mm \cdot d^{-1}}$ correspond to pit penetration times $\tau^{(1)}$ = 2, 1, 0.67 and 0.5 days (Eq. 4.32) and pit degradation rates by pressure $\dot{\alpha}_p$ = 7.86, 1.39, 0.5 and 0.25 $\mathrm{mm \cdot d^{-1}}$ as shown in Tab. 4.4.

Pit penetration time [d]	**Pit degradation rate** [$\mu\mathrm{m \cdot d^{-1}}$]	
τ	$\dot{\alpha}_c$ ($\kappa = 0.2$)	$\dot{\alpha}_p$ ($\beta_1 = 0.175, \beta_2 = -1.5$)
0.5	4	7.86
1	3	1.39
1.5	2	0.5
2	1	0.25

Table 4.4: Pit degradation rates $\dot{\alpha}_c$ (enzymatic, Eq. 4.23) and $\dot{\alpha}_p$ (pressure, Eq. 4.27) evaluated for the pit penetration times $\tau = \tau^1 = \tau^2 = 0.5$, 1, 1.5 and 2 days.

Penetration work and penetration capacity

Fig. 4.14(a) and Fig. 4.14(b) show the penetration work W_N (Eq. 4.29) and the penetration capacity Π_N (Eq. 4.30) of *P. vitreus* measuring as quantity Q the amount of degraded nutrients using same simulation setup as in Fig. 4.13. It is observed that the penetration work decreases with increasing hyphal growth rates, whereas the penetration capacity increases with increasing hyphal growth rates. In addition, higher pit degradation rates results in a higher penetration work and penetration capacity.

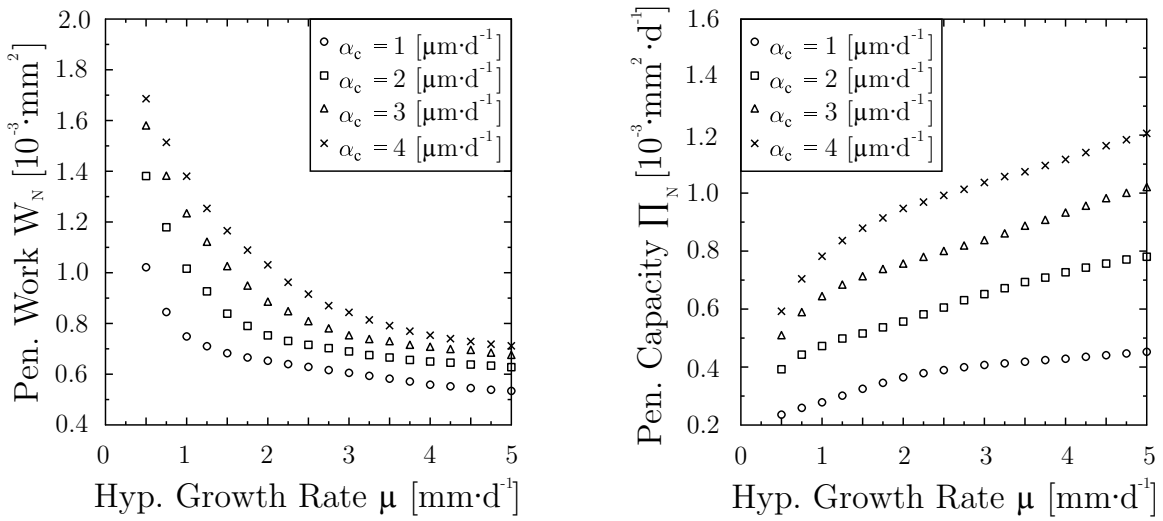

(a) (b)

Figure 4.14: The hyphal growth rate μ plotted versus (a) the penetration work (Eq. 4.29) and (b) the penetration capacity (Eq. 4.29) of *P. vitreus*. The symbols represent simulations for $\dot{\alpha}_c$ = 1, 2, 3 and 4 mm · d^{-1} using the same simulation setup as in Fig. 4.13. Each symbol represents the average over 1000 realizations and the uncertainty of the data points is within the range of the symbols.

4.3.4 Discussion

The growth of *Physisporinus vitreus*

The penetration behavior of *P. vitreus* into Norway spruce heartwood is supposed to be characterized by a stepwise capture of a wood tissue [55], because the aspirated and lignified bordered pits hinder the expansion of the mycelium (Fig. 4.9). Only the degrading of either the bordered pits or the cell wall enables the fungus to growth from one tracheid to another. Thereby the ratio between the velocity of the hypha within the tracheids (i.e. hyphal growth rate) and the pit degradation rate is of interest, because this ratio influences the density of the mycelium, the number of tips in the system and the penetration velocity of the growth front as shown by simulations (Figs. 4.12 and 4.13).

Penetration velocity

The FGM assumes that the hyphal growth rate (μ) and the pit degradation rate ($\dot{\alpha}_c$) are the key factors for the colonization of Norway spruce wood in its first stage of growth. Using the analytical model (Eq. 4.31) we are able to quantify the influence of both factors on the penetration velocity of *P. vitreus*. The results suggest that a doubling of the hyphal growth rate enables *P. vitreus* to reduce the pit degradation rate by a factor of four (Fig. 4.13), in order to reach a penetration velocity of 1 $\mathrm{mm \cdot d^{-1}}$ (Fig. 4.9(d)). The hyphal growth rate is mainly influenced by the water activity, temperature and pH [163], whereas the effect of environmental factors on the ability of *P. vitreus* to penetrate the bordered pits is unknown. Thus, changing the incubation conditions offers an optimization of the bioincising process (see section 'Optimization of bioincising' below).

The measured hyphal growth rates between approximately 0.5 and 1.5 $\mathrm{\mu m \cdot d^{-1}}$ (Fig. 4.13) are in good agreement with *in vivo* experiment of *P. vitreus* at standard conditions (C. Stührk, oral communication) and therefore confirm the model assumptions. It is possible to estimate for the first time the pit degradation rate of *P. vitreus*. The simulations in combination with laboratory experiments show that the pit degradation rates ($\dot{\alpha}_c$ and $\dot{\alpha}_p$) are approximately 1 to 4 and 0.3 - 8 $\mathrm{\mu m \cdot d^{-1}}$ for a penetration either by enzymes or pressure (Tab. 4.4).

Optimization of bioincising

A discrete modelling approach is used to study the biotechnological process of bioincising, because such a model provides information about the impact of *P. vitreus*, e.g. the amount of degraded pits, and therefore enables an optimization of the bioincising process. For example, the simulation shows that, an increase of the hyphal growth rate from 1 to 2 $\mathrm{\mu m \cdot d^{-1}}$ results in an increase of the growth velocity of the mycelium from 0.8 to 1.75 $\mathrm{\mu m \cdot d^{-1}}$ and an increase of the penetration capacity from 0.5 to 0.6 $\mathrm{mm^2 \cdot d^{-1}}$ using a pit degradation rate of 2 $\mathrm{\mu m \cdot d^{-1}}$ (Figs. 4.13 and 4.14). A penetration capacity of 0.5 to 0.6 $\mathrm{mm^2 \cdot d^{-1}}$ indicates that, for the tracheid framework given in Fig. 4.10(a), the growth front of the mycelium penetrating 1 $\mathrm{mm \cdot d^{-1}}$ into the wood degrades approximately 0.5 to 0.6 micrometer pit membranes in total, which is a measure for the permeability

of the wood [55]. Moreover, the penetration capacity may figure as a measure for the efficiency of wood-decay fungi to colonize wood, since a high pit degradation rate may facilitate the capture of their resource. Thus, it would be interesting to measure and compare various penetration capacities from several wood-decay fungi, e.g. choosing as quantity of interest the biomass, amount of degraded pits or permeability.

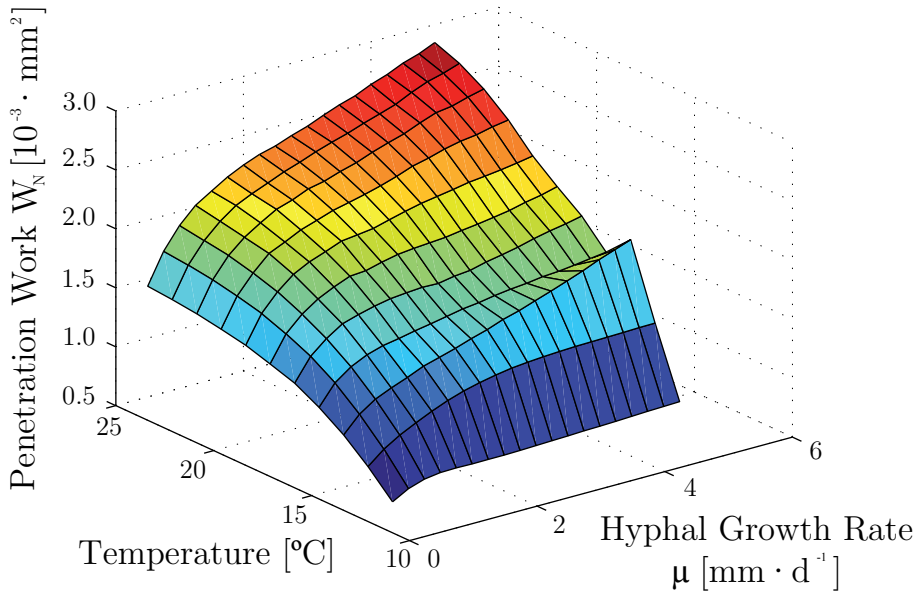

Figure 4.15: The hyphal growth rate μ plotted versus the penetration work (Eq. 4.29) evaluated for temperatures between 12.5 and 25°C a water activity level of 0.990 using the simulation setup of Fig. 4.13 and $a = 0.3$ [58]. Each point represents the average over 1000 realizations and the uncertainty of the data points is less than 0.1 W_N

The last step would be an optimization of bioincising on a larger scale using the modelling framework as described above. On a macroscopic scale, the influence of the distribution of the fungal inoculum on the surface of wood blocks is of interest, because the penetration velocity of *P. vitreus* in radial (i.e. rays) and longitudinal (i.e. tracheids) direction is much higher than in tangential direction. Thus, combining environmental factors with the distribution of the pellets on the wood surface will assist the design of incubation conditions that are required to induce a certain degree of wood permeability by *P. vitreus*. However, this final step of optimization is difficult, for two main reasons. First, a careful validation

of the model assumption on this scale is very time- and cost intensive, e.g. using CLSM [187]. Second, modelling the growing fungus on larger time scales requires the implementation of processes such as anastomosis, autolysis of fungal cells or the degradation of the wood cell walls. Such additional parameters increase the complexity of the FGM and may hinder an efficient optimization of the bioincising process.

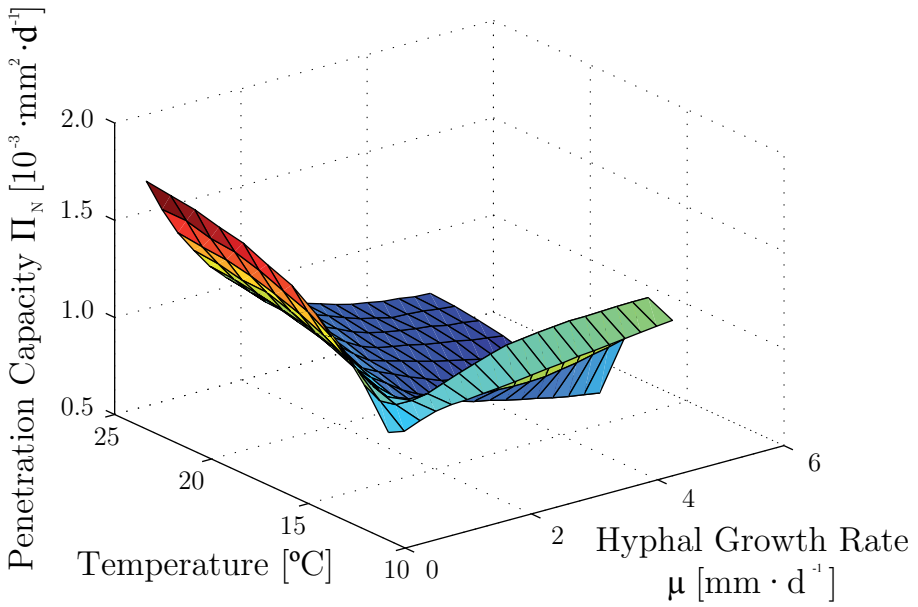

Figure 4.16: The hyphal growth rate μ plotted versus the penetration capacity (Eq. 4.30) evaluated for temperatures between 12.5 and 25°C a water activity level of 0.990 using the simulation setup of Fig. 4.13 and $a = 0.3$ [58]. Each point represents the average over 1000 realizations and the uncertainty of the data points is less than 0.1 Π_N

4.4 Norway spruce wood

4.4.1 Introduction

Hyphal growth and the impact of a fungus are inextricably linked to the underlying substrate and the extracellular digestion of organic matter. The interplay among the chemical composition of the substrate and the concentration of its

components, the geometrical structure of the substrate and fungal enzymes determine the growth of fungi. Normally, the natural resources of fungi are physically and chemically complex and structured in space, and often the natural nutrient sources are not continuously uniform, but spatially discrete and heterogeneously distributed. The discrete form of the nutrient source depends on the modelling scale, as well as the porous structure of many natural substrates such as soils or wood.

Inspired by their highly adapted growing strategy I propose to model wood-decay fungi from a 'substrate' viewpoint by reducing the enormous complex wood structure to the main fungal pathways connecting the pores, i.e. in the case of the fungus *P. vitreus* the bordered pits, and considering the mycelium as discrete objects. Such models, which are classified as 'vector models', have been developed by many authors in the past (e.g. Boswell et al. [21] and references therein) and are often subdivided into lattice-based (e.g. Boswell [18]) and lattice-free (e.g. Carver & Boswell [28]) approaches according to Boswell & Hopkins [19]. The present model uses a lattice free discrete modelling approach because of the relevant characteristic length scales of wood range over three orders of magnitude from about approximately 2 - 50 µm (lumen size in latewood, the distance between the pits) to about 2 - 5 mm (length of tracheids, width of a growth ring). Thereby reducing the wood structure to its connectivity (i.e. solely the pits) may be less cost-intensive than discretizing the wood structure by using a regular lattice based on the micrometre scale.

The focus of my investigation was the effect of microscopic parameters, such as the degradation rate, degree of opening of pits and pellet (i.e. starting node) concentration, on macroscopic system properties, such as the penetration depth of the fungus, biomass, distribution of destroyed pits and resultant changes in the wood's permeability. By comparing the macroscopic system properties obtained from simulations with the results of laboratory experiments we hope to improve the understanding on how a complex and difficult to observe system, such as fungus-wood, interacts on the microscopic scale under defined conditions. For this purpose a lattice-free 3D FGM is devised that considers hyphae and nutrients as discrete structures. This FGM is, to my knowledge, the first to simulate hyphal growth and the impact of wood-decay fungi.

4.4.2 Simulation

A typical simulation is shown in Fig. 4.17 using the model parameters given in Tab. 4.5 and one pellet (initial node).

Substrate (wood)			
Tracheid width/height/length	$w_1/w_2/w_3$	0.001 - 0.04/0.04/2	mm
Pit density early-wood	$\rho_{ET}(\rho_{ER})$	$0.02\rho_{ET}/2$	mm^{-1}
Pit density latewood	$\rho_{LT}(\rho_{LR})$	$\rho_{ER}/2\rho_{ER}/2$	mm^{-1}
Mycelium (fungus)			
Mean hyphal growth rate	μ	1	mmd^{-1}
Mean edge length	λ	0.05	mm
Growth cut-off length	θ	$w_1/20$	mm
Growth cut-off angle	ξ	90	$\circ$
Growth costs	ϵ	0	$\mathrm{mol}\cdot\mathrm{mm}^{-1}$
Pit initial nutrient	ν	4×10^{-13}	mol
Pit initial degradation rate	α_I	$\nu/20$	mol
Pit degradation rate	α_c	$0.45\times\nu$	mold^{-1}
Pit opening	κ	0.1	$\mathrm{mol}\cdot\mathrm{mol}^{-1}$
Apical branching threshold	β_t	$0.6\times\nu$	mol
Lateral branching threshold	β_s	$0.35\times\nu$	mol
Simulation			
Initial pellet density	n_k^0	12	mm^{-2}
Initial number of Spitzenkörper	n_s^0	1	-
Initial nutrient concentration	n_n^0	$(3/2)\times\beta_t$	mol
Initial orientation	n_c^0	[0 0 1]	-

Table 4.5: Parameters used in the development of the FGM. A rectangular Cartesian coordinate system with the base vectors e_1, e_2 and e_3 is used, where the unit vectors $e_r = e_1$, $e_t = e_2$, and $e_l = e_3$ denote the radial (R), tangential (T), and longitudinal (L) directions as shown in Fig. 2.2.

A rectangular Cartesian coordinate system with the base vectors e_1, e_2, e_3 is used,

where the unit vectors $e_r = e_1$, $e_t = e_2$, and $e_l = e_3$ denote the radial, tangential, and longitudinal directions, as shown in Fig. 2.2. The mean hyphal growth rate μ was estimated by laboratory experiments [163]. The wood sample consisted of 1575 tracheids and 96711 pits. At the beginning of the simulation all pits are closed ($\kappa < n$) and have the same initial amount of nutrient ν. Initially, the pellet has the attributes $n_s^0 = 1$, $n_n^0 = 3\beta_t/2$ and $n_c^0 = e_1 = [0; 0; 1]$. In order to model unlimited extension of the specimen in the radial and tangential directions, periodic boundary conditions are imposed to all faces of the specimen, normal to the main growth direction. When a hypha passes through such a face, it reappears at the opposite face. The simulation ends when all nutrients are exhausted or a specific number of time steps is reached. In Fig. 4.17 the simulation was interrupted after 4000 iteration steps ($\sim$ 2.5 d).

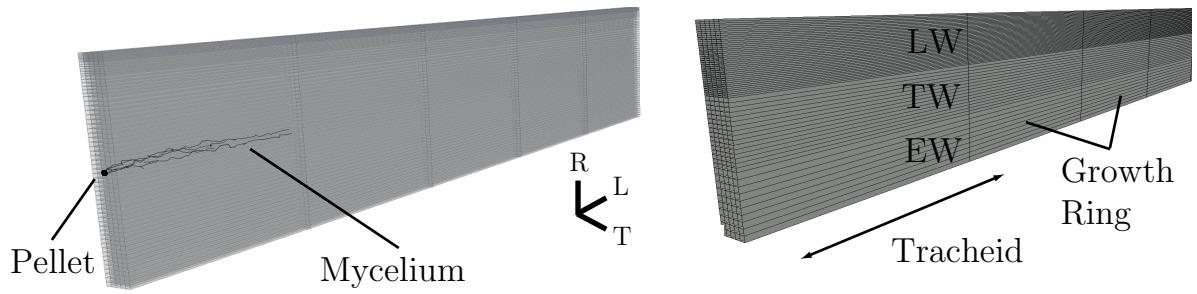

Figure 4.17: Specimens used throughout the study. (a) Typical simulation: penetration of the fungus (black) after 1 d (approximately 100 iteration steps of the FGM) in the longitudinal direction using the parameters shown in Tab. 4.5. The wood sample (grey) consists of 1575 tracheids and 96711 pits. Periodic boundary conditions are applied to the specimen's faces, normal to the tangential (T) and radial (R) directions. In this case fungal growth started from a single initial node (pellet) with one tips. (b) In order to analyze fungal activity in early-wood (EW), transition-wood (TW), and latewood (LW) we used specimens consisting of 25, 40, and 100 tracheids mm^{-1}, respectively, in the radial direction, with a pellet density $n_k^0 = 25\ 1 \cdot \text{mm}^{-2}$. Thus, EW, TW, and LW occupy the same volume.

4.4.3 Results and discussion

The growth and impact of wood-decay fungi is complex because of the heterogeneous structure of the substrate and the mechanism of the growing mycelium of these higher fungi. In the longitudinal direction the tracheids determine the course of the growing mycelium, whereas in the radial direction the rays canalize the hyphae. In the tangential direction the pits are the main pathway for the fungus to move from tracheid to tracheid. In the presented model the rays are not considered in order to reduce the complexity of the substrate. Therefore, the discussion will focus on the penetration of *P. vitreus* in the longitudinal and tangential directions only.

In order to demonstrate the ability of the proposed model to simulate the growth and impact of wood-decay fungi, the growth pattern, growth characteristics and the impact of the fungus on the substrate are discussed . The results obtained from the simulations are compared with experimental results. Unless otherwise specified, the parameters given in Tab. 4.5 are used throughout.

Growth pattern

Fig. 4.18 shows the modelled growth of *P. vitreus* in the heartwood of Norway spruce after 1, 1.5, 2, and 2.5 d, starting from a single pellet. The wood specimen consisted of 1516 tracheids and 96711 pits. Periodic boundary conditions were applied to surfaces in the tangential and radial directions. The hypha enters a tracheid and grows from pit to pit. The tracheids canalize the growth of the fungus in the longitudinal direction because of their cylindrical lumens and the initially closed pits. During growth along the tracheid in a longitudinal direction, the tip node of the hypha splits several times, depending on the apical branching threshold. If the end of a tracheid is reached, the spread of the mycelium in the longitudinal direction ceases and the mycelium becomes more dense, because of uptake of nutrients and lateral branching occurs. After some time, the membranes of the bordered pits open ($F_j^{(m)} < \kappa$) and the fungus is able to colonize an adjacent tracheid, beginning the colonization process again. Therefore, the fungus colonizes the substrate in the stepwise growth pattern shown in Fig. 4.18(d): only a few leading hyphae penetrate the adjacent tracheids in the longitudinal direction,

while the bulk of the mycelium consists of nodes with coordinates $r_i \cdot e_l < w_3$. Laboratory experiments confirmthis characteristic growth pattern of *P. vitreus* [187].

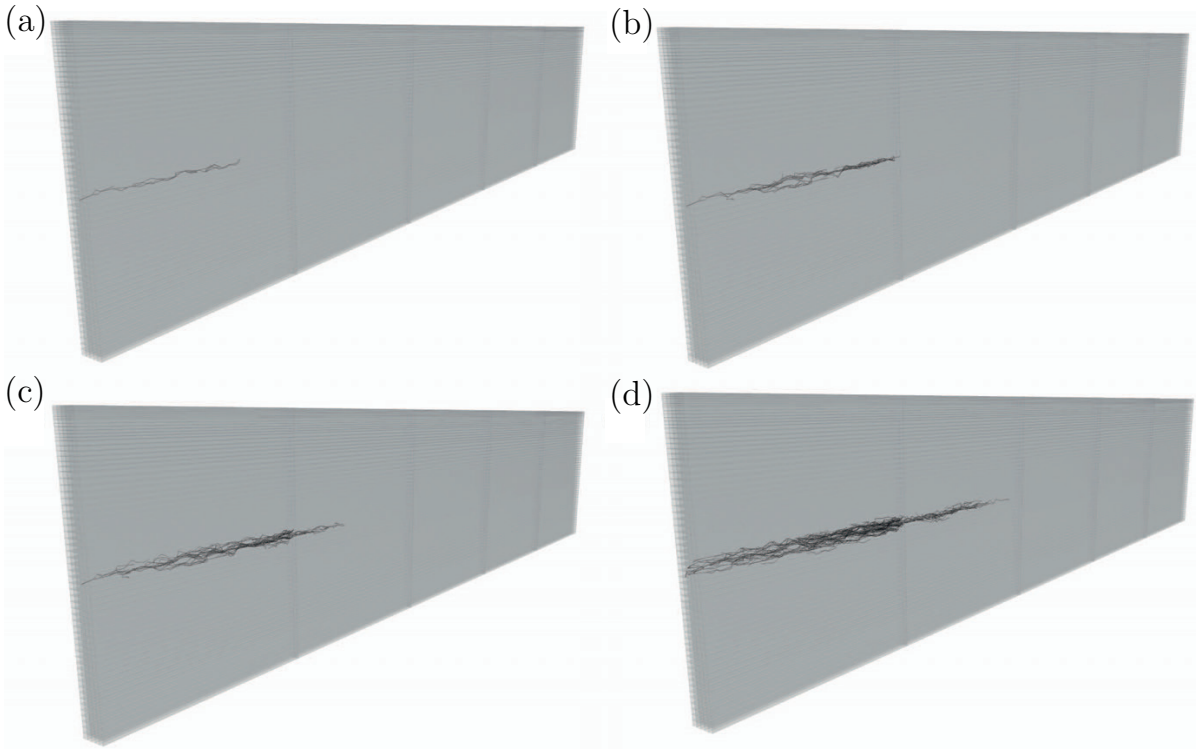

Figure 4.18: Evolution of the mycelium. (a) - (d) Growth of the fungus *Physisporinus vitreus* in heartwood of Norway spruce after 1, 1.5, 2, and 2.5 d, starting from a single pellet. The wood specimen consisted of 1516 tracheids and 96711 pits. Periodic boundary conditions were applied to surfaces in the tangential and radial directions. The model parameters are given in Tab. 4.5. After 2 d, only a few leading hyphae have penetrated into adjacent tracheids in the longitudinal direction and the bulk of the mycelium remains in the first section of the specimen (nodes with coordinates $r_i \cdot e_l < w_3$).

Growth characteristics

In order to analyze the characteristics of growing mycelium in wood the same system and parameters are used as shown in Fig. 4.18, but with a different pellet density $n_k = 105\ l \cdot \mathrm{mm}^{-2}$, totalling 45 pellets. A mean hyphal growth rate of $\mu =$

$1\text{mm} \cdot \text{d}^{-1}$ corresponds to $a_w = 0.972$, 22°C, and pH 5 [160]. Fig. 4.19 shows the evolution of the number of tips N_S with time. After 2 d the mycelium consists of approximately 52000 nodes and edges and 6400 tips. After a transient phase, the number of tips increases exponentially (see inset in Fig. 4.19). Between 0.2 and 1.8 d they fit the law $a \cdot exp(t/\tau)$ with the parameters a = 49.8 and $\tau = 0.4$ and between 1.5 and 2.25 d a = 188 and $\tau = 0.56$. Thus, between 0.2 and 1.4 d it takes approximately 1 d to increase the number of tips by a factor of 10. Most tips arise from apical branching and the first lateral branching occurs after approximately 0.5 d. The transient phase is more pronounced, with lateral rather than apical branching. Between 1 and 2.25 d the ratio of the number of tips arising from apical and lateral branching is approximately constant.

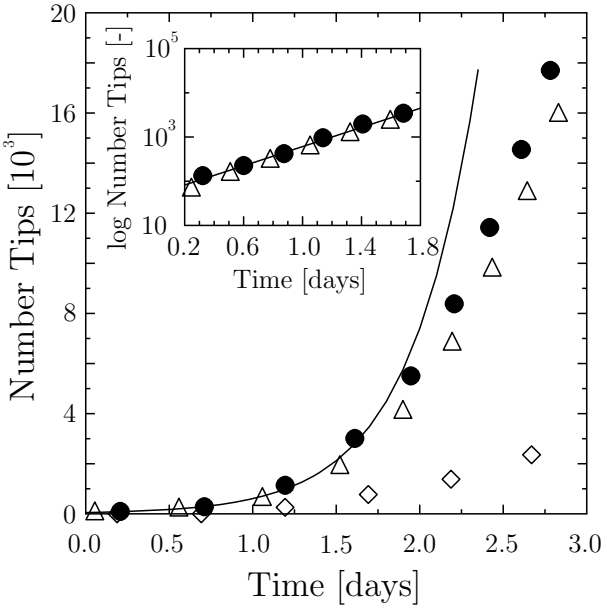

Figure 4.19: The number of tips plotted against time for a mean hyphal growth rate of $\mu = 1.0$ mm $\cdot$ d^{-1}. Between 0.2 h and 1.8 d the tips evolution fits an exponential law a exp(t/τ) with the parameters a = 49.8 and $\tau = 0.38$. Most tips arise from apical branching. Between 1.4 and 2.25 d the ratio of the number of tips arising from apical and lateral branching is approximately constant. Each line represents the average over nine realizations and the uncertainty of the data points is within the range of the symbols.

For *P. vitreus*, a_w is the most influential factor on the growth rate [160]. The different phases of growth, with a mean hyphal growth rate μ varying from 1 ($a_w =$

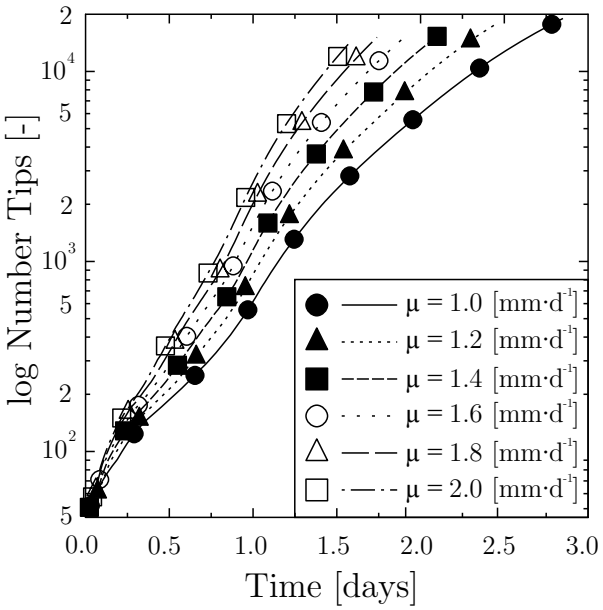

Figure 4.20: The number of tips plotted against time for hyphal growth rates varying from $\mu = 1.0$ to $\mu = 2.0$ mm $\cdot$ d^{-1}. During 2 d of growth there are a transient phase and two phases of approximately exponential expansion. Generally, the penetration of the fungus is characterized by alternating exponential (unrestricted) and restricted growth at a specific frequency. Each line represents the average over nine realizations and the uncertainty of the data points is within the range of the symbols.

0.972) to 2 ($a_w = 0.982$) mmd^{-1}, are shown in Fig. 4.20. For the different growth rates the penetration depth and shape of the growth front are similar. During 2 d of growth one observes a transient phase and two phases of approximately exponential expansion. The mechanism is the same as the one shown in Fig. 4.18. In the transient phase the hyphae initiated from the pellets the mycelium is extended by one edge, but the branching rate is low because of the low nutrient concentration. In this phase all branching is apical. After 12 h the transient phase ends and the mycelium starts to grow exponentially, as long as the first row of tracheids in the longitudinal direction is colonized. After approximately 36 h the growth front penetrates adjacent tracheids in the longitudinal direction and reaches a phase of continuous tip production after 1.5 d, again as long as the next row of tracheids in the longitudinal direction is reached. Generally, the penetration of the fungus is characterized by alternating exponential (unrestricted) and restricted growth at a specific frequency. Obviously, this frequency depends on the length of the tracheids in the longitudinal direction. Experimental results

seems to be in agreement with the observed growth pattern (Fig. 4.21).

During unrestricted growth, the total hyphal length and the number of tips of the mycelium increase at the same rate. In the present model between 0.5 and 1.5 d the HGU is approximately 350 and 550 µm for $\mu = 1.0$ and $\mu = 2.0$, respectively. The smaller the mean hyphal growth rate the denser the mycelium. Fig. 4.22 shows the HGU plotted for different mean hyphal growth rates against time. Between 1 and 2.5 d the HGU oscillates around 350 and 550 µm for $\mu = 1.0$ and $\mu = 2.0$, respectively. After 10 and 28 h the penetration depth of the growth front increases by more than w_3 and $2 \cdot w_3$, respectively. Thus, the oscillation occurs because of the stepwise invasion of the substrate in the longitudinal direction. The alternation of restricted and unrestricted growth phases seems to be a characteristic of *P. vitreus* on a mesoscopic length scale. Obviously, the present model overestimates the fluctuations in the HGU because of the simple substrate used. In reality, the lengths of the tracheids are Gaussian distributed [22] and there are defects in the overlapping regions. Additionally, on the macroscopic length scale, the lengths of the tracheids increase from the pit to the bark of a tree and the fluctuations in the HGU may be smoothened out. In order to analyze the characteristics of the observed fluctuations, further qualitative and quantitative experiments and simulations are necessary.

Impact on early- and latewood

The distribution of pits in Norway spruce wood is heterogeneous. Because of the different function of the tracheids in early-wood (nutrient transport) and latewood (stability of tree), most of the bordered pits are located in the early-wood tracheids and both the size and number of bordered pits in latewood are smaller. Therefore, the intensity of fungal activity in the first stage of growth strongly correlates with the underlying substrate, because of the different amounts and availability of nutrients in early- and latewood.

Fig. 4.23 shows the number of open pits plotted against time for different mean hyphal growth rates. The number of open pits increases exponentially with time, and surprisingly, there are no fluctuations resulting from the stepwise growth.

In order to analyze fungal activity in early-, transition-, and latewood we use a

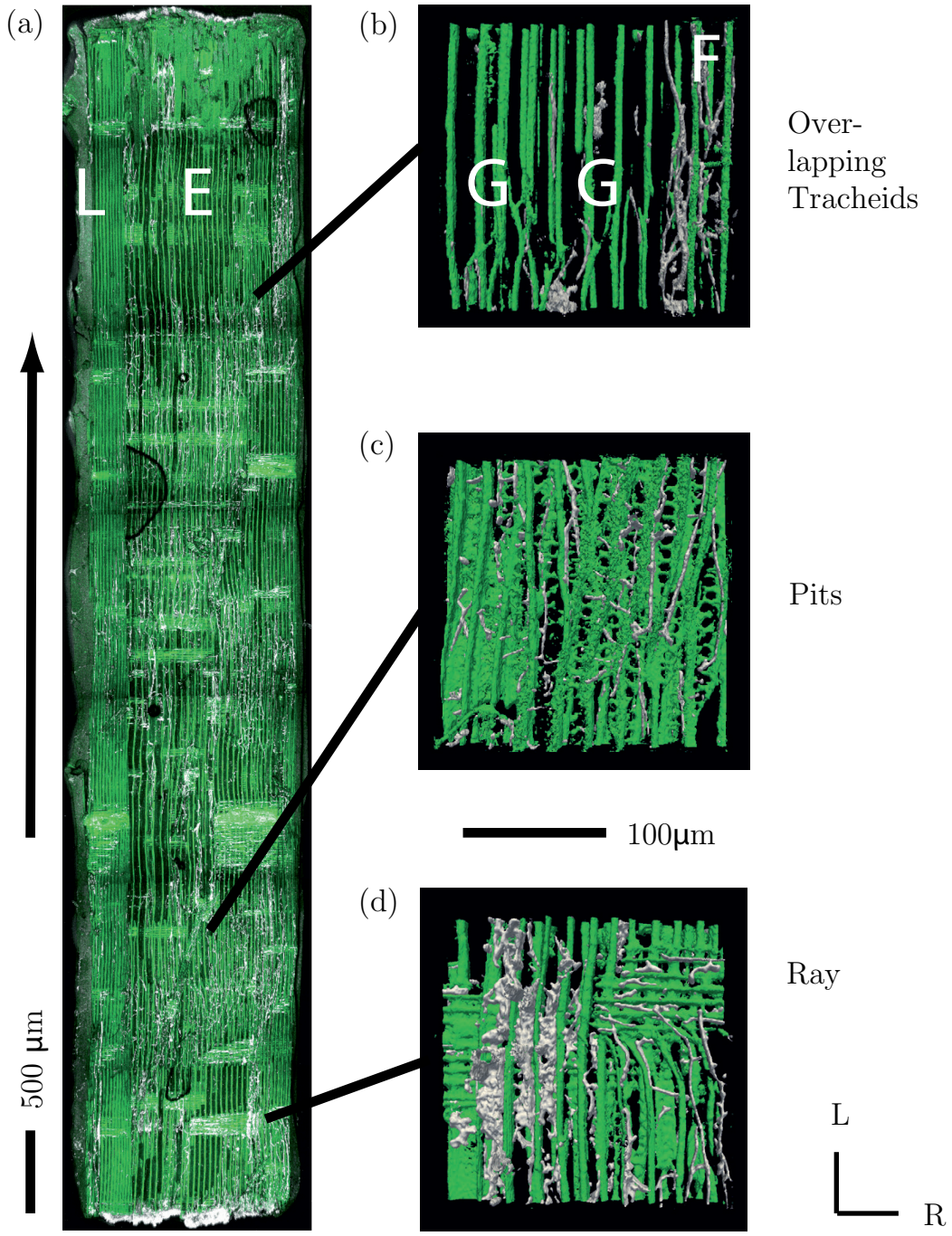

Figure 4.21: (a) Penetration of the white-rot fungus *Physisporinus vitreus* (white) into a longitudinal-tangential section of Norway spruce heartwood (green) visualized by CLSM. The fungus is stained with the actin-specific fluorescence marker Alexa Fluor 660 + WGA. Wood has an autofluorescence at about 350 nm and is transparent for CLSM up to 200 nm. Wood and hyphae are visualized and rendered via iso-surfaces. The terms E and L denote early- and latewood. (b) - (d) show an overlapping region, the fungal activity at the pits and a ray respectively. The terms F and G denote blocked and leading hyphae.

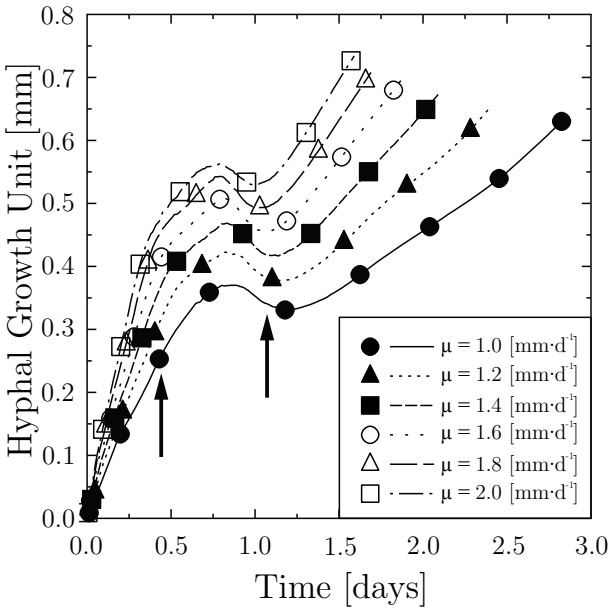

Figure 4.22: The HGU plotted for different hyphal growth rates. The HGU is defined as the ratio of the total length of the mycelium and the total number of tips. For unrestricted growth, the HGU is a constant. Between 0.5 and 1.5 d the HGU oscillates around 350 and 550 µm for $\mu = 1.0$ and $\mu = 2.0$, respectively. The oscillation occurs because of the stepwise invasion of the substrate by the fungus in the longitudinal direction. The alternation of restricted and unrestricted phases of growth seems to be a characteristic of *Physisporinus vitreus*. After 10 and 28 h the penetration depth of the growth front increases more than w_3 and $2 \cdot w_3$, respectively (arrows). Each line represents the average overnine realizations and the uncertainty of the data points is within the range of the symbols.

model specimen with 25, 40, and 100 tracheids mm^{-1}, respectively, in the radial direction, with a pellet density of 25 mm (Fig. 4.17(a)). Thus, early-, transition-, and latewood occupy the same volume. The simulation parameters are the same as shown in Tab. 4.5, except for the growth cost ϵ. Fig. 4.24 shows the mycelium, the distribution of remaining nutrients and the number of open pits (Eq. 4.2) for all pits occupied by more than one node after 2.5 d of incubation for $\epsilon \in [10^{-4}, 10^{-3}]$.

Generally, there is much higher fungal activity in early- and transition-wood than in latewood with regard to the amount of mycelium, the growth front and the number of degraded pits. Because of the strong correlation between the number of open pits and the remaining nutrients the focus of my analysis is on the number of open pits. The difference in the number of open pits in early-, transition-,

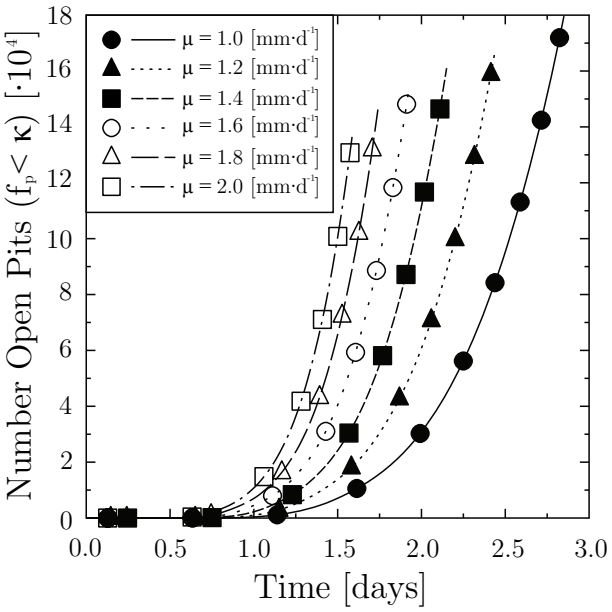

Figure 4.23: The number of open pits plotted against time for different mean hyphal growth rates increases exponentially with time. Surprisingly, there are no fluctuations in the evolution of the number of open pits arising from the stepwise growth. Each line represents the average over nine realizations and the uncertainty of the data points is within the range of the symbols.

and latewood for $\epsilon = 10^{-4}$ and $\epsilon = 10^{-3}$ is approximately 35%, 11%, and 43%, respectively. In total, after 2 d approximately 77% and 75% of the occupied pits are open for $\epsilon = 10^{-4}$ and $\epsilon = 10^{-3}$, respectively, while the absolute number of open pits is approximately 17% higher in Fig. 4.24(c) than in Fig. 4.24(d). As anticipated, the cost of growing affects the number of occupied pits and the growth front: the higher the growth cost the smaller the polarity and therefore the velocity of the fungus.

A detailed view of the distribution of open pits in measurement Fig. 4.24(c) shows that, surprisingly, there is a significant difference in the number of open pits: after 2 days of incubation approximately 71%, 91%, and 55% of occupied pits are open in early-, transition-, and latewood, respectively. Because of the linear degradation rate $\dot{\alpha}_c$, we would expect approximately the same proportion of open pits, but the mean number of nodes per pit in transition-wood is higher than in early- and latewood. Thus, the initial degradation rate plays an important role by opening the pits and therefore enhancing the spread of the mycelium in the tangential and radial directions. Latewood seems to be less accessible to hyphae than early- and transition-wood.

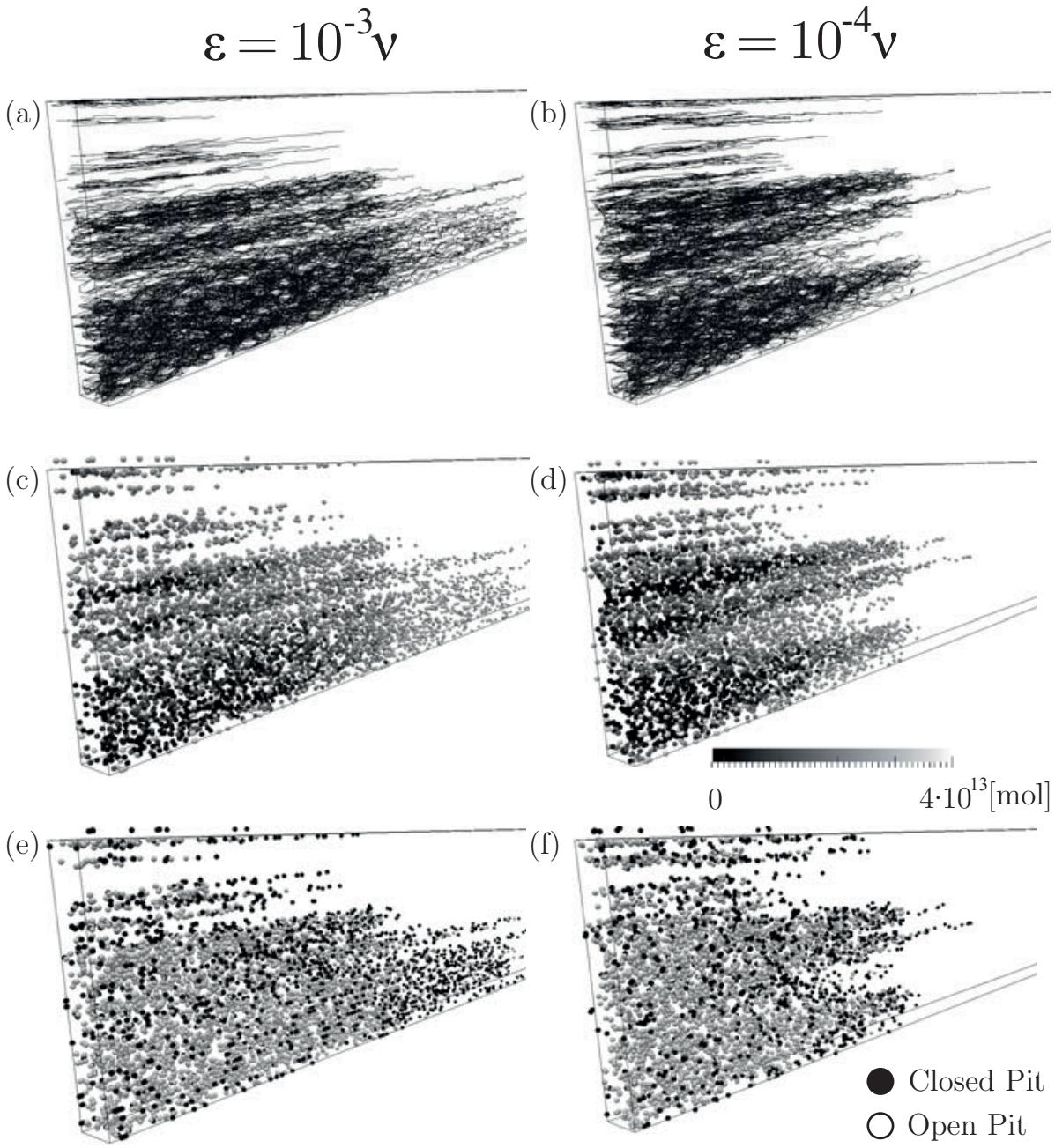

Figure 4.24: Fungal activity characterized by the mycelium (a, b), the distribution of remaining nutrients given in mol (c, d), and the number of open pits (e, f) (see Eq. 4.2) for all pits occupied by more than one node after 2.5 d of incubation for $\epsilon \in [10^{-4}, 10^{-3}]$ mol $\cdot$ mm^{-1}. There is much higher fungal activity in early- and transition-wood than in latewood with regard to the amount of mycelium, the growth front and the number of degraded pits.

The lower accessibility of latewood regions by *P. vitreus* was also supposed by Lehringer et al. [99], because of the cavities and notches that are mainly in the latewood. Perhaps *P. vitreus* creates its own voids in order to colonize regions of Norway spruce with fewer and smaller pits. If we compare the distributions between studies, there is a difference: Lehringer et al. [99] found no significant differences between the degradation of bordered pit membranes in early- and latewood whereas in my simulation the number of strongly degraded pits ($f_i^{(m)} < 0.2 \cdot \nu$) was higher in early-wood than in latewood (Fig. 4.24). However, this result depends on the definition of 'strongly degraded' and the incubation conditions. Thus, further qualitative and quantitative experiments and simulations are necessary to explain the colonization strategy of the fungus.

Permeability

Wood-decay fungi have to create new pathways in order to growth and capture the nutrients of a resource such as Norway spruce heartwood. The alteration of the permeability is an inherent part of their colonization strategy and characterizes wood-decay fungi. The white-rot fungus *P. vitreus* degrades the initially closed bordered pit membranes of Norway spruce wood. Since the permeability of Norway spruce heartwood is dominated by the hydraulic resistance of the pits [143], their degradation by *P. vitreus* has a drastic influence on the permeability even in its first stage of growth. The gas permeability K of Norway spruce may be given by

$$K = k_q \cdot Q = \frac{\eta \cdot L \cdot B_1}{A \cdot \Delta B \cdot \overline{B}} \tag{4.36}$$

which is Darcy's law describing the flow of a gas through a porous medium such as wood [173]. η denotes the dynamic viscosity of air, L is the specimen length in flow direction, A is the specimen area perpendicular to the flow direction, Q is the volumetric flow rate, B_1 is the pressure behind the specimen, $\Delta B = B_1 - B_2$ is the pressure difference and $B = B_1 + B_2/2$ the average pressure. Lehringer [97] measured the gas permeability of Norway spruce wood samples after $t = 3$, 5, 7, 9 weeks of incubation with *P. vitreus* by exposing cylindric samples with a radius

and length of 20mm to a pressure difference ΔB and measuring the volumetric flow rate Q. Since the absolute pressure and the pressure difference were fixed during the measurement, we can give a rough prediction of the permeability's time evolution by assuming

$$K(t) = K_0 + k_q \cdot Q(t) \approx K_0 + k_q^* \cdot \frac{N_{p,open}(k_q^* \cdot t)}{N_{p,tot}(k_q^* \cdot t)} \tag{4.37}$$

where K_0 is wood's intrinsic permeability, $N_{p,tot}$ is the total number of pits and $N_{p,open}$ is the number of open pits per volume, which can be derived from the model (Fig. 4.23). k_q^* and k_t^* are unknown constants. k_q^* links the volumetric flow rate Q with the number of pits per volume and k_t^* scales the time in order to account for different observation times and incubation conditions of the wood samples *in vitro* and *in silico*.

Fig. 4.25 shows the time evolution of the gas permeability estimated by the model of Eq. 4.37 using $K_0 = 0.048$ Darcy, $k_t^* = 27$, $k_q^* = 0.14$ m^2. The progression of the open pits is measured over 3 d in a volume of about 4 mm^3 using the FGM with the parameters given in Tab. 4.5 and $\mu = 1.2$ mm $\cdot$ d^{-1}. The permeability model, which has an error smaller than 0.02 Darcy, is compared to the experiments of Lehringer [97].

The factor k_t^* implies that we need about 4 weeks to reach the same permeability for samples with a 6000 times bigger volume. Additionally, the model prediction is within the error of the experimental permeability measurements even in a later stage of fungal growth, which is characterized by an attack of the cell walls besides the degradation of the bordered pits. The results suggests, that the permeability changes even in a later stage of fungal growth is not mainly affected by distribution of the degraded bordered pits and the clustered decay pattern of cell walls. The permeability changes may be principally explained by the total number of open pits.

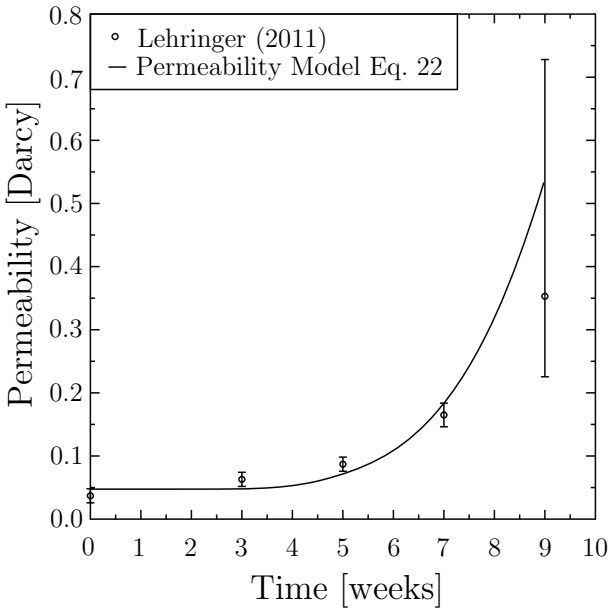

Figure 4.25: Time evolution of the gas permeability estimated by the model of Eq. 4.36 using $K_0 = 0.048$ Darcy, $k_t^* = 27$, $k_q^* = 0.14$ m^2 and compared to the experiments of Lehringer et al. [97]. The progression of the open pits is measured over 3 d in a volume of about 4 mm^3 using the FGM with the parameters given in Tab. 4.3 and $\mu = 1.2$ mm $\cdot$ d^{-1}

4.4.4 Summary

This section presented a 3D mathematical model of hyphal growth and the impact of the white-rot fungus *P. vitreus*. The model focuses on the structure of the wood (i.e. nutrients and substrate) and the tree-like network of the fungus (i.e. the mycelium), the evolution of which with time is governed by key processes such as polarization, uptake and transport of nutrients and the cost of growth. The model reduces the enormously complex growth of *P. vitreus* to a pit-to-pit motion of individual hyphae.

I found that the fungus captures the substrate in a stepwise pattern, with alternating phases of restricted and unrestricted growth, and we compared the simulation results qualitatively and quantitatively with experimental results [187, 99, 97]. One observes that fungal activity in early-wood is much higher than in latewood after 2 d of incubation, whereas Lehringer et al. [99] found no significant differences in fungal activity. The discrepancy in these findings may be explained by the different observation times, but further qualitative and quantitative experi-

ments and simulations are necessary to explain the colonization strategy of the fungus.

In particular, the influence of tracheid length on the penetration velocity of wood-decay fungi in the longitudinal direction is of interest, as well as the impact of the fungus on the substrate (e.g. changes in permeability). In order to simulate the permeability changes induced by *P. vitreus*, a more accurate wood model in terms of pit distribution and pit size, as well as parenchymal cells, is essential. Images from synchrotron radiation tomography show the anatomical features of wood, such as pits and rays, and confocal laser scanning microscopy offers a technique for measuring the evolution and spatial distribution of biomass in wood. These microscopic techniques will enable the development of a more realistic model that includes anastomosis, metabolism and the presence of an inhibitor.

Generally, hyphal growth models are limited up to the centimetre scale because of the growth of millions of hyphal tips in the small specimens of wood. However, we consider that the present model enables analysis of the effects of microscopic parameters, such as the degradation rate and degree of opening of pits, on macroscopic system properties such as penetration depth of the fungus, biomass, distribution of destroyed pits in early- and latewood and the alteration of the permeability. This understanding of how complex systems (e.g. fungus - wood) interact under defined conditions is crucial for the biotechnological applications of *P. vitreus*.

5 Permeability of fungally-modified Norway spruce wood

5.1 Introduction

The previous section presented a rough prediction of the permeability of infested wood (Eq. 4.37). The FGM is limited to relative small sample size and therefore it is proposed to study the impact of *P. vitreus* on a macroscopic scale using a hydraulic model. Such kind of models were developed by many authors in the past for analyzing the permeability of wood [33, 32, 142, 16] or studing the impact of fungi [67]. A review of the topic is presented by Siau [173]. However, most of the studies dealt with the anatomy of wood, e.g. the size and distribution of the pits, whereas a few analyzed the impact of wood-decay fungi. Lehringer et al. [101] presents a review on various techniques for improving liquid permeability.

5.2 Model

The basic idea of my 3D hydraulic model of Norway spruce wood is to reduce the complex wood structure to a framework of cell walls, whereby each cell wall has an effective hydraulic resistance. Underlying cell wall elements, such as the pits, intrinsic holes or any kind of fungal impact, determine the effective hydraulic resistance of each cell wall. The advantage of this approach is the low number of degrees of freedom to model the full heterogeneity of a Norway spruce growth ring, whereas a drawback is the detailed knowledge needed to construct an appropriate wood structure. For example, a $2 \times 2 \times 2$ mm block of a growth ring has approximately 3000 degrees of freedom. A standard desktop computer easily solves such a system of equations and therefore we can focus on the effective hydraulic resistance, i.e. the bordered pits and the impact of *P. vitreus* on the

cell walls.

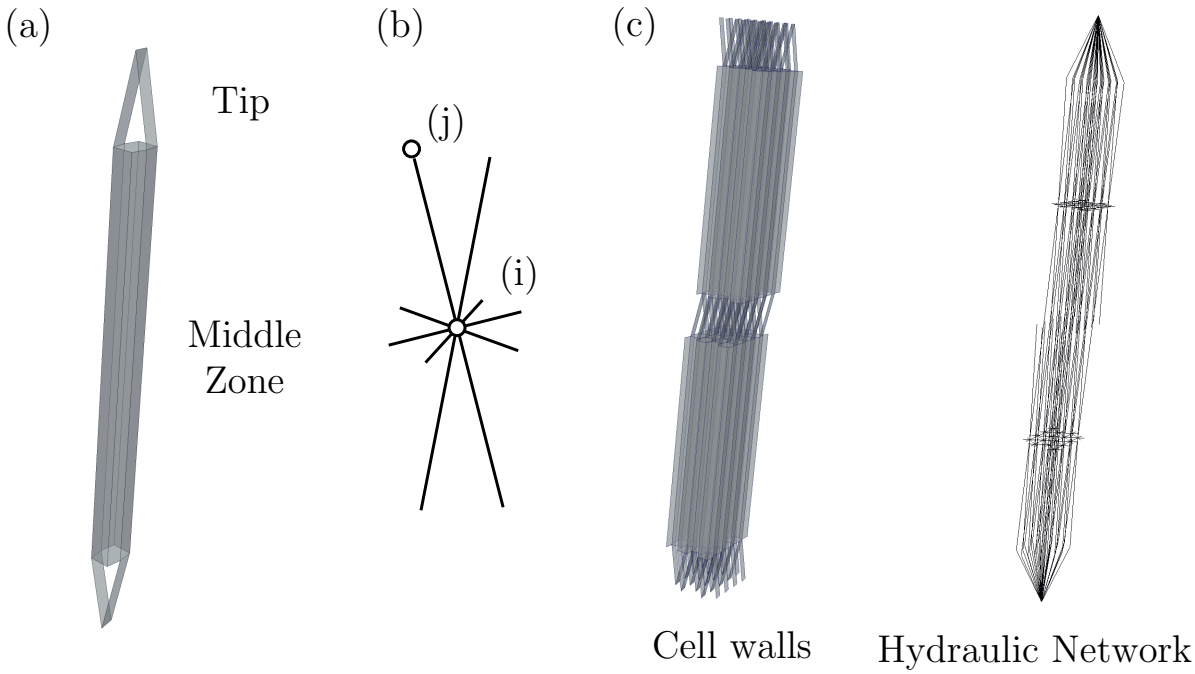

Figure 5.1: (a) The proposed model considers a tracheid as a polyhedron with 10 faces. Each cell wall represents one degree of freedom and has an effective hydraulic resistance, which is determined by cell wall elements such as bordered pits. (b) The hydraulic network of such a tracheid is represented by 10 branches (cell walls) and one node (lumen). (c) shows a tracheid framework and the corresponding hydraulic network.

Inspired by the anatomical study of Lewis [106] a Norway spruce tracheid is modelled as a polyhedron with 10 faces (Fig. 5.1).

The middle zone of the tracheid has a rhombic shape (Fig. 2.3), whereas the tips are represented by four faces connecting the cell walls over the cross. The hydraulic network of such a tracheid is represented by 10 branches (cell walls) and one node (lumen) assuming that only the pits in the cell walls influence the flow between adjacent tracheids as shown in Fig. 5.1(b). A Norway spruce growth ring is constructed by assembling single tracheids and adjusting their height l_R according to Eq. 2.2 (Fig. 5.1(c)). In order to model the flow of a fluid, e.g. air, through the network of Fig. 5.1(c), it is assumed that (a) the fluid is incompressible and (b) the pressure drop Δp between two nodes (i.e. adjacent

lumen) is proportional to the flow Q through that branch [9], i.e.

$$\Delta p = R_h \cdot Q, \tag{5.1}$$

where R_h is the hydraulic resistance between node (i) and (j) (Fig. 5.1(b)). The hydraulic resistance and related measures are defined in Tab. 5.1 according to Choat et al. [29].

Measure	Symbol	Unit	Relation
Hydraulic conductance	k_h	$\left[\frac{\mathrm{m}^3}{\mathrm{s}\cdot\mathrm{MPa}}\right]$	$\Delta p = \frac{1}{k_h} \cdot Q$
Hydraulic conductivity	K_h	$\left[\frac{\mathrm{m}^4}{\mathrm{s}\cdot\mathrm{MPa}}\right]$	$\Delta p = \frac{L}{K_h} \cdot Q$
Hydraulic resistance	R_h	$\left[\frac{\mathrm{s}\cdot\mathrm{MPa}}{\mathrm{m}^3}\right]$	$\Delta p = R_h \cdot Q$
Hydraulic resistance	r_h	$\left[\frac{\mathrm{s}\cdot\mathrm{MPa}}{\mathrm{m}^4}\right]$	$\Delta p = r_h \cdot L \cdot Q$
Area-specific pit resistance	r_p	$\left[\frac{\mathrm{s}\cdot\mathrm{MPa}}{\mathrm{m}}\right]$	$\Delta p = \frac{r_p}{A} \cdot Q$

Table 5.1: Resistance, conductance, conductivity and resistivity are defined according to Choat et al. [29]. Δp is the pressure drop between two nodes and Q is the flow through that branch of length L.

As a first rough assumption the flow of gas through a capillary, e.g. the canal of a pit, may be given by the law of Darcy-Weissbach [15], i.e.

$$R_h(t) = \frac{128 \cdot \eta l}{\pi \cdot d(t)^4}, \tag{5.2}$$

where η is the kinematic viscosity and l and d is the length and diameter of the capillary respectively. The diameter of the capillary is a function of time, in order to model the impact of the fungus, and may be estimated both from the FGM (Ch. 3) and tomographic microscopy (Sec. 4.1).

Steady-state flow in a hydraulic network can be solved using a direct stiffness procedure [9].

5.3 Results and discussion

Fig. 5.2 shows a hydraulic network of a section of a Norway spruce growth ring consisting of 1840 tracheids. The size of the system is approximately 4 mm in longitudinal, 2 mm in radial and 0.5 mm in tangential direction. The growth ring is constructed according to the fibre geometry measured in Fig. 2.5. Each cell wall has an area-specific pit resistance $r_p = 1 \cdot 10^{-3}$ GPa $\cdot$ s $\cdot$ m^{-1} according to Choat et al. [29]. The applied pressure difference (from the top to the bottom) is 0.5 MPa resulting in a permeability of the system of approximately 0.05 Darcy.

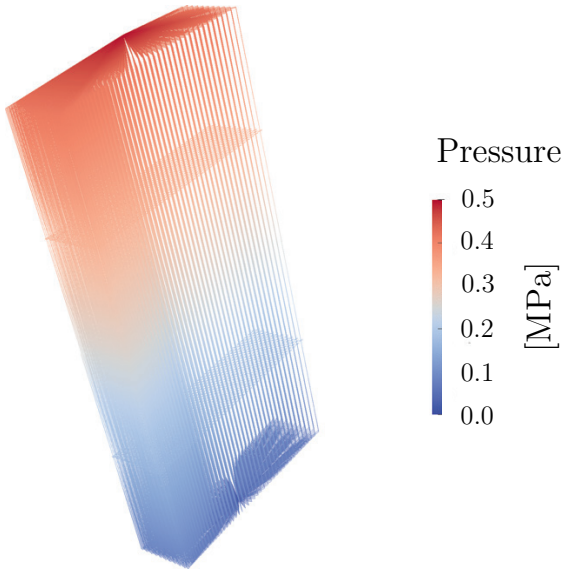

Figure 5.2: Flow through a tracheid network. A pressure drop of 0.5 MPa results in a permeability of approximately 0.05 darcy.

The present model is a preliminary study and does not consider effects such as the expansion of the gas or non-linear pressure drop, which typically occur at the bordered pits [173]. However, the study may demonstrate the potential of such hydraulic models for analyzing the impact of wood-decay fungi.

6 Conclusion

This thesis presents a novel microscopy technique for the automated quantification of microscopic cell wall elements (i.e. the pits) or the impact of wood-decay fungi, as well as novel mathematical models for the study of wood-decay fungi both in homogeneous environments (i.e. Petri dishes) and in physically and chemically complex structured environments (i.e. wood). These methods were used to study the basic phenomena of the growth and impact of the biotechnological relevant white-rot wood-decay fungus, *Physisporinus vitreus*, in Norway spruce wood on the microscopic, mesoscopic and macroscopic scales. Understanding the key processes that determine the interaction between wood and fungus on a microscopic scale will enable optimization of macroscopic system properties, such as permeability, of bioincised wood. This chapter summarizes the main findings and critically discusses the models and results in the context of future developments in the field of wood-decay fungi.

Microscale: wood anatomy

First, the anatomy of infested Norway spruce wood was studied using high-resolution synchrotron X-ray tomographyic microscopy. I developed a technique for the three-dimensional analysis of cell wall elements in Norway spruce wood, such as pits, intrinsic defects, hyphae and the cell wall alterations induced by fungi. The presented technique makes use of the characteristic cylindrical shape of the Norway spruce tracheids by mapping these three-dimensional elongated objects to a two-dimensional image using cylindrical projection. This final two-dimensional map of a tracheid's cell wall enables, for the first time, fast and efficient automated computation of the cell wall elements' properties (e.g. three-dimensional position, orientation, frequency, size, shape and intensity). These properties are sensitive to the morphological processing of the tracheidal two-

dimensional map, but validation of the obtained decay pattern, intrinsic defects or the position of the pits on a cell wall is easily possible using electron or light microscopy. Despite this success, the method is not a substitution for classical destructive histological staining techniques using light or laser scanning microscopy, because even state-of-the-art synchrotron topographic microscopy does not provide information about the nanoscopic composition of the wood.

Second, based on this cylindrical projection technique, the three-dimension distribution of bordered pits within a Norway spruce growth ring was studied. Measuring the position, size, frequency and orientation of the bordered pits was essential for the development of accurate models of the wood's anatomy for simulating the permeability of infested Norway spruce wood.

Mesoscale: modelling the growing fungus

Physisporinus vitreus degrades the bordered pits in its first stage of colonizing Norway spruce heartwood. In order to reduce the complex interaction between *P. vitreus* and Norway spruce wood to a defined number of parameters, I modelled the evolution of the mycelium by pit-to-pit growth of the hyphae. Using this modelling approach, called a fungal growth model (FGM), the simulation of *P. vitreus* in both wood and Petri dishes is possible.

As the first step, colonies of *P. vitreus* were analyzed on Petri dishes as a homogeneous quasi two-dimensional environment. By comparing simulations of the FGM with laboratory experiments of fungal colonies growing on MEA I showed that the combined effects of water activity, temperature and pH on the radial growth rate of fungal mycelia on the macroscopic scale may be explained by a power law for the costs of hyphal maintenance and expansion on the microscopic scale. Information about the response of the fungal mycelium at the microscopic level to environmental conditions is essential for simulating and optimizing its behaviour in complex structure substrates such as wood. In the second step, the model was use to investigate the mycelium's growth front in a two-dimensional wood-like environment. A combination of laboratory experiments with the FGM suggested that *P. vitreus* requires approximately 12 - 48 hours to penetrate through a bordered pit, depending on the hyphal growth rate and the mode of pit penetration.

Furthermore, I introduced universal measures (i.e. penetration velocity, penetration work and penetration capacity) that may support optimization of bioinicising. At the very least, I simulated the growing fungus in a three-dimensional Norway spruce growth ring. Simulations suppose that the growth of the fungus is characterized by stepwise capture of the wood tissue, resulting in a fluctuation of the hyphal growth unit. In addition, permeability changes may be mainly explained by the total number of open pits.

Macroscale: modelling permeability

On the macroscopic scale, the impact of *P. vitreus* on the wood structure is simulated by means of a hydraulic model, in which each tracheid is represented by a polyhedron with 10 faces. Knowledge of the distribution of the pits, obtained by tomographic microscopy, enables calculation of the precise corresponding hydraulic resistance of each cell wall, based on the resistance of a single pit. This permeability model links the microscopic degradation of the pits (measured using the FGM or high-resolution synchrotron data) with the macroscopic permeability of a wood sample. While submitting this thesis, this was ongoing work and conclusive remarks were not possible. However, the preliminary study demonstrates the potential of this approach and therefore completes my view on the growth and impact of *P. vitreus* on the micro-, meso- and macroscopic scale.

Bioincising: optimization by means of the FGM

I developed a framework for the optimization of bioincising. The FGM was used to study the influence of environmental factors, the penetration behaviour of the fungus and the effect of the chemical and physical structure of the resource on the growing mycelium. However, the last step, which would be optimization of the bioincising process on a larger scale, was not performed, for two main reasons. First, a careful validation of the model assumptions was no longer possible. Second, the simulation of the growing fungus on larger time scales requires the implementation of additional processes such as anastomosis.

The presented lattice-free approach is a simplification of the complex interaction

between wood and fungus and might have a tendency to use rules that do not have a direct biological representation, but the FGM has two main advantages. First, I think a lattice-free approach is elegant for modelling the growth of the fungus, *P. vitreus*, in its first stage of wood colonization, because the relevant characteristic length scales of wood range over three orders of magnitude from about 2 - 50 µm (the distance between the pits; lumen size in latewood) to about 2 - 5 mm (length of tracheids; width of a growth ring). Therefore, reducing the wood structure to its connectivity (i.e. solely the pits) may be less cost-intensive than discretization of the wood structure by using a regular lattice-based method on the micrometre scale. Second, nearly all available models focus on the growing mycelium or the distribution of nutrients and not on the creation of new pathways into the substrate. I think this type of fungal impact needs more attention, especially because the creation of new pathways is often accompanied by altered permeability of the substrate and therefore offers an elegant way of verifying and investigating the influence of microscopic parameters of mathematical models of fungal growth in soil or wood on the macroscopic scale.

Modelling wood-decay fungi: future developments

The drawback of modelling wood-decay fungi on the colony scale is the very time- and cost-intensive validation of the model's assumptions by means of laboratory experiment - an essential process for the development and application of any model - because tomographic microscopy techniques for the visualization of growing hyphae within an opaque material such as wood are not available to date or are still in development. Therefore, I see future developments in other fields; in particular, the use of mathematical models for studying the impact of wood-decay fungi on the permeability and acoustic properties of wood.

The permeability of infested wood is revealing about the colonization strategy of wood-decay fungi. It would be interesting to know how various wood-decay fungi affect the permeability of their resource over time. I see great benefits in using mathematical models for such comparative studies, because hydraulic models are able to link the microscopic decay pattern with macroscopic system properties (i.e. permeability) for which established laboratory experiments exist. As shown in this thesis, such hydraulic models are based on a small number of well-defined

parameters, because modern (phase-contrast) tomographic microscopy techniques in combination with quantitative image processing techniques provide a full three-dimensional picture of both untreated and infested wood.

Fungi are able to alter the mechanical properties of wood. For example, the excellent degradation pattern of *P. vitreus* makes it available as an agent for biotechnological applications such as the improvement of tonewood. This application, in which the fungus was successfully used to produce tonewood for a violin estimated in a blind test by over 100 listeners to be of higher quality than a Stradivari, fascinates me because I have had a passion for playing the viola for more than 20 years. The 'Stradivari' effect of the fungus seems to be related to its delignification of the cell wall, but the underlying mechanism leading from microstructural cell wall alterations to the excellent resonance properties of the wood is still unknown. Mathematical models may give deeper insights into the complex interaction between fungus and wood. Hopefully, the present work will illuminate additional aspects of the behaviour of the exceptional organism, *P. vitreus*, for a better understanding of the mystery of superior violins.

Bibliography

[1] The biotech Stradivarius. *Nature Biotechnology*, 28(1):6, 2010. 3, 29

[2] A. D. Araujo, W. B. Bastos, J. S. Andrade, and H. J. Herrmann. The distribution of local fluxes in porous media. *Physical Review E*, 74(1):010401, 2006. 35

[3] D. J. Ashton, T. C. Jarrett, and N. F. Johnson. Effect of Congestion Costs on Shortest Paths Through Complex Networks. *Physical Review Letters*, 94(5):058701, 2005. 36

[4] D. J. Bailey and C. A. Gillian. Biological control of pathozone behaviour and disease dynamics of rhizoctonia solani. *New Phytologist*, 136(2):359–367, 1997. 36

[5] S. L. Bardage and G. Daniel. The ability of fungi to penetrate micropores: implications for wood surface coatings. *Material und Organismen*, 31(4):233–245, 1998. 55, 81, 82

[6] S. Bartnicki-Garcia, D. D. Bartnicki, G. Gierz, R. López-Franco, and C. E. Bracker. Evidence That Spitzenkörper Behavior Determines the Shape of a Fungal Hypha: A Test of the Hyphoid Model. *Experimental Mycology*, 19(2):153–159, 1995. 24

[7] S. Bartnicki-Garcia, F. Hergert, and G. Gierz. Computer simulation of fungal morphogenesis and the mathematical basis for hyphal (tip) growth. *Protoplasma*, 153(1-2):46–57, 1989. 24, 36

[8] M. Baschung and D. Pflug. *Aufstockungen mit Holz*. Lignum, Le Mont-sur-Lausanne, 2008. 21

[9] K. J. Bathe. *Finite Element Procedures*. Prentice-Hall, Inc., New Jersey, 1996. 111, 112

[10] J. Bauch, W. Liese, and R. Schultze. The morphological variability of the bordered pit membranes in gymnosperms. *Wood Science and Technology*, 6(3):165–184, 1972. 12, 13

[11] B. A. D. Begoude, R. Lahlali, D. Friel, P. R. Tondje, and M. H. Jijakli. Response surface methodology study of the combined effects of temperature, pH, and aw on the growth rate of Trichoderma asperellum. *Journal of Applied Microbiology*, 103(4):845–854, 2007. 66

[12] A. D. Bell. The Simulation of Branching Patters in Modular Organisms. *Philosophical Transactions of the Royal Society of London B*, 313(1159):143–159, 1986. 35

[13] L. Boddy and A. D. M. Rayner. Origins of Decay in Living Deciduous Trees: The Role of Moisture Content and a Re-Appraisal of the Expanded Concept of Tree Decay. *New Phytologist*, 94(4):623–641, 1983. 26

[14] L. Boddy, J. M. Wells, C. Culshaw, and D. P. Donnelly. Fractal analysis in studies of mycelium in soil. *Geoderma*, 88(3-4):301–328, 1999. 22

[15] G. Bollrich. *Technische Hydromechanik 1 - Grundlagen*, volume 1. 2000. 111

[16] A. J. Bolton and J. A. Petty. A model describing axial flow of liquids through conifer wood. *Wood Science and Technology*, 12(1):37–48, 1978. 109

[17] R. G. Bolton and L. Boddy. Characterization of the spatial aspects of foraging mycelial cord systems using fractal geometry. *Mycological Research*, 97(6):762–768, 1993. 22

[18] G. P. Boswell. Modelling mycelial networks in structured environments. *Mycological Research*, 112(9):1015–1025, 2008. 36, 65, 92

[19] G. P. Boswell and S. Hopkins. Linking hyphal growth to colony dynamics:

Spatially explicit models of mycelia. *Fungal Ecology*, 1(4):143–154, 2009. 35, 92

[20] G. P. Boswell, H. Jacobs, F. A. Davidson, Gadd, and K. Ritz. Functional Consequences of nutrient translocation in mycelial fungi. *Journal of Theoretical Biology*, 217(4):459–477, 2002. 36

[21] G. P. Boswell, H. Jacobs, K. Ritz, G. M. Gadd, and F. A. Davidson. The Development of Fungal Networks in Complex Environments. *Bulletin of Mathematical Biology*, 69(2):605–634, 2007. 36, 65, 92

[22] J. Brändström. Micro- and ultrastructural aspects of Norway spruce tracheids: a review. *IAWA Journal*, 22(4):333–353, 2001. 9, 10, 13, 51, 99

[23] C. R. Brodersen, E. F. Lee, B. Choat, S. Jansen, R. J. Phillips, K. A. Shackel, A. J. McElrone, and M. A. Matthews. Automated analysis of three-dimensional xylem networks using high-resolution computed tomography. *New Phytologist*, 191(4):1168–79, 2011. 48

[24] H. Brunswik. Untersuchungen über die Geschlechts- und Kernverhältnisse bei der Hymenomyzetengattung Coprinus. *Botanische Abhandlungen*, 5:1–152, 1924. 24

[25] A. T. Bull and A. P. J. Trinci. The Physiology and Metabolic Control of Fungal Growth. *Advances in Microbial Physiology*, 15:1–84, 1977. 35

[26] M. J. Carlile. The Success of the Hypha and Mycelium. In N. A. R. Gow and G. M. Gadd, editors, *The Growing Fungus*, volume 1, pages 3–19, 1995. 25

[27] M. J. Carlile, S. C. Watkinson, and G. W. Gooday. *The fungi*. Elsevier Academic Press, second edition, 2001. 73

[28] I. Carver and G. P. Boswell. A Lattice-Free Model of Translocation-Induced Outgrowth in Fungal Mycelia. *IAENG International Journal of Applied Mathematics*, 38(4):02, 2008. 36, 63, 92

[29] B. Choat, A. R. Cobb, and S. Jansen. Structure and function of bordered

pits: new discoveries and impacts on whole-plant hydraulic function. *New Phytologist*, 177(3):608–626, 2008. 47, 111, 112

[30] B. Chopard, H. J. Herrmann, and T. Vicsek. Structure and growth mechanism of mineral dendrites. *Nature*, 353(6343):409–412, 1991. 35

[31] D. Cohen. Computer simulation of biological pattern generation processes. *Nature*, 216:246–248, 1967. 36, 66

[32] G. Comstock. Directional Permeability Of Softwoods. *Wood and Fiber Science*, 1(4):283–289, 1970. 78, 109

[33] G. L. Comstock and W. A. Côté. Factors affecting permeability and pit aspiration in coniferous sapwood. *Wood Science and Technology*, 2(4):279–291, 1968. 47, 109

[34] S. Cragg, A. Pitman, and S. Henderson. Developments in the understanding of the biology of marine wood boring crustaceans and in methods of controlling them. *International Biodeterioration & Biodegredation*, 43(4):197–205, 1999. 1

[35] J. W. Creffield. *Wood destroying insects, wood borers and termites*. CSIRO Publications, East Melbourne, 1991. 1

[36] P. W. Crous, W. Gams, J. A. Stalpers, V. Robert, and G. Stegehuis. MycoBank: an online initiative to launch mycology into the 21st century. *Studies in Mycology*, 50:19–22, 2004. 22

[37] G. Daniel. Use of electron microscopy for aiding our understanding of wood biodegradation. *FEMS Microbiology Reviews*, 13(2-3):199–233, 1994. 76, 78

[38] F. A. Davidson. Mathematical modelling of mycelia: a question of scale. *Fungal Biology Reviews*, 21(1):30–41, 2007. 35, 36

[39] F. A. Davidson, B. D. Sleeman, A. D. Rayner, J. W. Crawford, and K. Ritz. Large-Scale Behavior of Fungal Mycelia. *Mathematical and computer modelling*, 24(10):81–87, 1996. 36

[40] G. Deflorio, S. Hein, S. Fink, H. Spiecker, and F. W. M. R. Schwarze. The

application of wood decay fungi to enhance annual ring detection in three diffuse-porous hardwoods. *Dendrochronologia*, 22:123–130, 2005. 29

[41] D. Derome, M. Griffa, M. Koebel, and J. Carmeliet. Hysteretic swelling of wood at cellular scale probed by phase-contrast X-ray tomography. *Journal of Structural Biology*, 1731:180–190, 2010. 39, 47

[42] S. Dickson and P. Kolesik. Visualisation of mycorrhizal fungal structures and quantification of their surface area and volume using laser scanning confocal microscopy. *Mycorrhiza*, 9(4):205–213, 1999. 33, 35

[43] I. Dill and G. Kraepelin. Der Abbau von Lignin/Cellulose durch Weissfäule-Pilze: Einfluss spezifischer ökologischer Faktoren. *Forum Holzforschung*, 11:484–489, 1988. 27

[44] D. Donaldson. Cellulose microfibril aggregates and their size variation with cell wall type. *Wood Science and Technology*, 41(5):443–460. 14

[45] L. Edelstein. The Propagation of Fungal Colonies: A Model for Tissues Growth. *Journal of Theoretical Biology*, 98:679–701, 1982. 36

[46] S. J. Eichhorn and R. J. Young. The Young's modulus of a microcrystalline cellulose. *Cellulose*, 8(3):197–207, 2001. 16

[47] K. E. L. Eriksson, R. A. Blanchette, and P. Ander. *Microbial and Enzymatic Degradation of Wood and Wood Components*. Springer, Berlin. 1

[48] G. B. Ermentrout and L. Edelstein-Keshet. Cellular automata approaches to biological modeling. *Journal of Theoretical Biology*, 160(1):97–133, 1993. 35, 36

[49] D. Fengel. Structure and function of the Mebrane in Softwood Bordered Pits. *Holzforschung*, 26(1):1–9, 1972. 13, 14

[50] D. Fengel and G. Wegener. *Wood - Chemistry, Ultrastructure, Reactions*. Walter de Gruyter, Berlin, 1984. 9, 14, 15

[51] M. Fricker, L. Boddy, and D. Debber. Network organisation of mycelial fungi. In K. Esser, R. J. Howard, and N. A. R. Gow, editors, *The Mycota* -

Biology of the fungal cell, volume 8, pages 309–330, Berlin, 2007. Springer. 28, 30, 35, 65

[52] M. Fricker, J. Runions, and I. Moore. Quantitative fluorescence microscopy: From Art to Science. *Annual Review of Plant Biology*, 57(1):79–107, 2006. 34

[53] M. J. Fuhr, C. Lehringer, M. Schubert, F. W. M. R. Schwarze, H. J. Herrmann, and F. K. Wittel. Modelling the permeability of wood infested by the basidiomycete Physisporinus vitreus. *in preparation*, 2011. 4

[54] M. J. Fuhr, M. Schubert, and F. W. M. R. Schwarze. Three-dimensional distribution of bordered pits in Norway spruce wood. *in preparation*, 2011. 4

[55] M. J. Fuhr, M. Schubert, F. W. M. R. Schwarze, and H. J. Herrmann. Modelling the hyphal growth of the wood-decay fungus Physisporinus vitreus. *Fungal Biology*, 115:919–932, 2011. 4, 30, 33, 47, 65, 67, 68, 74, 76, 79, 88, 90

[56] M. J. Fuhr, M. Schubert, F. W. M. R. Schwarze, and H. J. Herrmann. Penetration capacity of the white-rot basidiomycete Physisporinus vitreus. *submitted to Applied Microbiology and Biotechnology*, 2012. 4

[57] M. J. Fuhr, C. Stührk, B. Münch, F. W. M. R. Schwarze, and M. Schubert. Automated Quantification of the Impact of the Wood-decay fungus Physisporinus vitreus on the Cell Wall Structure of Norway spruce by Tomographic Microscopy. *Wood Science and Technology*, DOI: 10.1007/s00226-011-0442-y, 2011. 4, 33, 34, 48, 49

[58] M. J. Fuhr, C. Stührk, M. Schubert, F. W. M. R. Schwarze, and H. J. Herrmann. Modelling the effect of environmental factors on the hyphal growth of the basidiomycete Physisporinus vitreus. *Journal of Basic Microbiology*, 5:1–8, 2011. 4, 74, 76, 90, 91

[59] M. J. Fuhr, C. Stührk, F. W. M. R. Schwarze, M. Schubert, and H. J. Herrmann. Modelling hyphal growth of the bioincising fungus Physisporinus vitreus. In *IRG 41th Annual Meeting, Biarritz*, Stockholm, Sweden, 2010.

IRG. 33

[60] G. Gierz and S. Bartnicki-Garcia. A Three-Dimensional Model of Fungal Morphogenesis Based on the Vesicle Supply Center Concept. *Journal of Theoretical Biology*, 208(2):151–164, 2001. 24

[61] W. Gindl, C. Hansmann, N. Gierlinger, M. Schwanninger, B. Hinterstoisser, and G. Jeronimidis. Using a water-soluble melamine-formaldehyde resin to improve the hardness of Norway spruce wood. *Journal of Applied Polymer Science*, 93(4):1900–1907, 2004. 1

[62] M. Girbardt. Der Spitzenkoerper von Polystictus Versicolor (L.). *Planta*, 50:47–59, 1957. 24

[63] M. Girbardt. Die Ultrastruktur der Apikalregion von Pilzhypen. *Protoplasma*, 67:413–441, 1969. 24

[64] R. C. Gonzalez, R. E. Woods, and S. L. Eddins. *Digital Image Processing Using MATLAB*. Gatesmark Publishing, second edition, 2009. 40

[65] A. Goriely and M. Tabor. Mathematical modeling of hyphal tip growth. *Fungal Biology Reviews*, 22(2):77–83, 2008. 36

[66] S. N. Gray, J. Dighton, S. Olsson, and D. H. Jennings. Real-time measurement of uptake and translocation of 137Cs within mycelium of Schizophyllum commune Fr. by autoradiography followed by quantitative image analysis. *New Phytologist*, 129(3):449–465, 1995. 63

[67] F. Green and C. A. Clausen. Production of Polygalacturonase and Increase of Longitudinal Gas Permeability in Southern Pine by Brown-Rot and White-Rot Fungi. *Holzforschung*, 53(6):563–568, 1999. 109

[68] F. Green, C. A. Clausen, T. A. Kuster, and T. L. Highley. Induction of polygalacturonase and the formation of oxalic acid by pectin in brown-rot fungi. *World Journal of Microbiology and Biotechnology*, 11(5):519–524, 1995. 20

[69] F. Green and T. L. Highley. Mechanism of brown-rot decay: Paradigm or

paradox. *International Biodeterioration & Biodegradation*, 39(2-3):113–124, 1997. 28, 47, 76, 78

[70] F. Green, J. L. Tschernitz, T. A. Kuster, and T. L. Highley. Hydrolysis of bordered pits during colonization of conifers by brown-rot fungi. In *26th Annual Meeting Helsingør, Denmark 11-16 June 1995.* International Research Group on Wood Preservation, 1995. 76, 78

[71] D. Gross and A. Schmutz. *Jahrbuch Wald und Holz*. Bundesamt für Umwelt BAFU, Bern, 2010. 20

[72] U. G. Hacke and S. Jansen. Embolism resistance of three boreal conifer species varies with pit structure. *New Phytologist*, 182(3):675–686, 2009. 47

[73] A. Hafner, J. Fischer, and J. Francuz. Rettungsgrabungen in einer endneolithischen Pfahlbausiedlung am Bielersee. *Archäologie Bern*, pages 76–79, 2008. 1

[74] A. Hafner, J. Fischer, and J. Francuz. Rettungsgrabungen 2008 in der von Erosion bedrohten Pfahlbausiedlung. *Archäologie Bern*, pages 110–113, 2009. 1

[75] J. A. Hailwood and S. Horrobin. Absorption of water by polymers: Analysis in terms of a simple model. *Transactions of the Faraday Society*, 42:B084–B092, 1946. 19

[76] S. D. Harris, N. D. Read, R. W. Roberson, B. Shaw, S. Seiler, P. Plamann, and M. Momany. Polarisome meets spitzenkörper: microscopy, genetics, and genomics converge. *Eukaryotic cell*, 4(2):225–229, 2005. 24, 58

[77] P. Hass, F. K. Wittel, M. Mendoza, M. Stampanoni, H. J. Herrmann, and P. Niemz. Adhesive penetration in beech wood: Experiments. *Wood Science and Technology*, 46(1-3):243–256, 2011. 20

[78] H. J. Herrmann. Simulation of random growth processes. In *The Monte Carlo Method in Condensed Matter Physics*, volume 71, pages 93–120, Berlin, 1992. Springer. 35

[79] P. C. Hickey, D. J. Jacobson, N. D. Read, and N. L. Glass. Live-cell imaging of vegetative hyphal fusion in Neurospora crassa. *Fungal Genetics and Biology*, 37(1):109–119, 2002. 28

[80] C. A. S. Hill. *Wood Modification: Chemical, Thermal and Other Processes.* John Wiley & Sons, Ltd, Chichester, UK, 2006. 1

[81] C. Hillebrand and C. Lehringer. *The impact of Physisporinus vitreus.* Bachelor's Thesis, EMPA, Dübendorf, Switzerland, 2010. 80

[82] W. E. Hillis. *Wood Extractives.* Academic Press, New York, 1962. 20

[83] V. K. Horvath and H. J. Herrmann. The Fractal Dimension of Stress Corrosion Cracks. *Chaos, Solitons and Fractals*, 1(5):395–400, 1991. 35

[84] S. A. Hutchinson, P. Sharma, K. R. Clarke, and I. Macdonald. Control of Hyphal Orientation in Colonies of Mucor Hiemalis. *Transactions of the British Mycological Society*, 75(2):177–191, 1980. 36

[85] J. Ihssen, M. Schubert, F. W. M. R. Schwarze, and L. Thöny-Meier. Efficient production of Al(OH)3-immobilized laccase with aHeterobasidion annosum strain selected by microplatescreening. *Journal of Applied Microbiology*, 110(4):924–934, 2011. 27

[86] B. Illman and B. Dowd. High Resolution Microtomography for Density and Spatial Informeation about Wood Structures. In U. Bonse, editor, *Proceedings of SPIE on Developments in X-ray Tomography II*, pages 198–204. Society of Photo-Optical Instrumentation Engineers, 1999. 34

[87] T. C. Jarrett, D. J. Ashton, M. Fricker, and N. F. Johnson. Interplay between function and structure in complex networks. *Physical Review E*, 74(2):026116, 2006. 22, 30

[88] D. Jones, B. Tjeerdsma, M. Spear, and C. A. S. Hill. Properties of wood following treatment with a modified hot oil. In H. Militz and C. A. S. Hill, editors, *Wood modification: Processes, properties and commercialisation*, pages 202–207, Göttingen, 2005. 1

[89] A. Jorissen, F. Bongers, B. Kattenbroek, and W. Homan. The influence of acetylation of radiata pine in structural size on its strength properties. In H. Militz and C. A. S. Hill, editors, *Wood modification: Processes, properties and commercialisation*, pages 108–115, Göttingen, 2005. 1

[90] T. Kerr and I. W. Bailey. The cambium and its derivative tissue. X. Structure, optical properties and chemical composition of the so-called middle lamella. *Journal Of The Arnold Arboretum*, 15:329–349, 1934. 14

[91] W. Knebel and E. Schnepf. Confocal laser scanning microscopy of fluorescently stained wood cells: a new method for three-dimensional imaging of xylem elements. *Trees - Structure and Function*, 5(1):1–4, 1991. 33

[92] R. Kohli, A. B. Herrmann, and J. Babel. *Szenarien zur Bevölkerungsentwicklung der Schweiz 2010 bis 2060.* Bundesamt für Statistik BFS, Neuchatel, 2010. 21

[93] F. F. P. Kollmann and W. A. Côté. *Principles of wood science and technology. I. Solid wood.* Springer, Berlin, 1984. 19

[94] Z. Koran. Intertracheid pitting in the radial walls of black spruce tracheids. *Wood Science*, 7(2):111–115, 1974. 13

[95] P. B. Laming and B. J. H. Terwelle. Anomalous tangential pitting in Picea Abies (L.) Karst. (European Spruce). *IAWA Bulletin*, 4:3–10, 1971. 13

[96] A. Lamour, F. van den Bosch, A. J. Termorshuizen, and M. J. Jeger. Quasi-steady state approximation to a fungal growth model. *IMA Journal of Mathematics Applied in Medicine and Biology*, 19(3):163–183, 2002. 36

[97] C. Lehringer. *Permeability improvement of Norway spruce wood with the white rot fungus Physisporinus vitreus.* PhD thesis, Göttingen, Germany, 2011. 26, 27, 28, 104, 105, 106

[98] C. Lehringer, M. Arnold, K. Richter, K. Schubert, F. W. M. R. Schwarze, and H. Militz. Bioincised Wood as Substrate for Surface Modification. In *European Conference on Wood Modification 2009*, 2009. 2, 28, 65, 76

[99] C. Lehringer, K. Hillebrand, K. Richter, M. Arnold, F. W. M. R. Schwarze, and H. Militz. Anatomy of bioincised Norway spruce wood. *International Biodeterioration & Biodegradation*, 64(5):346–355, 2010. 2, 12, 23, 27, 28, 29, 33, 44, 104, 106

[100] C. Lehringer, G. Koch, R.-B. Adusumalli, W. M. Mook, K. Richter, and H. Militz. Effect of Physisporinus vitreus on wood properties of Norway spruce. Part 1: Aspects of delignification and surface hardness. *Holzforschung*, 65(5):711–719, 2011. 2, 29

[101] C. Lehringer, K. Richter, F. W. M. R. Schwarze, and H. Militz. A review on promising approaches for liquid permeability improvement in softwood. *Wood and Fiber Science*, 41(4):373–385, 2009. 2, 28, 109

[102] C. Lehringer, B. Saake, V. Živković, K. Richter, and H. Militz. Effect of Physisporinus vitreus on wood properties of Norway spruce. Part 2: Aspects of microtensile strength and chemical changes. *Holzforschung*, 65(5):721–727, 2011. 2, 29

[103] R. Lejeune, J. Nielsen, and G. V. Baron. Morphology of Trichoderma reesei QM 9414 in submerged cultures. *Biotechnology and Bioengineering*, 47(5):609–615, 1995. 36

[104] F. Lens, J. S. Sperry, M. A. Christman, B. Choat, D. Rabaey, and S. Jansen. Testing hypotheses that link wood anatomy to cavitation resistance and hydraulic conductivity in the genus Acer. *New Phytologist*, 190(3):709–23, 2011. 47

[105] R. D. Levine. *Molecular Reaction Dynamics*. Cambrige University Press, Cambridge, UK, 2005. 67

[106] F. T. Lewis. The sape of the tracheids in the pine. *The American Journal of Botany*, 22(8):741–762, 1935. 12, 110

[107] C. M. Liddell and D. Hansen. Visualizing complex biological interactions in the soil ecosystem. *The Journal of Visualization and Computer Animation*, 4(1):3–12, 1993. 36

[108] W. Liese and J. Bauch. On the closure of bordered pits in conifers. *Wood Science and Technology*, 1(1):1–13, 1967. 13

[109] W. Liese and I. Johann. Experimentelle untersuchungen über die feinstruktur der hoftüpfel bei den koniferen. *Naturwissenschaften*, 24:579–80, 1954. 13

[110] W. Liese and R. Schmid. Licht- und elektronenmikroskopische Untersuchungen über das Wachstum von Bläuepilzen in Kiefer- und Fichtenholz. *Holz als Roh- und Werkstoff*, 19(9):329–337. 76, 78, 80

[111] Lignatec. *Bauten in Holz - Brandschutz Anforderungen*. Lignum, Zurich, 2005. 3, 21

[112] H. Lindström. Fiber Length, Tracheid Diameter, and Latewood Percentage in Norway Spruce: Development from Pith Outward. *Wood and Fiber Science*, 29(1):21–34, 1997. 6

[113] J. M. Lopez and H. J. Jensen. Generic model of morphological changes in growing colonies of fungi. *Physical Review E*, 65(2):021903, 2002. 36

[114] C. Mai, U. Kües, and H. Militz. Biotechnology in the wood industry. *Applied Microbiology and Biotechnology*, 63(5):477–494, 2004. 2, 29

[115] A. Majcherczyk and A. Hüttermann. Bioremediation of wood treated with preservatives using white-rot fungi. In A. Bruce and J. W. Palfreyman, editors, *Forest products biotechnology*, pages 129–140, London, UK, 1998. Taylor and Francis. 29, 65

[116] H. Mäkinen, T. Jyske, and P. Saranpää. Variation of tracheid length within annual rings of Scots pine and Norway spruce. *Holzforschung*, 62(1):123–128, 2008. 10

[117] D. Mannes, F. Marone, E. Lehmann, M. Stampanoni, and P. Niemz. Application areas of synchrotron radiation tomographic microscopy for wood research. *Wood Science and Technology*, 44(1):67–84, 2010. 39, 48

[118] S. C. Mayo, F. Chen, and R. Evans. Micron-scale 3D imaging of wood

and plant microstructure using high-resolution X-ray phase-contrast microtomography. *Journal of structural biology*, 171(2):182–8, Apr. 2010. 44

[119] M. McGovern, A. Senalik, G. Chen, F. C. Beall, and H. Reis. Detection and assessment of wood decay using x-ray computer tomography. volume 7647, page 76474B, 2010. 34

[120] M. Mendoza, P. Hass, F. K. Wittel, P. Niemz, and H. J. Herrmann. Adhesive penetration in beech wood Part II: penetration model. *arXiv*, 1007.0761. 20

[121] A. Meskauskas, M. D. Fricker, and D. Moore. Simulation colonial growth of fungi with the Neighbour-Sensing model of hyphal growth. *Mycological Research*, 108(11):1241–1256, 2004. 36

[122] K. Messner, K. Fackler, P. Lamaipis, W. Gindl, E. Srebotnik, and T. Watanabe. Biotechnological wood modification. In *Proceedings of the International Symposium on Wood-based Materials*, pages 45–49, Vienna, Austria, 2002. 29, 65

[123] F. Meyer. Topographic distance and watershed lines. *Signal Processing*, 38(1):113–125, July 1994. 40

[124] K. Mitsui and L. Tolvaj. Acetylation of photo-thermally treated wood. In H. Militz and C. A. S. Hill, editors, *Wood modification: Processes, properties and commercialisation*, pages 156–159, Göttingen, 2005. 1

[125] M. Mooser, M. Forestier, and M. Pittet-Baschung. *Surélévations en bois : densifier, assainir, isoler*. Presses Polytechniques et Universitaires Romandes, Lausanne, 2010. 21

[126] B. Munch, P. Trtik, F. Marone, and M. Stampanoni. Stripe and ring artifact removal with combined wavelet - Fourier filtering. *Optics Experss*, 17(10):8567–8591, 2009. 40

[127] U. Neuhäusler, G. Schneider, W. Ludwig, and D. Hambach. Phase contrast X-ray microscopy at 4 keV photon energy with 60Â nm resolution. *Journal de Physique IV (Proceedings)*, 104:567–570, Mar. 2003. 39

[128] J. Nielsen. Modelling the morphology of filamentous microorganisms. *Trends in Biotechnology*, 14(11):438–443, 1996. 35

[129] P. Niemz. *Physik des Holzes und der Holzwerkstoffe*. DRW-Verlag, 1993. 8, 15, 16, 17, 18, 19

[130] S. S. of Engineers and Architects. *SIA 260:2003 - Basis of structural design*. SIA, Zurich, 2003. 3

[131] S. S. of Engineers and Architects. *SIA 265:2003 - Timber Structure*. SIA, Zurich, 2003. 3

[132] N. Otsu. A threshold selection method from gray-level histograms. *IEEE Trans. Sys., Man., Cyber.*, 9:62–66, 1979. 40

[133] E. Panagou, V. Kodogiannis, and G. Nychas. Modelling fungal growth using radial basis function neural networks: The case of the ascomycetous fungus Monascus ruber van Tieghem. *International Journal of Food Microbiology*, 117(3):276–286, July 2007. 66

[134] E. Z. Panagou, P. N. Skandamis, and G. J. E. Nychas. Modelling the combined effect of temperature, pH and aw on the growth rate of Monascus ruber, a heat-resistant fungus isolated from green table olives. *Journal of Applied Microbiology*, 94(1):146–156, 2003. 66

[135] S. Parnell, F. van den Bosch, and C. A. Gilligan. Large-Scale Fungicide Spray Heterogeneity and the Regional Spread of Resistant Pathogen Strains. *Phytopathology*, 96(5):549–555, 2006. 36

[136] D. V. Patel and C. N. J. Mcghee. Contemporary in vivo confocal microscopy of the living human cornea using white light and laser scanning techniques: a major review. *Clinical and Experimental Ophthalmology*, 35(1):71–88, Feb. 2007. 34

[137] R. B. Pearce. Tansley Review No. 87. Antimicrobial Defences in the Wood of Living Trees. *New Phytologist*, 132(2), 1996. 26

[138] P. W. Perrin. Review of Incising and Its Effects on Strength and Preservative

Treatment of Wood. *Forest Products Journal*, 28(9):27–33, 1978. 1

[139] B. Petric and V. Scukanec. Volume percentage of tissues in wood of conifers grown in Yugoslavia. *IAWA Bulletin*, 2:3–7, 1973. 9

[140] R. C. Pettersen. *The chemical composition of wood*, pages 57–126. Advances in chemistry series 207. American Chemical Society, 1984. 20

[141] J. A. Petty. The Aspiration of Bordered Pits in Conifer Wood. *Proceedings of the Royal Society of London. Series B, Biological Sciences*, 181(1065):395–406, 1972. 2

[142] J. A. Petty. Laminar flow of fluids through short capillaries in conifer wood. *Wood Science and Technology*, 8(4):275–282, Dec. 1974. 109

[143] J. A. Petty and R. D. Preston. Permeability and structure of the wood of Sitka spruce. *Proceeding of the Royal Society of London B*, 175:149–166, 1970. 47, 104

[144] N. J. B. Plomley. Formation of the colony in the fungus Chaetomium. *Australian Journal of Biological Sciences*, 12:53–64, 1958. 32

[145] J. I. Prosser. *Mathematical modelling of fungal growth*, pages 319–335. Chapman and Hall, 1995. 35, 36

[146] A. D. M. Rayner. *Degrees of Freedom - Living in Dynamic Boundaries*. Imperial College Press, 1997. 23

[147] A. D. M. Rayner and L. Boddy. *Fungal Decomposition of Wood*. John Wiley & Sons, 1988. 1, 12, 23, 25, 26, 65, 76

[148] N. D. Read, A. Lichius, J. Shoji, and A. B. Goryachev. Self-signalling and self-fusion in filamentous fungi. *Current Opinion in Microbiology*, 12:1–8, 2009. 28

[149] C. M. Regalado and B. D. Sleeman. Aggregation and collapse in a mechanical model of fungal tip growth. *Journal of Mathematical Biology*, 39(2):109–138. 36

[150] C. Reynaga-Pena, G. Gierz, and S. Bartnicki-Garcia. Analysis of the role of the Spitzenkörper in fungal morphgenesis by computer simulation of apical branching in Aspergillus niger. *Proc. Natl. Acad. Sci. USA*, 94:9096–9101, Aug. 1997. 24

[151] B. A. Richardson. *Wood preservation.* Spon Press, 2001. 1

[152] K. Richter. Perforation and impregnation methods to improve weather resistance of structural timber. Technical report, EMPA, Dübendorf, Switzerland, 1989. 1, 47

[153] M. Riquelme and S. Bartnicki-Garcia. Advances in understanding hyphal morphogenesis: Ontogeny, phylogeny and cellular localization of chitin synthases. *Fungal Biology Reviews*, 22(2):56–70, May 2008. 24

[154] M. Riquelme, C. Reynaga-Pena, G. Gierz, and S. Barnicki-Garcia. What determines growth direction in fungal hyphae. *Fungal Genetics and Biology*, 24:101–109, 1998. 64

[155] M. P. Sarén, R. Serimaa, S. Andersson, T. Paakkari, P. Saranpää, and E. Pesonen. Structural variation of tracheids in Norway spruce (Picea abies [L.] Karst.). *Journal of Structural Biology*, 136(2):101–109, 2001. 10

[156] O. Schmidt. Indoor wood-decay basidiomycetes: damage, causal fungi, physiology, identification and characterization, prevention and control. *Mycological Progress*, 6(4):261–279, Nov. 2007. 33

[157] O. Schmidt, U. Schmitt, U. Moreth, and T. Potsch. Wood decay by the white-rotting basidiomycete Physisporinus vitreus form a cooling tower. *Holzforschung*, 51(3):193–200, 1997. 23, 26, 27

[158] H. Schmidt-Vogt, W. Liese, and K. E. Rehfuess. *Die Fichte. Band 2/1: Wachstum, Züchtung, Boden, Umwelt, Holz*, volume 2. Verlag Paul Parey, 1986. 6, 13, 14, 17, 19

[159] M. Schubert. *In vitro und ad planta Studien zum Einsatz von Trichoderma-Arten für die Biologische Kontrolle Holz abbauender Pilze an Bäumen.* PhD thesis, Albert-Ludwigs-Universität Freiburg im Breisgau, 2006. 1, 23, 25,

26, 29, 62

[160] M. Schubert, V. Dengler, S. Mourad, and F. W. M. R. Schwarze. Determination of optimal growth parameters for the bioincising fungus Physisporinus vitreus by means of response surface methodology. *Journal of Applied Microbiology*, 106(5):1734–1742, 2009. 29, 61, 66, 69, 97

[161] M. Schubert and J. Ihssen. Behandlung von Nadelholz mit Laccase zur Verbesserung der Widerstandsfähigkeit gegenüber holzverfärbenden Pilzen. WHFF-Projekt Nr. 2009.03. Technical report, Swiss Federal Laboratories for Material Science and Technology (EMPA), St. Gallen, 2010. 5

[162] M. Schubert, S. Mourad, S. Fink, and F. W. M. R. Schwarze. Ecophysiological responses of the biocontrol agent Trichoderma atroviride (T-15603.1) to combined environmental parameters. *Biological Control*, 49(1):84–90, 2009. 61, 66

[163] M. Schubert, S. Mourad, and F. Schwarze. Radial basis function neural networks for modeling growth rates of the basidiomycetes Physisporinus vitreus and Neolentinus lepideus. *Applied microbiology and biotechnology*, 85(3):703–712, Jan. 2010. 2, 22, 25, 29, 66, 69, 71, 72, 73, 74, 89, 94

[164] M. Schubert, S. Mourad, and F. W. Schwarze. Statistical approach to determine the effect of combined environmental parameters on conidial development of Trichoderma atroviride (T-15603.1). *Journal of basic microbiology*, 50(6):570–580, Dec. 2010. 66

[165] M. Schubert and F. W. M. R. Schwarze. Response Surface Analyse (RSM) der Wirkung kombinierter Parameter auf das Wachstum von Physisporinus vitreus. *Holztechnologie*, 50:16–20, 2009. 29, 65

[166] M. Schubert, T. Volkmer, C. Lehringer, and F. W. M. R. Schwarze. Resistance of bioincised wood treated with wood preservatives to blue-stain and wood-decay fungi. *International Biodeterioration & Biodegradation*, 65(1):108–115, Jan. 2011. 27

[167] F. W. M. R. Schwarze, J. Engels, and C. Mattheck. *Fungal Strategies of Wood Decay in Tree*. Springer Verlag Berlin Heidelberg New York, 2nd

edition, 2004. 1, 12, 23

[168] F. W. M. R. Schwarze and H. Landmesser. Preferential degradation of pit membranes within tracheids by the basidiomycete Physisporinus vitreus. *Holzforschung*, 54(5):461–462, 2000. 2, 23, 28, 29, 55

[169] F. W. M. R. Schwarze, H. Landmesser, B. Zgraggen, and M. Heeb. Permeability changes in heartwood of Picea abies and Abies alba induced by incubation with Physisporinus vitreus. *Holzforschung*, 60(4):450–454, 2006. 2, 23, 27, 29, 76, 78

[170] F. W. M. R. Schwarze and M. Schubert. Enhance uptake of wood modification agents in 'bioincised' wood. In *The International Research Group on Wood Protection*, 2009. 2, 28, 29, 75, 76

[171] F. W. M. R. Schwarze and M. Schubert. Physisporinus vitreus: a versatile white rot fungus for engineering value-added wood products. *Journal of Applied Microbiology and Biotechnology*, 92(3):431–440, 2011. 27

[172] F. W. M. R. Schwarze, M. Spycher, and S. Fink. Superior wood for violins wood decay fungi as a substitute for cold climate. *New Phytologist*, 179(4):1095–1104, Sept. 2008. 3, 29, 44

[173] J. F. Siau. *Transport Processes in Wood*. Springer Series in Wood Science. Springer Verlag Berlin Heidelberg New York, 1984. 18, 47, 78, 104, 109, 113

[174] J. H. Sietsma and J. G. H. Wessels. *Apical Wall Biogenesis*. The Mycota. Springer-Verlag Berlin Heidelberg, 2 edition, 2006. 24

[175] J. Sirviö. Variation of cross sectional properties within single norway spruce tracheids. *Wood and Fibre Science*, 33(1):16–25, 2000. 13, 33

[176] J. Sirviö and P. Kärenlampi. Pits s natural irregularities in softwood fibers. *Wood and Fiber Science*, 30(1):27–39, 1998. 13, 47, 50, 51, 78

[177] O. Skyba. *Durability and physical properties of thermo-hygro-mechanically (THM)-densified wood*. PhD thesis, 2008. 17

[178] M. L. Smith, J. N. Bruhn, and J. B. Anderson. The fungus Armillaria

bulbosa is among the largest and oldest living organisms. *Nature*, 356:428–431. 22

[179] F. Soddell, R. Seviour, and J. Soddell. Using Lindenmayer Systems to Investigate How Filamentous Fungi May Produce Round Colonies. *Complexity*, 2, 1995. 36

[180] M. Spycher. *The application of wood decay fungi to improve the acoustic properties of resonance wood for violins*. PhD thesis, Albert-Ludwigs-Universität Freiburg im Breisgau, 2007. 29

[181] M. Spycher, F. Schwarze, and R. Steiger. Assessment of resonance wood quality by comparing its physical and histological properties. *Wood Science and Technology*, 42(4):325–342, Apr. 2008. 29

[182] U. Srinivasan, H. J. Staines, and A. Bruce. Influence of media type on antagonistic modes of Trichoderma spp. against wood decay basidiomycetes. *Material und Organismen*, 21:301–321, 1992. 27, 61

[183] A. J. Stamm. *Wood and Cellulose Science*. The Ronald Press Company, 1964. 16, 18, 19

[184] M. Stampanoni, A. Groso, A. Isenegger, G. Mikuljan, Q. Chen, A. Bertrand, S. Henein, R. Betemps, U. Frommherz, P. Böhler, D. Meister, M. Lange, and R. Abela. Trends in synchrotron-based tomographic imaging: the SLS experience. *Proceedings of SPIE*, 6318(1):63180M+, Sept. 2006. 39

[185] T. Strahm. Hochfestes Brettschichtholz aus Laubholz und mit hybridem Trägeraufbau: BSH GL 60 Träger. *Holzforschung Schweiz*, 1:7–8, 2011. 20

[186] C. Stührk. *Tomographische Visualisierung des Hyphensystems von Physisporinus vitreus in Fichtenholz (Picea abies) zur Optimierung des Bioincising Prozesses*. PhD thesis, EMPA St. Gallen, 2011. 30, 33, 35

[187] C. Stührk, M. Fuhr, M. Schubert, and F. W. M. R. Schwarze. Analyzing hyphal growth of the bioincising fungus Physisporinus vitreus with light-, confocal laser scanning- and, Synchrotron X-ray tomographic microscopy. In *Paper prepared for the 41st Annual Meeting Biarritz, France*, 2010. 26,

30, 33, 34, 35, 52, 74, 91, 96, 106

[188] N. Y. Su and R. H. Scheffrahn. *Termites as pests of buildings*, pages 437–453. Kluwer Academic Publishers, 2000. 1

[189] P. Sudbery and H. Court. *Polarised growth in fungi*, volume 8 of *The Mycota*, chapter 6, pages 137–166. Springer-Verlag Berlin Heidelberg New York, first edition, 2007. 24, 58

[190] R. J. Thomas and K. P. Kringstad. The Role of Hydrogen Bonding in Pit Aspiration. *Holzforschung*, 25(5):143–149, Jan. 1971. 13

[191] S. H. Tindemans, N. Kern, and B. M. Mulder. The diffusive vesicle supply center model for tip growth in fungal hyphae. *Journal of Theoretical Biology*, 238(4):937–948, Feb. 2006. 24, 36

[192] A. P. J. Trinci. A Study of the Kinetics of Hyphal Extension and Branch Initiation of Fungal Mycelia. *J Gen Microbiol*, 81(1):225–236, Mar. 1974. 32, 73

[193] P. Trtik, J. Dual, D. Keunecke, D. Mannes, P. Niemz, P. Stähli, A. Kaestner, A. Groso, and M. Stampanoni. 3D imaging of microstructure of spruce wood. *Journal of Sturctural Biology*, 159(1):46–55, 2007. 39, 47

[194] A. Tunbridge and H. Jones. An L-systems approach to the modelling of fungal growth. *The Journal of Visualization and Computer Animation*, 6(2):91–107, 1995. 36

[195] J. Van den Bulcke, M. Boone, J. Van Acker, M. Stevens, and L. Van Hoorebeke. X-ray tomography as a tool for detailed anatomical analysis. *Annals of Forest Science*, 66:508–519, 2009. 33, 48

[196] J. van den Bulcke, M. Boone, J. van Acker, and L. van Hoorebeke. Three-Dimensional X-Ray Imaging and Analysis of Fungi on and in Wood. *Microscopy and Microanalysis*, 15(5):395–402, 2009. 33, 34

[197] J. Van den Bulcke, B. Masschaele, M. Dierick, J. V. Acker, M. Stevens, and L. V. Hoorebeke. Three-dimensional imaging and analysis of infested

coated wood with X-ray submicron CT. *International Biodeterioration & Biodegradation*, 61(3):278–286, 2008. 35

[198] A. Wagenführ and F. Scholz. *Taschenbuch der Holztechnik*. Carl Hanser Verlag, 2008. 9, 15, 17, 19

[199] J. Webster and R. W. S. Weber. *Introduction to Fungi*. Cambridge University Press, The Edinburgh Building, Cambridge CB2 2RU, UK, third edition, 2007. 25

[200] D. Weiss. Supersonic Spores. *Discovery Channel Magazine*, (17):43–49, Apr. 2010. 29

[201] R. S. Williams. *Weathering of Wood*. CRC Press, 2005. 1

[202] F. K. Wittel. *Diskrete Elemente - Modelle zur Bestimmung der Festigkeit Evolution in Verbundwerkstoffen*. Kröplin, B, Pfaffenwaldring 2, 2006. 8, 10

[203] Y. Xiao, B. Kreber, and C. Breuil. Localisation of fungal hyphae in wood using immunofluorescence labelling and confocal laser scanning microscopy. *International Biodeterioration & Biodegradation*, 44(4):185–190, Dec. 1999. 33

[204] Y. Xiao, R. N. Wakeling, and A. P. Singh. Use of confocal microscopy in examining fungi and bacteria in wood. *Biofouling: The Journal of Bioadhesion and Biofilm Research*, 15(1):231–239, 2000. 33

[205] U. Yildiz, E. Dizman, H. Kalaycioglu, S. Yildiz, A. Temiz, and E. D. Gezer. The effects of chemical modification on the physical and mechanical properties of particleboards produced from alder and spruce chips. In H. Militz and C. A. S. Hill, editors, *Wood modification: Processes, properties and commercialisation*, pages 116–124, Göttingen, 2005. 1

Curriculum vitae

Matthias Jörg Fuhr

Date of birth	25/12/1982
Place of birth	Zurich ZH, Switzerland
Citizenship	Sufers GR, Switzerland

Education

Nov. 2008 - Nov. 2011	PhD in Computational Physics at ETH Zurich
Sep. 2008	Master of Science ETH in Civil Engineering
Feb. - July 2008	Master's thesis at The University of Tokyo
2006 - Jan. 2008	Master program at ETH Zurich in Civil Engineering
2003 - 2006	Bachelor program at ETH Zurich in Civil Engineering
1996 - 2003	Matura Typus B (Latin and English) Literargymnasium Rämibühl

List of publications

[1] M. J. Fuhr, C. Stührk, F. W. M. R. Schwarze, M. Schubert, H. J. Herrmann (2010): Modelling hyphal growth of the bioincising fungus Physisporinus vitreus. Paper prepared for the 41th Annual Meeting of the International Research Group on Wood Protection, Biarritz, France.

[2] C. Stührk, M. J. Fuhr, F. W. M. R. Schwarze, M. Schubert (2010): Analyzing hyphal growth of the bioincising fungus Physisporinus vitreus with light-,

confocal laser scanning- and, Synchrotron X-ray tomographic microscopy. Paper prepared for the 41th Annual Meeting of the International Research Group on Wood Protection, Biarritz, France.

[3] M. J. Fuhr, M. Schubert, F. W. M. R. Schwarze, H. J. Herrmann (2011): Modeling the hyphal growth of the wood decay fungus Physisporinus vitreus, Fungal Biology 115, pp. 919-932.

[4] M. J. Fuhr, C. Stührk, B. Münch, F. W. M. R. Schwarze, Mark Schubert (2011): Automated Quantification of the Impact of the Wood-decay fungus Physisporinus vitreus on the Cell Wall Structure of Norway spruce by Tomographic Microscopy, Wood Science and Technology, DOI: 10.1007/s00226-011-0442-y.

[5] M. J. Fuhr, C.< Stührk, M. Schubert, F. W. M. R. Schwarze, H. J. Herrmann (2011): Modelling the effect of environmental factors on the hyphal growth of the basidiomycete Physisporinus vitreus, Journal of Basic Microbiology 51, pp. 1-8.

[6] C. Stührk, M. J. Fuhr, M. Schubert, F. W. M. R. Schwarze, H. J. Herrmann (2011): Visualisierung und Modellierung des Bioincising Pilzes Physisporinus vitreus, Holzforschung Schweiz 2011/1, p. 13 - 16.

[7] M. J. Fuhr, M. Schubert, C. Stührk, F. W. M. R. Schwarze and H. J. Herrmann (2012). Penetration capacity of wood decay fungi into wood. in preparation.

[8] M. J. Fuhr, C. Stührk, F. W. M. R. Schwarze and M. Schubert (2012). 3D Distribution of bordered pits in Norway spruce wood. in preparation.

[9] M. J. Fuhr, C. Lehringer, M. Schubert, F. W. M. R. Schwarze, F. K. Wittel (2012). Permeability of Norway spruce wood colonized by Physisporinus vitreus. in preparation.